POLITECNICO DI MILANO

Scuola di Ingegneria Industriale e dell'Informazione

Corso di Laurea Magistrale in
Ingegneria Energetica

Evaluation of ORC processes and their implementation in solar thermal DSG plants

Relatore: Prof. Paolo SILVA

Co-relatore: M.Sc. Heiko SCHENK

Tesi di Laurea di:

Dalma DEGLI ESPOSTI Matr. 783376

Anno Accademico 2012 - 2013

Acknowledgements

Innanzitutto, vorrei ringraziare il Professor Paolo Silva per la sua infinita disponibilità e per avermi dato la possibilità di sviluppare questa tesi in Germania.
Un sincero ringraziamento va in particolare ad Andrea Giostri, che ha pazientemente messo a disposizione la sua conoscenza continuando a seguire il mio lavoro anche da lontano. Lo ringrazio per il supporto iniziale in quel di Stoccarda. Il primo mese in ufficio è stato come sentirsi a casa.

Besonderer Dank geht an meinen Betreuer M.Sc. Heiko Schenk vom DLR Stuttgart, der diese Masterarbeit ermöglicht hat. Ich bedanke mich bei ihm für die wöchentlichen jour fixe Termine, in denen er mir ausführlich zu allen Fragen und Problemstellungen mit Rat und Tat zur Seite stand. Weiterhin möchte ich mich bei allen Mitarbeitern des Instituts für Solarforschung am Standort Stuttgart für die angenehme und freundschaftliche Zusammenarbeit bedanken.

Il ringraziamento più grande va però a Mamma e Papà, per aver sempre creduto in me e avermi supportato in ogni momento e in ogni mia scelta da sempre. Un ringraziamento speciale va alla mia Nonna, per esserci sempre stata in ogni occasione.

Grazie alla mia Sis e a tutti gli Amici di Brixen, Milano e Torino che nonostante la lontananza sono sempre stati presenti, dimostrando quanto il nostro legame sia forte.
Inoltre, un doveroso ringraziamento va al mio collega di fiducia e ai “piccoli ing.”, che oltre ad esser stati miei compagni d’avventura al Politecnico, si sono rivelati degli ottimi amici.

Un grazie speciale va poi alla mia “Stuttgart-Family”, che ha contribuito a rendere piacevoli e divertenti questi mesi di permanenza all’estero.

Infine un pensiero va a tutte le persone che in questi anni hanno condiviso con me parte di questo percorso tra Milano, Monaco e Stoccarda. A chi c’era, c’è e c’è sempre stato. Grazie!

Index

Index of figures

Index of tables

Abstract

In recent years Direct Steam Generation (DSG) systems using water have been developed as an alternative to state-of-the-art parabolic trough plants with thermal oil. After a comprehensive research, first commercial DSG plants have already been realized. Organic Rankine Cycles (ORC) that have been widely used for electricity production with low-temperature heat (e.g. geothermal energy) are also suited for the implementation in solar thermal power plants. To the knowledge of the author, no previous research has been dedicated to the investigation of direct steam generation of an organic compound. The aim of this work is the evaluation of ORC processes that are promising for this application. Firstly, a deep analysis for finding the most suitable fluids for DSG was conducted. Particular interest was set on high-temperature applications and supercritical processes in order to value the best configuration. After defining two possible process layouts with siloxanes (a saturated cycle with octamethylcyclotetrasiloxane D4 and a supercritical cycle with hexamethyldisiloxane MM), a possible integration with a thermal storage system was investigated, focusing on the state-of-the-art indirect two-tank system. The feasibility of the charging and discharging processes of the storage system together with the performances of the whole plant system was assessed for both chosen configurations.

Keywords: Concentrated solar power plant (CSP), Organic Rankine cycle (ORC), direct steam generation (DSG), siloxanes

Sommario

Negli ultimi anni sono stati sviluppati sistemi a generazione diretta di vapore (DSG) con acqua come alternativa agli impianti parabolici con olio diatermico. Dopo accurati studi, sono stati realizzati i primi impianti DSG commerciali. Cicli Rankine a fluido organico (ORC), che sono ampiamente utilizzati per la produzione di energia elettrica da fonti termiche a bassa temperatura (energia geotermica), sono stati implementati anche in impianti solari termodinamici. Nessuna attività di ricerca è stata dedicata fino ad ora allo studio di generazione diretta di vapore di un composto organico tramite lo sfruttamento dell'energia solare. L'obiettivo principale di questa tesi è stato valutare i processi ORC che possono rivelarsi favorevoli a questo tipo di applicazione. Innanzitutto, è stata condotta una profonda analisi per identificare i fluidi più adatti ad essere utilizzati in un impianto DSG. Particolare interesse è stato rivolto verso applicazioni ad alta temperatura e processi supercritici, al fine di stabilire la migliore configurazione. Dopo aver definito due possibili processi con i silossani (un ciclo saturo con ottametilciclotetrasilossano D4 e un ciclo supercritico con esametildisilossano MM), è stata valutata una possibile integrazione con un accumulo termico, focalizzandosi sul sistema di accumulo indiretto a doppio serbatoio. La fattibilità dei processi di carica e scarica dell'accumulo termico è stata valutata, insieme alle prestazioni dell'impianto, per entrambe le configurazioni scelte.

Parole chiave: Solare termodinamico a concentrazione (CSP), ciclo Rankine a fluido organico (ORC), generazione diretta di vapore (DSG), silossani

Introduction

Background

World primary energy need has increased very rapidly in the last half century and is expected to continue to grow over the next years, due to a growing world population and the expanding economies. Nowadays the world energy production is still largely based on fossil fuels such as oil, natural gas and coal. Since fossil fuels are limited, a heavy increase of their market price is expected for the next decades. In addition, the burning of fossil fuels contributes greatly to global warming, air pollution and ozone depletion. These are the reasons why worldwide research and development in the field of renewable energy resources and systems has been carried out during the last decades [1]. Energy conversion systems that are based on renewable energy technologies appeared to have a beneficial impact on the sustainable development of the world. Because of the desiderable environmental and safety aspects it is widely believed that, along with other renewables, solar energy has strong potential to be a key technology for mitigating climate change and reduce CO_2 emissions [2]. Solar energy is one of the most abundant resources in the world. Its availability is greater in warm and sunny countries – those countries that, in accordance with the International Energy Agency forecasts, will experience most of the world's population and economic growth over the next years [3]. Among solar energy conversion systems, concentrated solar power (CSP), based on parabolic trough collectors, is one of the most developed technology to produce electricity and has been used in large power plants since the 1980s. In comparison with photovoltaic (PV) technologies, CSP has the advantage to decouple the solar energy source from electricity production if combined with a storage system. Therefore, the improvement of existing technologies based on CSP is becoming ever more crucial [4]. New technologies are currently being developed to increase performances and reduce the cost of the next-generation trough plants. In recent years direct steam generation (DSG) in the absorber tubes is seen as a promising option to further the competitiveness of this technology and first commercial plants have already been realized. Besides large-scale parabolic trough plants, competing small-scale technologies are also emerging and show a promising future. Decentralised small plants might be particularly relevant for remote rural areas of developing countries, isolated islands, or weak grids with insecure supply. Even in countries with well developed energy systems, small-scale and modular CSP can help ensure greater energy security and sustainability. In order to achieve a high efficiency conversion, modular solar thermal power plants coupled with the Organic Rankine Cycle have been widely proposed and

studied. Few commercial plants have been recently built and others are under construction [5].

Objectives

This thesis aims on the analysis and evaluation of ORC processes that could be suited for direct steam generation in parabolic trough power plants. Focus is set on the development of new power cycles that combine the direct steam generation of an organic medium in a parabolic trough plant. In this context, state-of-the-art trough collector and thermal storage system are considered.
Chapter 1 deals with concentrated solar power plants. First, the general design consideration are given, followed by the describtion of the four basic technologies: parabolic trough, linear Fresnel, solar tower, and parabolic dish. Finally, state-of-the-art parabolic trough power plants are presented.
Chapter 2 gives a technical background on organic Rankine cycles, focusing on the organic compounds and their thermodynamic characteristics. The chapter concludes with a brief review of the most employed ORC applications. The working fluid plays the main role in the optimization of the ORC. Therefore, Chapter 3 deals with the choice of the best suited organic working fluid. After a literature review of possible working fluids, a deep analysis for finding the most suitable fluids for a DSG application is carried out. The analysis includes both low and high temperature fluids.
Chapter 4 discusses ORC process layouts and gives thermodynamic optimization criteria to choose the best configurations. In accordance with the research fields of the Line Focus Systems division of DLR, particular interest is set on high-temperature and supercritical processes. The chapter concludes with a thermodynamic assessment of different storage system integrations.
In Chapter 5, the method for designing and modeling a solar plant through the simulation software EBSILON®Professional is presented. Initially, some general feature of the software are briefly introduced. Then, the implemented model of the two chosen plant configurations is described.
Chapter 6 deals with the assessment of the thermodynamic performances of both systems. Design and off-design analysis are carried out. Particular interest is set on the integration between the solar field and the storage system.

1 Concentrated solar power plants (CSP)

Solar thermal power systems were among the very first applications of solar energy. In the last 40 years, several large-scale experimental power systems have been constructed and operated, which led to the commercialization of some types of systems. Plants with a nominal capacity up to 80 MW_{el} have been in operation for many years [2]. Concentrating solar power (CSP) plants use mirrors to concentrate solar radiation and generate high-temperature heat that is used to drive turbines and generators, just like in a conventional power plant. One of the main challenge in designing these systems is to select the correct operating temperature. This is because the efficiency of the heat engine rises as its operating temperature rises, whereas the efficiency of the solar collector decreases as its operating temperature rises. For such applications exclusively concentration collectors are suited, since non-concentration solar collectors do not reach the necessary temperatures for conventional steam turbines. Unfortunately, concentrating collectors only work with beam radiation, also known as direct normal irradiation (DNI), whereas non-concentrating collectors or photovoltaic cells can also make use of diffuse radiation. Beam radiation is the fraction of solar radiation that arrives directly from sun and reaches the Earth's surface as a parallel beam; in contrast, the fraction of solar radiation that is deviated by clouds, atmospheric molecules, humidity and dust is called diffuse radiation. CSP plants perform best in areas with clear-sky conditions characterized by high values of DNI, such as the Sahara desert, southern Spain, oriental USA and Australia (Figure 1.1)

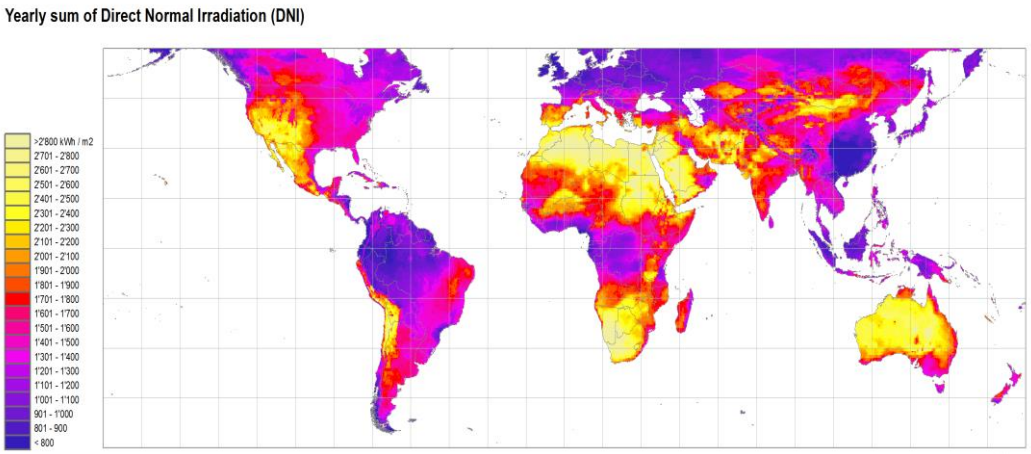

Figure 1.1: Global map of annual DNI [© METEOTEST; based on www.meteonorm.com]

For measuring DNI data there are various approaches. It can be measured with pyrheliometers from the ground, with satellite images or in a hybrid method where the advantages of the ground data (spatial accurateness) and the satellite data (availability of long time series) are combined. Today various institutions offer DNI data which differ in measurements and/or their analysis [6].

Solar energy, in contrast with fossil fuels, is not always available around the clock. Therefore, some CSP systems also integrate a thermal energy storage system (TES) or an auxiliary boiler, which allows them to operate during cloudy weather and nighttime.

1.1 State-of-the-art of concentrated solar power systems

Solar radiation is converted into thermal energy in the focus of solar thermal concentrating systems. There are four major different types of CSP technologies existing or under development: parabolic trough collectors (PTCs), linear Fresnel collectors (LFCs), solar towers and dish/Stirling engine systems.

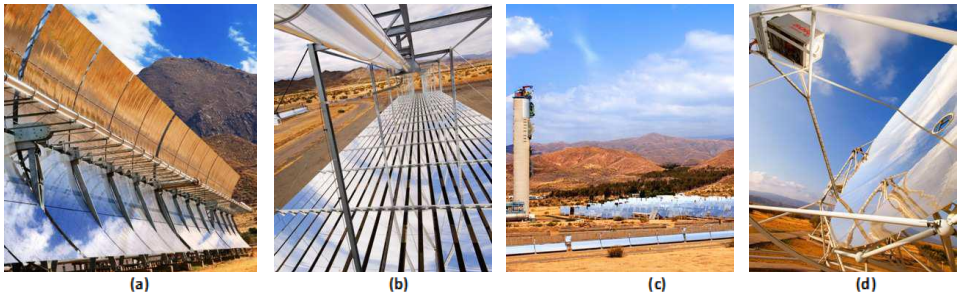

Figure 1.2: Main types of CSP: (a) Parabolic trough collectors; (b) Linear Fresnel collectors; (c) Solar Tower; (d) Solar dish (DLR)

These systems are classified by their focus geometry as either line-focus (PTCs and LFCs) or point-focus (solar towers and parabolic dishes). Usually, line-focus systems are built as single-axis tracking systems, as in the case of parabolic trough and linear Fresnel systems, which follow the sun along the solar altitude. Point focus systems are two-axis tracking systems in which concentrators follow the sun along both azimuth angle and altitude angle. The solar tracking is fundamental in concentrating concepts in order to follow the sun during its diurnal and seasonal motion and capture as much energy as possible. Concentration of direct solar radiation reduces the absorber surface area with respect to the collector aperture area and, thus, significantly reduces the overall thermal losses. The solar concentration ratio is defined as follows:

$$\boldsymbol{CR} = \frac{\boldsymbol{aperture\ surface\ area}}{\boldsymbol{absorber\ surface\ area}} = \frac{\boldsymbol{A_{ap}}}{\boldsymbol{A_{abs}}} \tag{1.1}$$

The radiation collected by the absorber is equal to the solar beam radiation multiplied by this solar concentration ratio.

Mainly due to the plants operating in California for more than two decades, parabolic trough systems are the most proven technology. Parabolic trough and linear Fresnel collectors, as well as power towers can be coupled to steam cycles with a net power output above 1 MW_{el}. Overall solar-to-electricity efficiencies, defined as the net power generation over incident beam radiation, are lower than

the conversion efficiencies of conventional steam cycles, because they include the conversion of solar radiative energy to heat within the collector and the conversion of the heat to electricity in the power block.

1.1.1 Parabolic trough

Parabolic trough collectors are the commercially most mature technology that generate heat at temperatures up to 400°C for solar thermal electricity generation. This is primarily due to the nine power plants operating in the Mojave Desert in California since the mid-1980s, known as solar electric generating systems (SEGS), with a total installed capacity of 354 MW_{el} [7]. These plants are based on large parabolic trough collectors concentrating sunlight onto a receiver pipe and providing steam to a Rankine power plant indirectly through a heat transfer fluid. The steam from the turbine is piped to a standard condenser and returns to the heat exchangers with pumps so as to be transformed again into steam. In the case of the Direct Steam Generation (DSG) in the solar field, the two-circuit system turns into a single-circuit system, where the solar field is directly coupled to the power block. The type of condenser depends on whether a large source of water is available near the power station. Since most of the plants are installed in desert areas, cooling is usually provided with a mechanical draft wet cooling tower or with air coolers. The major components of the systems are the collectors, the fluid transfer pumps, the power generation system, the natural gas auxiliary subsystem and the controls. During periods with low irradiation or during the night the systems can be operated with fossil fuel. Hybridising with fossil fuels can be done in several ways, either by using an auxiliary system for heating the HTF, or by introducing the fossil back-up system directly into the steam cycle, in the evaporation, superheat or reheat zones.

Figure 1.3: SEGS solar power plants III-VII at Mojave Desert, California

The solar field consists of many large single-axis tracking PTC, installed in parallel rows aligned on a north-south horizontal axis and track the sun from

east to west during the day. The typical PTC receiver, also called Heat Collector Element (HCE), is composed of an inner steel pipe, the absorber, surrounded by a glass tube, which limits convective heat losses with the environment. The absorber is covered with a selective high-absorptivity (greater than 90%), low-emissivity (less than 30% in the infrared) surface coating that reduces radiative thermal losses. With receiver tubes with glass vacuum tubes and glass pipes with an antireflective coating a higher thermal efficiency and better annual performance can be achieved, especially at higher operating temperatures. Receiver tubes with no vacuum are suited for working temperatures below 250°C, because thermal losses are not so critical at these temperatures. Typical state-of-the-art PTCs have aperture widths of about 6 m, total length is usually within 25 – 150 m and geometrical concentrating ratios between 60 – 85. The most well-known commercial PTC designs conceived for large solar thermal power plants are the LS-3 (manufactured by Luz) and the EuroTrough. The EuroTrough collector has been developed in order to reduced cost and it is an improvement of the LS-3. The main difference between these two collector designs is their steel structure.

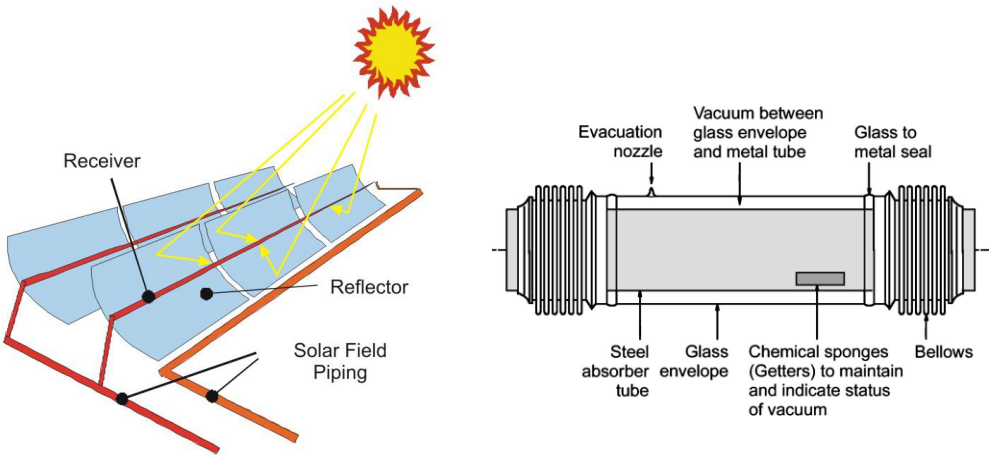

Figure 1.4: Schematic diagram of parabolic trough collectors and a detailed HCE (Flabeg Solar International)

As discussed before, parabolic trough collectors are characterized by both thermal and optical losses. Optical efficiency (η_{opt}) is the ratio between the quantity of solar radiation which reaches the absorber and the available solar radiation. Geometric and optical phenomena have a diminishing impact on the optical efficiency, such as shadowing, reflection of the mirrors, absorption of the absorber tube, as well as the transmittance of the protective glass envelope. The thermal efficiency (η_{th}) is defined as the ratio between radiation attaining the absorber and thermal energy effectively transferred to the HTF. The overall performance of parabolic trough collectors depends mainly on average

temperature of the HTF and on average irradiative solar intensity. Although the most famous examples of CSP plants are the SEGS plants in the United States and the Andasol 1, 2 and 3 in Spain, a number of projects are currently under development or construction worldwide. Due to the limited temperature of the HTF, commonly thermal oil, and also of its high cost, next generation of CSP aims at using molten salt or direct steam generation [8].

1.1.2 Linear Fresnel collectors

Linear Fresnel collectors (LFC) are the second type of commercially available line-focusing systems. The receiver is fixed above the primary mirrors and only these ones are tracked to the sun, whereas, in parabolic trough systems, the receiver rotates together with the mirrors. The primary mirror facets of the LFC are only slightly curved. The DNI is concentrated by the primary mirrors onto the receiver tube or indirectly by the secondary concentrator, which is mounted above the receiver. Since the aperture area consists of single ground-mounted mirror facets, wind load is reduced and a less rigid, and thus, less expensive collector structure can be used. As a consequence, the specific investment cost of a LFC is lower than the one of a PTC whereas on the other hand the optical performance of a linear Fresnel collector is lower: about 67% versus 75% of the PTC [9]. The final design of the LFC is thus a trade-off between high optical performance and low specific investment costs. At present, LFC technology is not mature as PTC, since only some pilot plants exist in Spain, Australia and the US. Regarding the process parameters (working temperature) and plant capacity, the same values as for the PTC apply. Different from state-of-the-art PTC plants, in LFC systems usually water is used as heat-transfer fluid in direct steam generation mode (DSG) [10].

Figure 1.5: Linear Fresnel reflector with one absorber (DLR/Novatec Solar)

1.1.3 Solar towers

Solar towers or central receiver systems use a field of distributed sun-tracking mirrors, called heliostats, to focus solar energy onto a receiver located atop a tall tower. The receiver achieves temperatures from 500 to over 1000°C and collects the sun's heat in a HTF (water-steam, liquid sodium or molten salt) that flows through the receiver and with this thermal energy a conventional power cycle is driven. Due to the increased process temperature, not only the Rankine cycle is applicable but also the Brayton cycle. As in line-focus systems, depending on the HTF various kind of storage systems can be integrated. It is clear that also in this case steam can be generated either directly and indirectly. Hence, newer systems favor the DSG approach [11].

Figure 1.6: Solar tower PS10 in Spain [12]

The collectors represent the largest cost in the system. In fact, heliostats consist of slightly curved mirrors mounted on a two-axes tracking system. Their concentration ratios are generally of 500 – 1000, much higher than that of line focusing systems (PTCs and LFCs). These increased higher concentration ratios allow higher operation temperatures, and thus, potentially higher conversion efficiencies of the power cycles. So far, only pilot plants (Solar One and Two in USA; prototype in Almería) or first commercial plants with capacities of up to 20 MW_{el} have been realized, as for example the PS10, PS20 and Gemasolar (also called Solar Tres) in Andalusia, Spain. All kinds of HTF have been used: mineral oil (Solar One), steam/DSG (PS10 and PS20) and molten salt (Gemasolar, Solar Two). Thus, this technology is less proven than the PTC option, but has the potential of increased efficiencies and reduced costs in the future.

1.1.4 Parabolic dish

Parabolic dish systems are point-focus collectors that track the sun on two axes like solar towers. They use a large parabolic silvered mirror as reflector to concentrate the sun's radiation onto a receiver, which is mounted above the dish at the focal point of the reflector. The receiver absorbs the reflected radiation and converts it into thermal energy. This heat can either be used directly in order to support chemical processes, but its most common application is power generation. The thermal energy is converted directly to electricity with a Stirling engine, connected to the receiver. In that manner, in contrast to parabolic trough systems, dish systems can generate electricity independently without piping losses or auxiliary consumption. Since parabolic dish collectors always point to the sun, their optical losses are lower than these of parabolic trough, Fresnel or tower systems. Dish units generally operate at concentration ratios of 600 up to 3000 which results in potentially highly efficient power conversion. In parabolic dish collectors temperatures of more than 1500°C can be reached [13]. Their principal advantages are a high solar-to-electricity conversion efficiency (over 30%) [14], modularity and flexibility. Due to wind loads, the size of the parabolic mirror is limited and the typical capacity of a single system is approximately 10 – 25 kW_{el}. Therefore, dish systems are particularly well suited for decentralized power supply and remote stand-alone power systems, such as water pumping or village power applications [15].

Figure 1.7: Parabolic dish (DLR)

1.2 Overview of existing parabolic trough power plants

There are two ways to integrate a PTC solar field in a Rankine steam cycle power plant:

1. indirectly, by heating a heat transfer fluid (HTF), typically a synthetic oil, in the solar field and using it to produce steam through a heat exchangers train;
2. directly, that is, generating steam in the solar field (DSG).

In both cases, with the thermal energy produced by the solar field a conventional steam cycle can be driven, such as Rankine with Superheat (SH), Rankine with Reheat (RH) and Rankine with Regeneration (RRg). Another option is an Organic Rankine Cycle (ORC), where water is replaced by an organic fluid that evaporates at a much lower temperature. If the radiation is sufficient, the system can work at operating full capacity only with the solar field. In order to ensure the production of electricity during periods of low radiation or during the night, the plants usually are equipped with an additional back-up boiler and some of them even with a TES.

Although the first PTC used DSG technology, and research in this area started in the 80s, at the same time as the commercial use of the HTF technology, during the last three decades commercial projects have not decided for it, due to the potential problems and uncertainties associated with the two-phase water/steam flow in the absorber tubes [8].

1.2.1 Parabolic trough plants with thermal oil

The SEGS plants were the first commercial power plants with thermal oil as heat transfer fluid. Being built from 1985 to 1991 in the Mojave Desert in California these plants are still in operation. The technology has proven to be commercially ready and new power plants, like the Andasol 1, 2 and 3 in Spain, are still based on the same system.

Figure 1.8 shows that the power plant can be subdivided into four locally separated units: the collector field, the storage system, the back-up-system, and the power block (PB). These systems consist fundamentally of two separate fluid circuits: a HTF circuit and a water steam circuit. The HTF is heated up from 290°C to 393°C inside the receiver tube of the solar field in order to return to a series of heat exchangers in the PB, where it is used to generate high-pressure superheated steam (100 bar, 371°C) for the power block. The PB is a conventional thermal power station made up of several components like those

used in fossil fuel power stations. The thermal energy of the steam is converted into mechanical energy by a steam turbine and finally to electric energy by a generator.

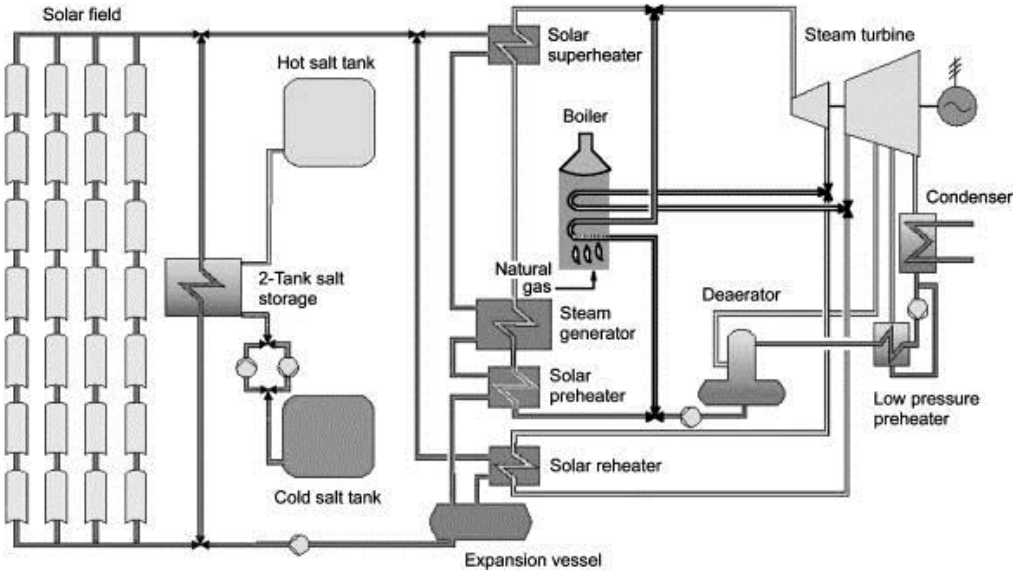

Figure 1.8: Schematic configuration of a parabolic trough power plant with oil as HTF (Flabeg Solar International)

In state-of-the-art parabolic trough plants, synthetic oil is used as HTF. The reason is that the vapor pressure of the thermal oil is much lower than that of water. Therefore, even at temperatures that are above the critical point of water (374°C), processes with thermal oil can remain in the liquid phase.

The thermal oil most widely used for temperatures up to 395°C is Therminol VP-1, which is an eutectic mixture of 73.5% biphenyl oxide and 26.5% diphenyl. Although it is flammable, safety and environmental protection requirements can be satisfied. The main limitations are its chemical stability that limits the maximum temperature of the steam Rankine cycle and the costs of the oil-related equipment [16]

The selection of the HTF affects also the type of TES that can be used in the power plant. Nowadays, the most commonly used storage concept in parabolic trough systems with thermal oil is the indirect two-tank storage system with molten salt (Andasol power plants, Spain). An indirect two-tank storage system, as the name said, uses two reservoirs, a hot and a cold tank to store thermal energy. In comparison with oil, molten salt presents some advantages as it is non-flammable, non-toxic and has a lower cost.

1.2.2 Parabolic trough plants with molten salt

An innovative possibility is using molten salt as HTF in the solar field, instead of thermal oil, in order to allow using the same fluid in both the SF and the TES [17]. If molten salt is used in this way, the TES concept will become direct. Figure 1.9 shows a schematic configuration of a solar power plant with PTCs and molten salt as HTF.

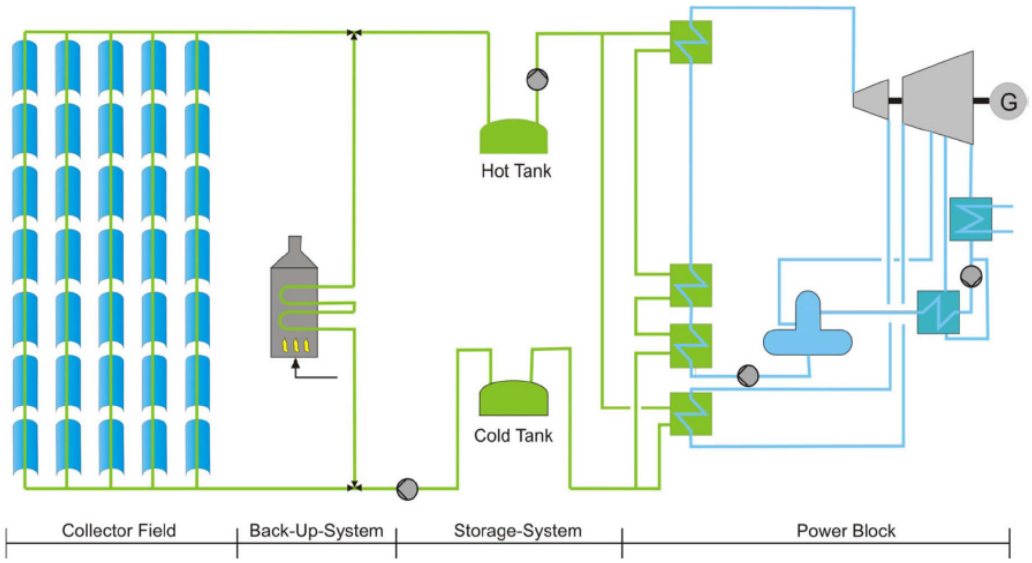

Figure 1.9: Schematic configuration of a parabolic trough power plant with molten salt as HTF (DLR)

If enough solar radiation is available, the molten salt from the cold tank is pumped through the solar field, heated up to the design temperature and finally stored in the hot tank. An auxiliary heater connected parallel to the collector field, can also heat the molten salt to the design temperature. As long as there is hot salt available in the hot tank, electricity can be produced on demand. As in case of thermal oil, the molten salt circulates through a heat exchanger in order to produce steam in the power block, and returns to the cold tank.

This technology offers a significant reduction in the cost of TES, eliminating the need of heat exchangers, and allows reaching a higher maximum temperature in the cycle compared to the one with synthetic oil. On the other side the disadvantage is that molten salt freezes at relatively high temperatures (220°C in the case of Solar Salt [18]) and much more care must be taken to make sure that the salt HTF does not freeze in the solar field.

A demonstration plant using this kind of technology was developed in Italy near Syracuse in 2004 by a joint venture between ENEA and ENEL, along with other smaller private companies, through a project called Archimede [19].

1.2.3 Parabolic trough plants with DSG

DSG refers to the direct generation of steam in the solar field, which makes the steam generator unnecessary. The solar field is divided into different sections performing the various stages of heat exchange: preheating, evaporation and superheating. Figure 1.10 shows the overall scheme of a parabolic trough power plant with DSG in the solar field.

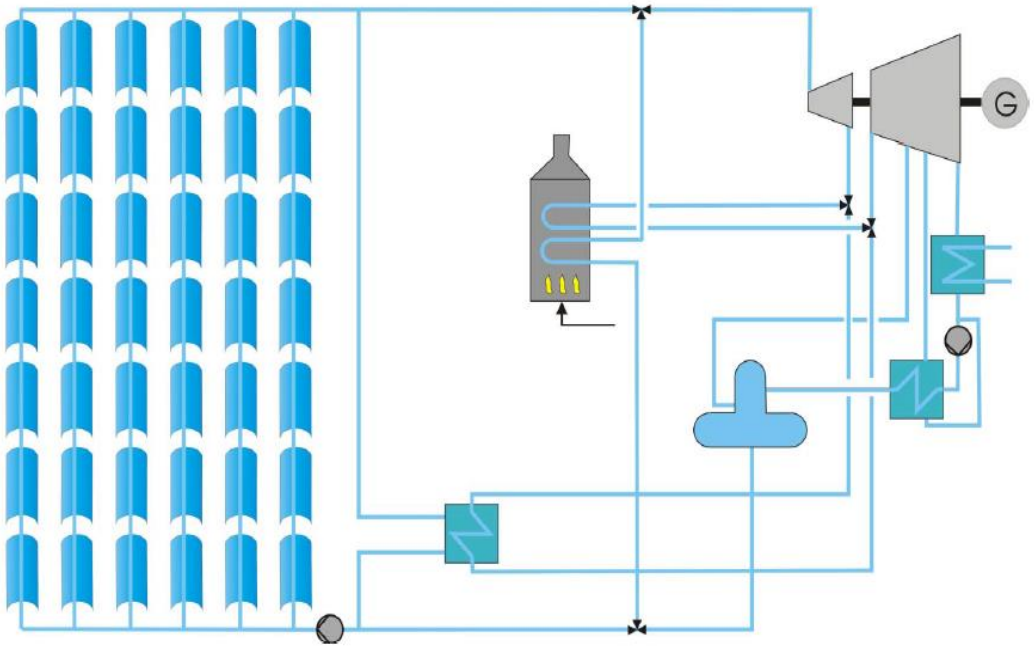

Figure 1.10: Schematic configuration of a parabolic trough plant with DSG (DLR)

Only in the recent years parabolic trough systems with DSG have been successfully tested under real solar conditions at the Plataforma Solar de Almería for example during the DISS (Direct Solar Steam) [20, 21] and INDITEP [22] projects. DSG has technical advantages over HTF technology [23]. With this configuration the steam temperature is not limited by thermal oil, but can reach values from 400°C to 550°C, increasing the thermal efficiency of the Rankine cycle. Although DSG increases the cost of the solar field piping by increasing the solar field fluid working pressure to above 100 bar, DSG leads to a simplified plant configuration that reduces the investment and O&M costs. Due to the constant temperature during phase transition, the thermal efficiency

of the collector is higher. Furthermore, compared to systems with thermal oil, in DSG systems the overall plant efficiency increases while environmental and operational risks, as fire hazard in case of leaks, are reduced.

The disadvantages of this technology concern the use of water/steam as a two-phase flow. In fact, the required control systems are more complex and expensive, due to the two-phase flow inside the absorber tubes and the different thermodynamic properties of water and steam.
The water flow must always be faster than a minimum required to avoid stratified flow in the evaporation zone, as shown in Figure 1.11. In fact, stratified flow lead to thermal stresses in the absorber tubes as the mirror facing side of the tube is cooled by water whereby the top part is only cooled by steam [24].

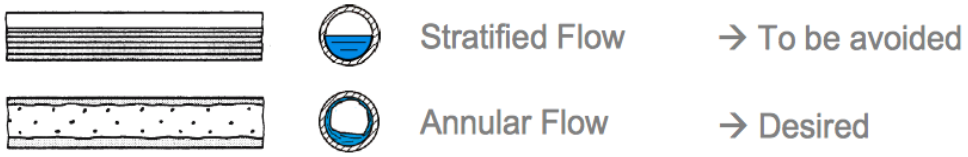

Figure 1.11: Representation of the stratified and anular flow in the evaporation zone [25]

From a technical point of view, three basic DSG collector field processes are possible [21]:

Once Trough System: In this system water is pre-heated, evaporated and superheated in a single collector loop. This system is the simplest and potentially the cheapest but the control of the outlet temperature in the receiver tube is complex due to the moving endpoint of the preheating, evaporation and superheating sections in the loop.

Injection System: In this system water is injected in several points of the receiver tube. This system presents the problem of a complex measurement and control operation.

Recirculation System: In this system the collector loop is divided in two sections. In the first section the water is preheated and evaporated, while in the second the water is superheated. In between the two sections there is a water-steam separator, where the water content in the mixture is separated and sent back to the solar collector inlet.

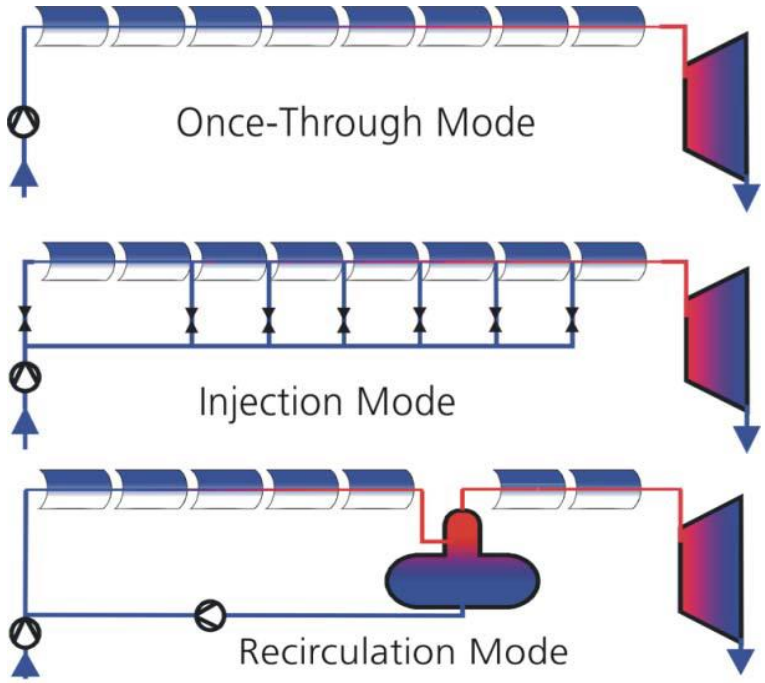

Figure 1.12: Three basic DSG processes (DISS)

The projects DISS and INDITEP have shown that the recirculation concept is the most feasible option for commercial application. Test results showed good stability of the recirculation process even with a low recirculation ratio, thus, making possible the use of small inexpensive water/steam separators in the solar field [26]. In order to further bring down the costs of a DSG solar field, the once-through concept is currently under development and demonstration through the research project DUKE [27].

The two-phase fluid poses a major challenge and current state-of-the-art TES are not suitable for DSG plants as they are not cost-competitive for large storage capacities. Therefore, different projects and development activities were performed in order to find innovative storage concepts. In the DISTOR project performed by DLR, a storage system, subdivided in three parts, was proposed. A phase change material (PCM) storage system was used to store latent heat of the evaporation phase and a concrete storage system for the sensible heat during the pre-heat and the super-heating phase [28, 29]. Another attractive option for facilitating the operation of DSG plants in case of saturated cycles is represented by short time direct storage systems called steam accumulators [30]. A system analysis, including integrated TES, pointed out the large influence of TES on the project investment cost of a DSG plant. A big effort in the development of a commercial storage system for DSG is still needed to make this kind of plant competitive in the market [31].

1.2.4 Parabolic trough plants with ORC

In the recent years several ORC companies investigated the integration of an organic Rankine cycle, typically used in geothermal and biomass applications, with parabolic trough solar systems (Figure 1.13). Systems under consideration range in size from 100 kW_{el} to 10 MW_{el}.
Design studies indicate that optimized ORC systems, in those cases, could be more efficient than more complex steam cycles operating at the same solar field outlet temperature [7]. The general concept is to create a Micro CSP system that, like a traditional trough plant, consists of a solar field circuit and an ORC power block connected via a heat exchangers train. The main difference is that the whole system with the ORC is smaller, modular and highly packaged. An ORC optimized for a 300°C operating temperature should allow a significant increase in the efficiency of small-size parabolic trough plants. In addition, at these temperatures, thermal storage is economically feasible.

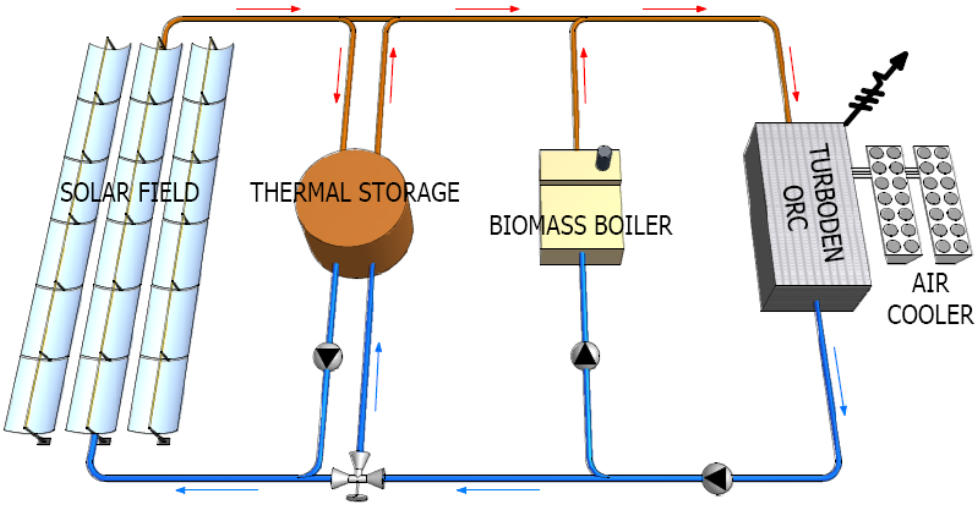

Figure 1.13: Schematic configuration of a parabolic trough power plant with ORC [5]

NREL analyzed a 1-MW ORC trough plant configuration in Saguaro, Arizona. The Saguaro solar power plant, completed in 2006, is the first to combine solar trough technology with an ORC power block provided by Ormat. N-pentane is the selected working fluid, allowing for a cycle efficiency higher than 20%, with an overall solar-to-electricity efficiency at the design point of 12.1% [32, 33].
The second micro-scaled CSP plant is the Holaniku at Keahole Point, developed by Sopogy in the Kona desert, Hawaii. The plant produces 2 MW of thermal energy that can be used to generate up to 500 kW of electricity through an ORC power block. In addition, the site includes up to two hours of thermal energy storage based on the indirect-two-tank storage system [34].

.

2 Organic Rankine Cycle Background

During the last two decades a great interest has risen in Organic Rankine Cycles, mainly because of the possibility to exploit heat sources at low and medium temperature. Water is the working fluid of choice for the vast majority of large scale fossil-fired Rankine cycle powerplants. Steam Rankine cycles are well-suited for high-temperature applications, but generally at low temperatures the efficiency decreases significantly. ORC is a promising technology for decentralized power applications typically of the order of less than a few MW. There is a variety of ORC fluids with different thermodynamic characteristics available suited for different working temperature ranges. Therefore, one of the advantages of ORC processes is that the working fluid can be selected according to the temperature range of the heat source and heat sink. For example, ORC systems can be used in biomass-fired combined heat and power systems, solar thermal systems, geothermal systems and industrial waste heat recovery. The modularity and versatility of this technology allows also for the integration of ORC into small-scale combined cycle power plants as a bottoming cycle.

The chapter is organized as follows. In Section 2.1 a typical ORC configuration is introduced and discussed. Section 2.2 presents the main characteristics of pure organic fluids together with a briefly discussion regarding the possibility of using mixtures. In Section 2.3 the main differences between steam Rankine cycles and ORCs are highlighted, in particular focusing on thermodynamic properties and turbine design considerations. Finally, Section 2.4 shortly reviewed the state-of-the-art ORC applications and some of the most innovative concepts being studied recently.

2.1 Typical configuration

The basic principles of the Organic Rankine Cycle (ORC) are similar to those of the steam Rankine cycle, but the main difference is that an organic working fluid with a lower boiling point and a higher vapor pressure is used instead of water. As shown in Figure 2.1, in the ideal cycle four processes can be identified:

1. **Isentropic pump (1 – 2)**
2. **Isobaric evaporation (2 – 5):** The boiler can be divided into three zones: preheating (2 – 3), evaporation (3 – 4) and superheating (4 – 5).
3. **Isentropic expansion (5 – 6)**
4. **Isobaric condensation (6 – 1):** The heat exchanger can be subdivided into the desuperheating (6 – 7) and the condensation (7 – 1) zones.

In the real cycle, the presence of irreversibilities lowers the cycle efficiency. These irreversibilities mainly occur during the expansion, in the heat exchangers and in the pump [35].

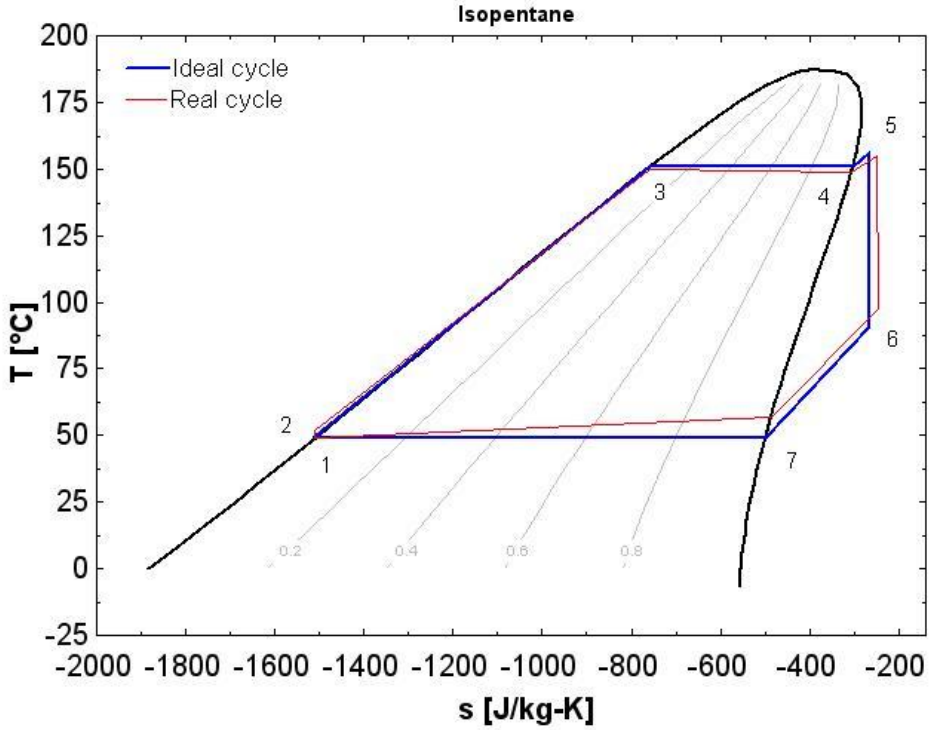

Figure 2.1: T-s diagram for the ideal/real ORC cycle using isopentane as working fluid

ORC presents a layout simpler than that of the conventional steam Rankine cycle: there is an evaporator or single heat exchanger to perform the three evaporation phases (preheating, evaporation and superheating), an expansion turbine, a condenser and a pump. In such systems, a regenerator is normally installed between the pump outlet and the turbine outlet to improve the performance of the system. The regenerator recovers the heat from the turbine exhaust to preheat the liquid in order to reduce the amount of heat released and the one needed to vaporize the fluid in the evaporator. Figure 2.2 shows a typical configuration of an ORC with (right) and without (left) regenerator.

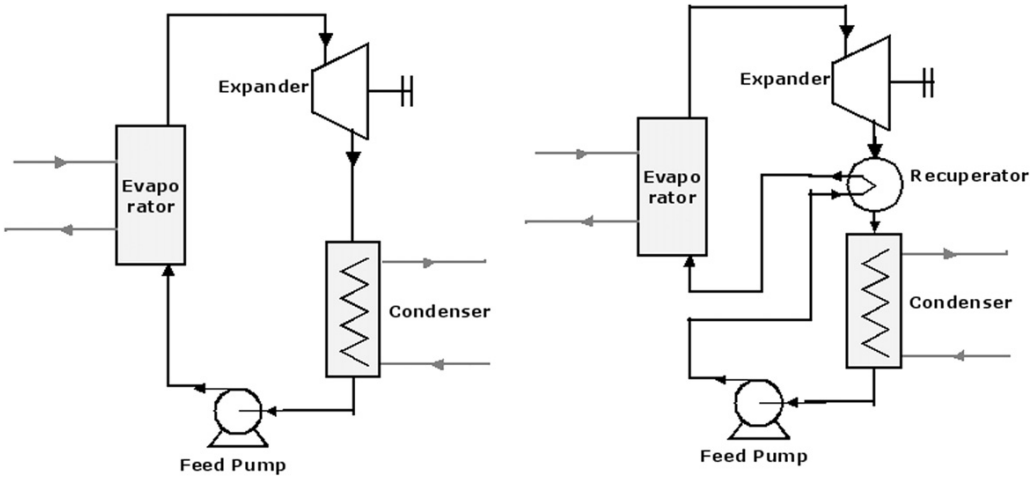

Figure 2.2: Component diagrams of a basic ORC (left) and a regenerative ORC (right) [36]

Compared to conventional water steam cycles, ORC systems are less complex and need less maintenance, which is partly explained by their modular feature: a similar ORC system can be used, with little modifications, in conjunction with various heat sources and applications, as presented further [36].

2.2 Organic working fluids

The major difference between an ORC cycle and a conventional steam Rankine cycle is the working fluid. An organic compound refers to all those chemical compounds containing carbon with the exception of carbon oxides and derived salts. Organic compounds consist of a structure of carbon and hydrogen atoms, possibly combined with atoms of other chemical elements, such as nitrogen, sulfur, phosphorus, silicon, fluorine and chlorine. Both pure fluids and fluid mixtures proposed for ORC are classified as hydrocarbons and fluorocarbons, refrigerants, aromatic compounds, paraffins, siloxanes, and inorganic fluids. The thermodynamic performance of the cycle depends greatly on the type of fluid chosen to take advantage of the available heat source. As we will see in Chapter 3, the selection of the organic fluid plays the real key role.

2.2.1 Characteristics of the organic working fluids

In order to be able to exploit heat sources at variable and medium-low temperatures, it is necessary to make use of working fluids which certain properties, such as the low boiling point and with curves that adapt well to variations in the temperature of the sources themselves. In these cases, water loses much of its utility and the fluids thermodynamically more interesting are usually those organic compounds characterized by a high molecular mass, very complex molecules and sufficient thermal stability. The organic substance employed is usually characterized by a low boiling point, a low latent heat of evaporation and high density; such properties are preferable to increase the input flow to the turbine. Table 2.1 lists some organic fluids and their relevant thermodynamic properties: water is included for comparison. Organic fluids show a relatively lower heat of evaporation than that of water as a result of their higher molecular mass. This is the main reason for which organic fluids are used instead of water for heat recovery of low-medium temperature sources. In these cases, ORCs allow to achieve better efficiencies and higher power compared to conventional working fluids.

Table 2.1: Thermal properties of water and some organic working fluids

Working fluid	Molecular weight (kg/kmol)	Boiling Point (K)	Liquid density (kg/m^3)	Latent heat (kJ/kg)	Specific heat ratio
water	18	373.15	958.35	2257.00	1.33
R-123	152.93	300.97	1456.7	170.19	1.10
isopentane	72.15	300.98	612.08	343.28	1.09
n-butane	58.12	272.66	601.26	385.71	1.12

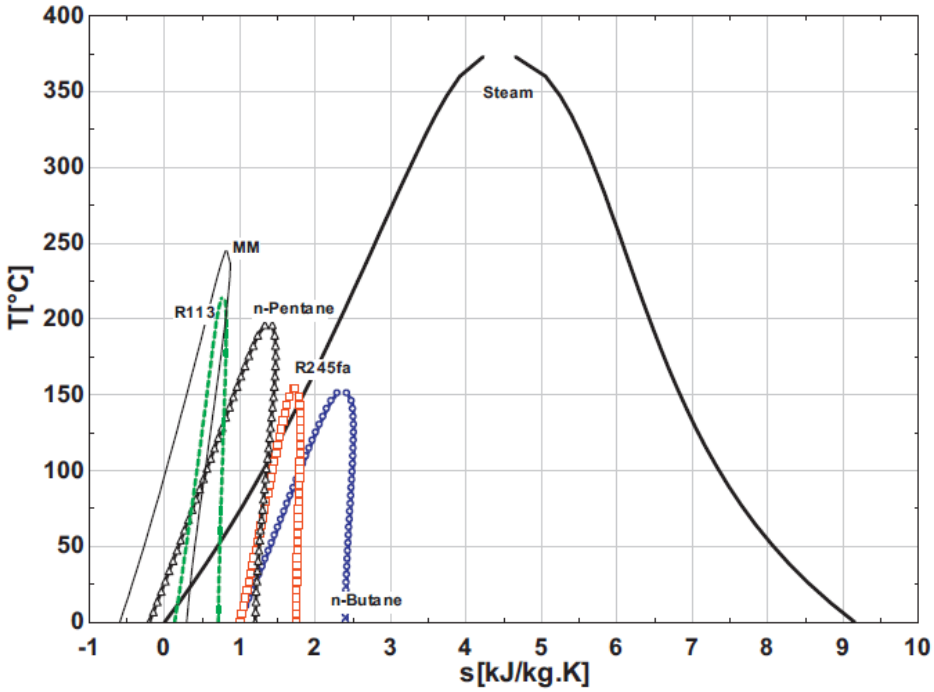

Figure 2.3: T-s diagram of water and various ORC fluids [37]

2.2.2 Classification of fluids based on the T-s diagram

Organic fluids, depending on the slope of the saturation vapor curve on a temperature-entropy diagram (dT/ds), can be classified into three groups:

1. *Dry fluids*, characterized by a positive slope and a large molecular weight; in this case the saturation curve in the T-s diagram is called retrograde.

2. *Wet fluids*, characterized by a negative slope and a low molecular weight.

3. *Isentropic fluids*, characterized by an infinite slope; in this case the saturation curve is almost vertical.

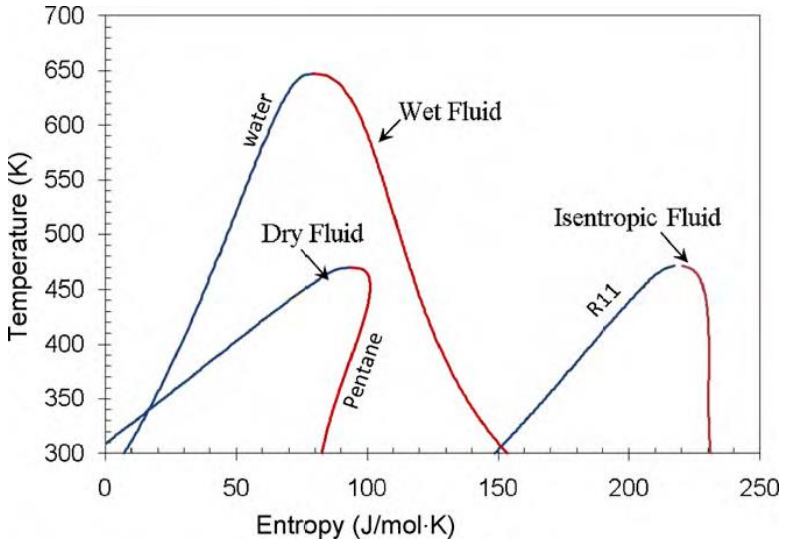

Figure 2.4: Saturation curves of a dry, wet and isentropic fluid [38]

Since the value of dT/ds leads to infinity for isentropic fluids, the inverse of the slope of the curve, defined as $\xi \approx dS/dT$, is used as a parameter to express the type of the fluid ($\xi > 0$: dry fluid, $\xi < 0$: wet fluid, $\xi \approx 0$: isentropic fluid) [38]. The type of saturation curve is closely related to the number of atoms of the molecule. The retrograde bells are typical for high molecular weight fluids, with a high number of atoms greater than 12, while the classic bells similar to that of water are typical of fluids with less than 8 atoms and smaller molecular weight [39].

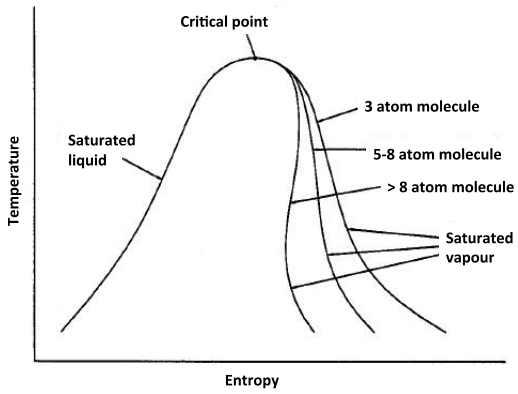

Figure 2.5: Effect of molecule size on the slope

Wet fluids are generally not suitable for ORC systems, because they require large enthalpy to become saturated and need to be superheated in order to avoid condensation during the expansion process and reduce the risk of blade erosion. Dry and isentropic fluids have better thermodynamic efficiencies, because they

do not require superheating. If the slope of the saturation curve is too positive, the fluid may exit the turbine at high temperatures; in this case, a regenerator is introduced in order to take advantage of the thermal energy of the fluid. A first selection of the fluid is carried out according to the slope of the saturation curve and organic fluids considered are usually either dry or isentropic.

2.2.3 Mixtures

Most of ORC applications are focused on pure component working fluids. However in some scientific work the utilization of organic fluid mixtures as working media for Rankine power cycles [40, 41] are mentioned as interesting. The main advantage in comparison to pure substances is represented by a non-isothermal phase change that leads to a better matching of working fluid and source/sink heat capacities. Figure 2.6 shows qualitatively the nature of the phase change for a two-component mixture in the T-s and T-x diagrams.

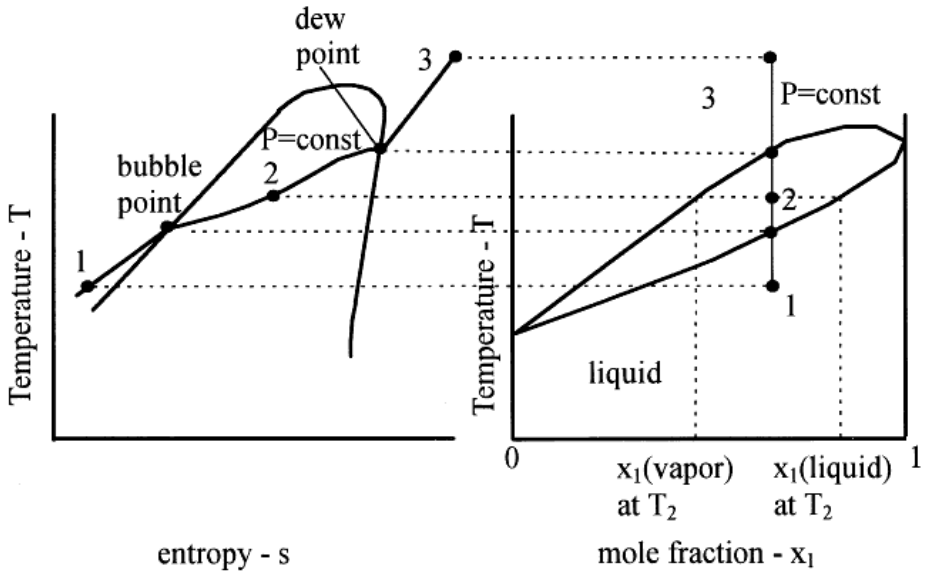

Figure 2.6: Qualitative representation of an isobaric phase change for a two-components mixture in the T-s and T-x (x = mole fraction) diagrams [40]

The compositions of liquid and vapour vary continuously along the isobar, and the compositions in the two phases are not the same. Another difference between mixtures and pure fluids occurs in the critical region. In this case, the critical point is not anymore characterised by the maximum value of temperature and pressure at which vapour and liquid coexists.

2.3 Comparison with the steam Rankine cycle

2.3.1 Thermodynamic and physical differences

Water and organic fluids are characterized by different properties, as summarized in Table 2.2. Water is inexpensive, non-toxic, non-flammable, chemically stable, has low environmental impact and low viscosity (and thus, lower friction losses and higher heat exchange coefficients). On the other hand, organic fluids may be relatively toxic and more expensive than water. With its low boiling point, a properly selected organic fluid can recover heat at much lower temperatures when compared to steam Rankine cycles.

Table 2.2: Summary of fluids properties comparison in steam and organic Rankine cycles

	Steam Cycle	**Organic Rankine Cycle**
Fluid	Water	Organic compound
Critical pressure	High	Low
Critical temperature	High	Low
Boiling point	High	Low
Condensing pressure	Low	Acceptable
Specific heat	High	Low
Viscosity	Low	Relatively high
Flammability	No	Yes, and depends on fluid
Toxicity	No	Yes, and depends on fluid
Environmental impact	No	High and depends on fluid
Availability	Available	Supply problem
Cost	Cheap	Expensive

As mentioned before, many of the thermodynamic characteristics and technological properties of an ORC are closely related to the position and shape of the saturation curve in the T-s diagram. Water is classified as a wet fluid, while the ideal fluids for ORCs are generally either dry or isentropic.

The first main difference between organic fluids and water in a Rankine cycle is their behavior when expanding from a saturated state through a turbine at low to moderate temperatures (200 - 400°C), as shown qualitatively in Figure 2.7.
In conventional Rankine cycles the isentropic expansion phase of water in the turbine occurs with a relatively low-quality two phase mixture (< 80%), while in ORCs it can take place without condensation phenomena, giving a very high performance and avoiding equipment damage. Hence, steam Rankine cycles require higher turbine inlet temperatures than ORC, leading to a more complex design characterized by superheating and reheating. This requires the use of

expensive high temperature materials for the turbine blades and the boiler.

In ORC systems, the turbine inlet temperatures are limited by the thermal stability of the fluid. Dry and isentropic organic fluids exit the turbine at a higher temperature than the condensing temperature. The available energy in this superheated turbine exhaust also gives the opportunity for energy recovery through a regenerator not present in a steam Rankine cycle, as discussed in Section 2.1.

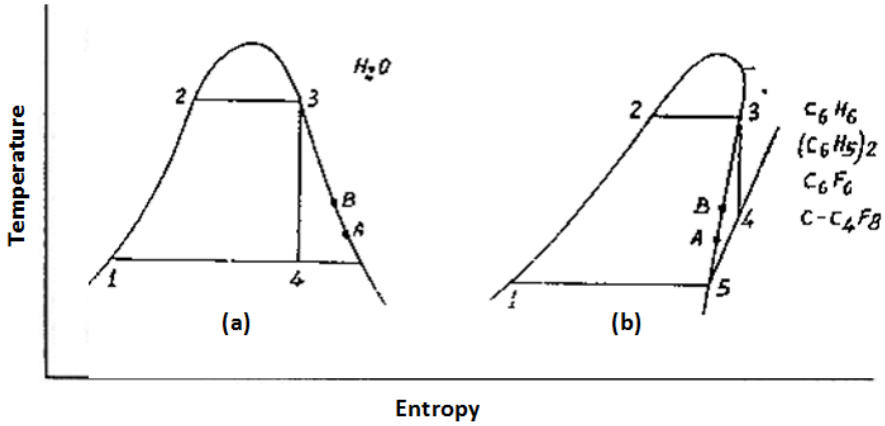

Figure 2.7: Rankine cycle for water (a) and for dry organic fluids (b)

In order to achieve high efficiencies, the condensing pressures of a steam Rankine cycle are extremely low, typically between 0.05 and 0.1 bar. The inevitable result of these sub-atmospheric condensing pressures is the infiltration of air in the circuit, and hence the need of a deaeration equipment. In contrast to that, the use of organic fluids allows operating at condensing pressures usually higher than the atmospheric pressure, while the saturation pressures, with equal levels of thermal source, are much higher. Super-atmospheric condensation enables the design of low or no-maintenance power cycles. This attribute is highly-desirable in remote and low-output applications where a full-time licensed maintenance staff is not a reasonable expectation. In contrast, the main disadvantage of ORC systems is the lower heat transfer coefficients of heat exchangers compared to the ones of water. This involves a reduction of the global coefficient of heat exchange surfaces and consequently more requests and therefore higher costs at the same thermal load of the heat exchanger.

Finally, an advantage of ORCs has also to be underlined in regard of thermodynamic cycle configurations. The limited critical pressure of organic fluids in comparison of that of water, makes supercritical cycles at low temperatures practically feasible [42].

2.3.2 Power and temperature range

Water is the best working fluid for all those energy sources with a maximum temperature of at least 300°C and power input higher than about 2 MW_{th} [43]. On the other side, organic fluids become a forced choice in the low/medium power range (from a few kW_{el} to several MW_{el}) and/or low maximum temperature (between 70 and 400°C), where using water encounters a number of techno-economic limits which mainly affect turbine design. Hence, the advantages of ORCs compared to traditional steam cycles become obvious when appropriate working fluids and operating conditions are selected:

1. In case of small-size plants, because using water would lead to really small volume flow rate at turbine inlet with an almost infeasible design of the first stage blades, which would result in poor efficiency;
2. At low maximum temperatures, a two-phase flow expansion necessarily results, leading to reduced efficiencies and turbine blade erosion.

Figure 2.8 presents the fields of application of ORC and steam cycle. It is clear that ORC allows for decentralized and small scale power generation.

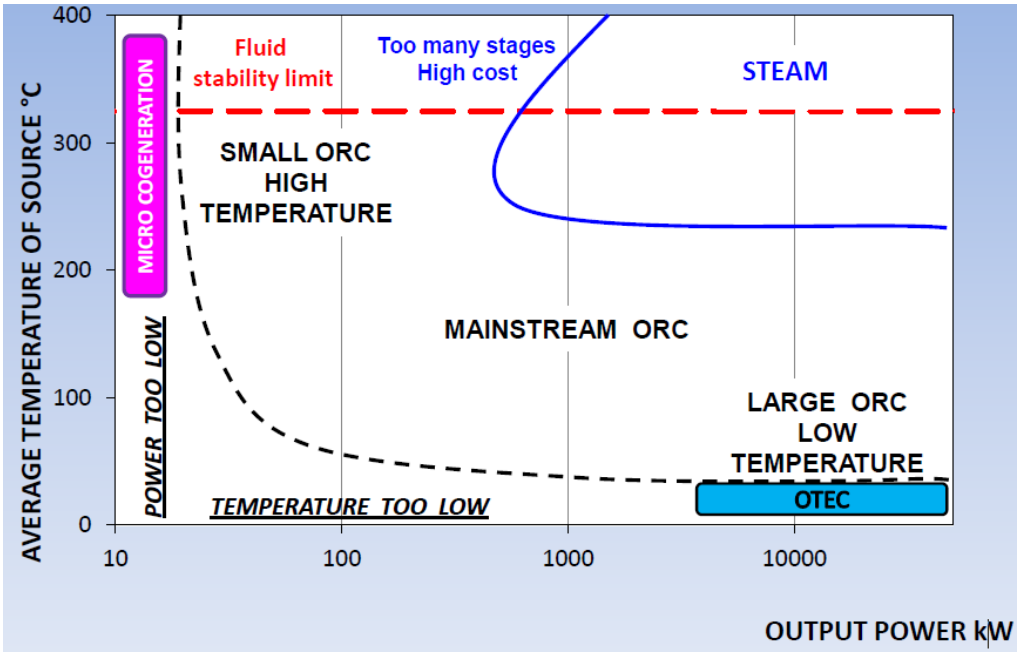

Figure 2.8: Field of applications in a temperature versus power diagram [44]

2.3.3 Turbine design

The working fluid nature plays a fundamental role in setting the practical feasibility of the turbine. The turbine's function is to expand steam to low pressure conditions, in order to produce mechanical power on the shaft that is converted into electrical power by a generator. In case of steam cycles, the pressure ratio and the enthalpy drop over the turbine are very high. As a consequence, steam turbines are complex and expensive, consisting of many expansion stages. These stages are also used as intermediate extraction points for a complex system of feedwater heaters, which serve to increase cycle efficiency and remove non-condensable gases. In ORCs, the average density of the fluids is much higher than that of water, being much higher the molecular mass; in this case it is clear that the isentropic enthalpy drop is much lower. Hence the turbine is very simple and, in respect of the reasonable volume flow rates, can involve only a single or a small number of expansion stages. This leads to a more economical system in terms of capital costs and maintenance. According to Equation (2.1), since Δh of the organic fluids are limited, at the same power level mass flow rates are high.

$$\boldsymbol{P = \dot{m}\,\Delta h} \tag{2.1}$$

The main advantage is that at high pressure the blade heights are constructively acceptable and not reduced as in the case of water.
The selection of fluids giving rise to proper volume flow rates allows optimum turbine sizes for any power level [45]. The turbine generally adopted are axial or radial centripetal (Figure 2.9).

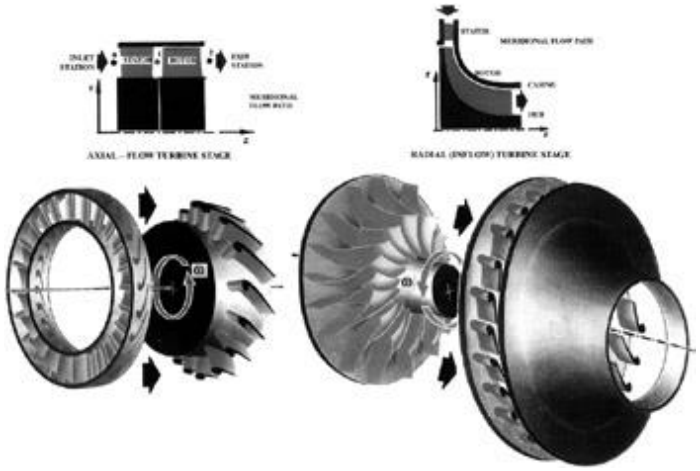

Figure 2.9: Axial and radial turbine stages [46]

The first are the most commonly used and found major applications in processes involving high volume flow rates and low enthalpy drops per stage, while for the other is the opposite. Modern configurations tend to adopt a variable geometry nozzle so as to optimize the efficiency of the expander in a wide range of environmental conditions and to obtain high performance in off-design conditions. The specific rotational speed N_s of the turbine can be calculated with Equation (2.2). From here, it can be inferred that a conventional steam turbine, in which the outlet volumetric flow rates are reduced while the enthalpy drops are high, requires a very high rotational speed. In this case the use of a gearbox is indispensable. The use of organic fluids allows instead a direct coupling of the turbine with the generator.

$$N_s = \frac{N\left(\sqrt{\dot{V}_{out,is}}\right)}{(\Delta h_{is})^{\frac{3}{4}}} \tag{2.2}$$

Therefore, another advantage resulting from the low rotational speed is a low mechanical stress of the turbine.

2.4 ORC applications

Owing to its low operating temperature, an organic Rankine cycle can suitably recover heat from various sources and this has already been demonstrated as the number of ORC plants installed worldwide is steadily increasing (Figure 2.10) [37].

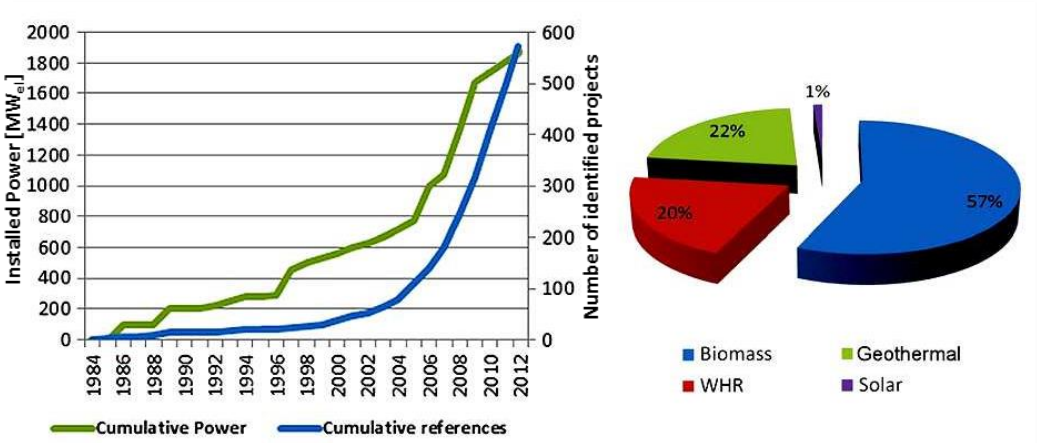

Figure 2.10: ORC market evolution and share of each application in terms of number of units adapted from [36]

The ORC technology is employed both in state-of-the-art and innovative applications:

Biomass combined heat and power

Biomass is widely available in a number of agricultural or industrial processes and can be used for the production of electricity in small to medium size scaled power plants. The problem of high specific investment costs for classic machinery such as steam boilers are overcome due to the low working pressures in ORC power plants. For small decentralized units, combined heat and power generation is required to ensure the profitability of the investment. Biomass CHP plants are mostly limited to 6-10 MW thermal power, corresponding to 1-2 MW electrical power. Most of these installations are in Europe, such as the plants built in Lienz Austria (1 MW_{el}), Sauerlach Bavaria (700 kW_{el}), Toblach South Tyrol (1.1 MW_{el}), and Fußach Austria (1.5 MW_{el}) [47].

Geothermal

Geothermal heat sources vary in temperature from a few tens of degrees up to 300°C. ORC is therefore perfectly adapted for this kind of application. These types of power plants are binary cycle since two fluids are involved in the cycle: liquid water/steam and the ORC cycle working fluid. However, it is important to keep in mind that for low-temperature geothermal sources (typically less than 100°C), the conversion efficiency is very low and geothermal plants are not economical. Higher temperature (> 150°C) geothermal heat sources enable combined heat and power generation, allowing the cooling water to be used for district heating. An example of a geothermal plant using the ORC process is the plant Neustadt–Glewe in Germany, which was the first geothermal power plant in Germany [48].

Waste heat recovery

Waste heat recovery is one of the most important development fields for ORC. It can be applied to heat and power plants (e.g.: a small scale cogeneration plant on a domestic water heater), or to industrial and farming processes such as organic products fermentation, hot exhausts from ovens or furnaces, flue-gas condensation or exhaust gases from vehicles. In such system, the waste heat is generally recovered by an intermediate heat transfer loop and used to evaporate the working fluid of the ORC.

CSP solar power plant

ORC can be used in the solar parabolic trough technology in place of the usual steam Rankine cycle in order to decrease investment costs at small scale. In fact, ORC allows power generation at lower capacities and with a lower collector temperature. Up to now, very few CSP plants using ORC are available on the market [33, 49], as mentioned in Section 1.2.4. Some very small scale-systems are being studied for remote off-grid applications, such as the proof-of-concept 3 kW_{el} system developed for rural electrification of a clinic in Lesotho [50].

Solar pond power systems

In a solar pond power plant, a conventional ORC system takes advantage of temperature gradients in salt-gradient solar pond systems. The maximum temperature reached by the water stored in these ponds is about 90-100°C.

Solar ORC-RO desalination systems

A solar ORC-RO system couples a solar thermal engine and a reverse-osmosis desalination plant. The solar thermal engine transforms the solar radiation into mechanical power via an ORC. The useful shaft power by mechanical coupling drives the high pressure pump of the RO desalination unit.

Ocean thermal energy conversion systems

This technology utilizes the temperature gradients (of at least 20°C) in oceans to drive a binary cycle.

Cold production

The shaft power of the ORC system is used to drive the compressor of a refrigeration system. This layout can be also used to produce heat if the ORC is coupled to a heat pump.

3 The choice of the organic working fluid

Before we move on to study in detail the thermodynamic cycles, the important matter of the choice of the organic working fluid has to be considered. In fact, the working fluid plays a key role in the optimization of the cycle and its selection has great implications for the design and performance of the whole plant [45]. Several scientific studies on the selection of working fluids for different types of heat sources and temperature ranges were carried out as for example in [38, 51-53]. While there are many available choices for working fluids, there are also many constraints on that selection that are related to the thermodynamic properties of the fluids, as well as considerations of health, safety and environmental impact. A set of possible working fluid candidates for this work are identified using heuristic knowledge about the processes based on similar systems. These candidates are then classified in respect of their operating temperatures in low temperature (< 250°C) and high temperature (> 250°C) fluids.

3.1 Selection criteria

In order to identify the most suitable organic working fluids the following criteria are taken into account:

- *Thermodynamic properties*
  A good working fluid for the ORC applications should have the following thermodynamic properties:

  - an appropriate low critical temperature and pressure, in order to allow performing supercritical cycles;

  - high vapor density, in order to have an acceptable volume flow rate;

  - low viscosity in both the liquid and vapor phases, in order to achieve high heat transfer coefficients and low friction losses in the heat exchangers;

  - high thermal conductivity, in order to achieve high heat transfer coefficients in the heat exchangers.

- *Thermal and chemical stability at operating temperatures*
  The maximum heat source temperature is limited by the chemical stability of the working fluid in order to avoid deterioration and decomposition at high temperatures.

- *Low or zero ODP (Ozone Depletion Potential)*
  ODP is a measure of the impact of a substance on the stratospheric ozone layer measured relative to R11 ($ODP_{R11} = 1$) [54]. For currently used fluids the ODP is less than 1, while it is always 0 for natural fluids.

- *Low or zero GWP (Global Warming Potential)*
  GWP is a measure of how much heat a substance traps in the atmosphere and it is expressed as a factor of carbon dioxide, chosen at unity [55]. It is calculated over a specific time interval, commonly 20, 100 or 500 years. The values have been defined for other fluids by the IPCC (Intergovernmental Panel on Climate Change) [56] in 1994, but they are constantly updated. For all synthetic fluids values are far greater than one.

- *Low toxicity and flammability*
  The ANSI/ASHRAE Standard 34 [57] identifies two classes related to toxicity and three groups related to flammability. For toxicity the TLV *(Threshold Limit Value)* indicator is used. It is the level to which it is believed an individual can be exposed day after day without adverse health effects. The suffix TWA *(Time Weighted Average)* indicates the average exposure to which an individual may be exposed during a usual work week of eight hours a day for five days without suffering consequences.

  CLASS A: refrigerants with TLV-TWA > 400 ppm (lower toxicity)
  CLASS B: refrigerants with TLV-TWA < 400 ppm (higher toxicity)

  The three groups identified for flammability are the following:

  GROUP 1: No flame propagation. Group consisting of all substances that do not show flame propagation at a temperature of 21°C and at atmospheric pressure.
  GROUP 2: Lower flammability. Group consisting of all substances with a lower flammability limit > 0.1 kg/m^3 at a temperature of 21°C and at atmospheric pressure and characterized by a heat of combustion < 19 MJ/kg.
  GROUP 3: Higher flammability. Group consisting of all substances with

a lower flammability limit ≤ 0.1 kg/m^3 at a temperature of 21°C and at atmospheric pressure and characterized by a heat of combustion ≥ 19 MJ/kg.

Table 3.1: Classification of Safety groups under the ANSI/ASHRAE Standard 34 [57]

	Lower Toxicity	Higher Toxicity
Higher Flammability	A3	B3
Lower Flammability	A2	B2
No Flame Propagation	A1	B1

According to Table 3.1, A1 fluids should be preferred.

- *Low costs and good availability*
  Fluids already used in commercial application are easier to obtain at a reasonable cost.

In according to Drescher [58], the fluids might be chosen in the adequate temperature range. The two main parameters are the maximum and minimum process temperature. The upper limit of the maximum process temperature is the fluid stability and material compatibility. The melting temperature should be below the ambient temperature, otherwise the fluid may solidify during shutdown time.

3.2 Screening of available fluids

Generally speaking, it is not easy to satisfy all the selection criteria mentioned above, especially in case of high temperature applications, where the problem of thermal stability became the important one. In order to identify the most suitable fluids for a DSG application a pre-selection was made, taking into account fluids that can be found in literature and state-of-the-art applications. Available fluids were firstly compared on the basis of their chemical stability, flammability, toxicity and potential to cause environmental harm. Cost was not considered as an influential factor among fluids, since no accurate data were presented in order to permit an appropriate evaluation.

The investigated organic fluids fall under five broad chemical groups:

1. Simple aliphatic hydrocarbons, such as butane, pentane, and hexane;

2. Fluorinated or halogenated hydrocarbons, including most refrigerants;

3. Aldehydes and ketones – variations on simple hydrocarbons which can be chosen so as to combine the benefits of hydrocarbons and refrigerants;

4. Aromatic hydrocarbons, combining high stability with good expansion properties and generally boiling well above ambient temperatures;

5. Siloxanes – a subgroup of silicones containing Si-O bonds with organic radicals characterized by an extremely high chemical stability at high temperatures.

Based on the critical temperature, which limits the evaporation temperature in subcritical cycles, fluids can be grouped in three categories [37]:

1. High temperature fluids (T_{crit} > 250°C)

2. Medium temperature fluids (150 < T_{crit} < 250°C)

3. Low temperature fluids (T_{crit} < 150°C)

Table 3.2: Classification of fluids based on their critical temperature

Low-temperature (LT) (<150°C)			**Medium-temperature (MT) (150-250°C)**			**High-temperature (HT) (>250°C)**		
Fluids	T_{crit} (°C)	p_{crit} (bar)	Fluids	T_{crit} (°C)	p_{crit} (bar)	Fluids	T_{crit} (°C)	p_{crit} (bar)
						N-Heptane	267.0	27.36
			N-Butane	152.3	37.96	Cyclohexane	280.5	40.75
R32	78.1	57.82	R245fa	154.0	36.51	Benzene	288.9	49.06
Propane	96.7	42.51	SES36	177.4	28.40	MDM	291.1	14.15
R134a	101.1	40.59	R123	183.7	36.62	N-Octane	296.2	24.97
R227ea	101.8	29.25	R365mfc	186.9	32.66	D4	313.3	13.32
R152a	113.3	45.17	N-pentane	196.5	33.70	Toluene	318.6	41.26
Ammonia	132.3	113.3	Hexane	234.6	30.34	MD2M	325.8	12.27
I-Butane	134.8	36.29	Methanol	240.2	81.04	D5	346.1	11.60
R236ea	139.3	35.02	Ethanol	240.8	61.48	D6	372.7	9.61
			MM	245.4	19.39	N-Butylbenzene	388.0	n/a
						Tribromomethane	422.9	n/a

As shown in Table 3.2, most of the typical working media adopted in low or medium temperature applications are refrigerants. Figure 3.1 highlights the relationship between the critical temperature and the critical pressure of the screened working fluids. Fluids with high critical temperatures are characterised by low critical pressures.

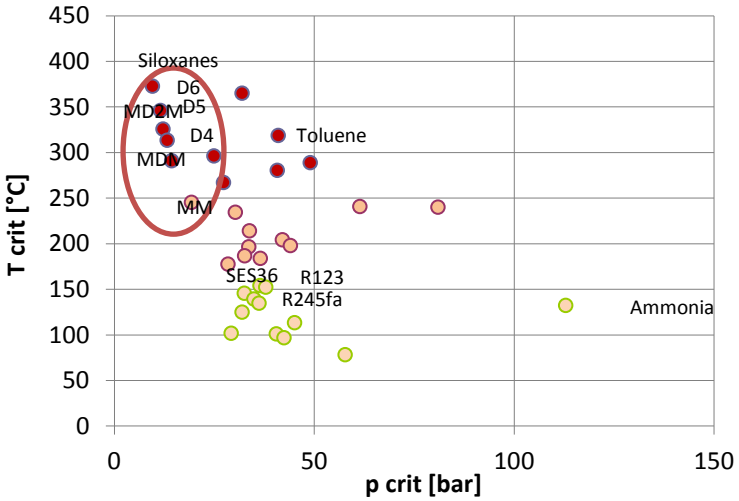

Figure 3.1: Critical temperature as function of the critical pressure of the screened organic fluids

Chlorofluorocarbons (CFCs) and hydrochlorofluorocarbons (HCFCs) are not considered in this screening, since some of them have already been phased out, while some other will be phased out in 2020 or 2030 in accordance with the Montreal Protocol established in 1987. For a long time this type of fluids have been commercially available and rationally employed as working fluids for ORC power generation from low-grade heat [45]. However, the inconvenience is that their ozone-depleting potential is elevated. Hence, transitional compounds, such as e.g. hydrofluorocarbons (HFCs) have been utilized to replace them as refrigerants. Table 3.3 summarizes the most important environmental characteristics of the working fluids, while Figure 3.2 gives a graphical overview of the ODP and GWP, which are considered the most important indexes.

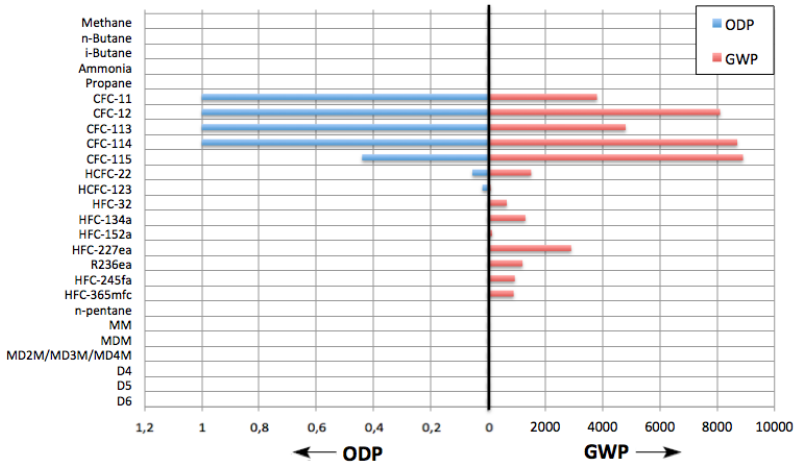

Figure 3.2: Graphical overview of the ODP and GWP indexes of some organic fluids

Table 3.3: Environmental characteristics of the investigated organic fluids

Fluids	TLV-TWA (ppm)	Autoignition temperature (°C)	Safety group	Athmospheric Lifetime (yrs)	ODP	GWP (100 yrs)
Water	-	-	A1	n/a	0	<1
Methane	1000	580	A3	1 2	0	21
n-Butane	1000	405	A3	<1	0	~0
i-Butane	1000	460	A3	<1	0	<10
Ammonia	25	651	B2	5-10 days	0	0
Propane	1000	450	A3	<1	0	~0
Substances controlled and being phased out by the Montreal Protocol						
CFC-11	1000	-	A1	45	1	3800
CFC-12	1000	-	A1	100	1	8100
CFC-13	1000	-	A1	640	1	
CFC-113	1000	-	A1	85	1	4800
CFC-114	1000	-	A1	300	1	8700
CFC-115	1000	-	A1	1.7	0.44	8900
HCFC-22	1000	632	A1	12	.055	1500
HCFC-123	50	n/a	B1	1.4	.02	90
Hydrofluorocarbons/Hydrocarbons						
HFC-32	1000	648	A2	5.6	0	650
HFC-134a	1000	>743	A1	14.6	0	1300
HFC-152a	1000	455	A2	1.4	0	140
HFC-227ea	1000	n/a	A1	34.2	0	2900
R236ea	n/a	n/a	n/a	10.7	0	1200
HFC-245fa	400	412	B1	8.8	0	930
HFC-365mfc	1000	532	n/a	8.6	n/a	890
SES36	n/a	580	n/a	n/a	n/a	n/a
n-pentane	600	309	A3	n/a	0	~20
hexane	n/a	234	n/a	n/a	n/a	n/a
methanol	n/a	385	n/a	n/a	n/a	n/a
ethanol	n/a	363	n/a	n/a	n/a	n/a
n-heptane	n/a	215	n/a	n/a	n/a	n/a
cyclohexane	n/a	245	A3	n/a	n/a	n/a
benzene	n/a	555	n/a	n/a	n/a	n/a
n-octane	n/a	220	n/a	n/a	n/a	n/a
toluene	n/a	480	n/a	2-500 days	n/a	n/a
n-butylbenzene	n/a	412	n/a	n/a	n/a	n/a
tribromomethane	n/a	n/a	n/a	n/a	n/a	n/a
Siloxanes						
MM	n/a	340	n/a	10-30 days	0	n/a
MDM	n/a	482	n/a	10-30 days	0	n/a
MD2M/MD3M/MD4M	n/a	n/a	n/a	10-30 days	0	n/a
D4	n/a	384-387	n/a	10-30 days	0	n/a
D5	n/a	372	n/a	10-30 days	0	n/a
D6	n/a	n/a	n/a	10-30 days	0	n/a

3.2.1 ORC fluids classified by application

Currently, in mostly applications a limited number of fluids is used: refrigerants and short chained alkanes are typically adopted for low temperature applications, while siloxanes find their application in the higher temperature range (300°C and above). For example, as shown in Table 3.4, octamethyltrisiloxane (MDM) is already used in biomass cogeneration and heat recovery applications (CHP) [5]. This fluid has advantages due to its favourable thermodynamic properties (critical pressure and temperature), which leads to high cycle efficiencies.

Table 3.4: Organic working fluid classified by application

Classification	Application	ORC working fluid
High Temperature (> 250°C)	Biomass	MDM
	Waste heat recovery (WHR)	Siloxanes
Low Temperature (<250°C)	Waste heat recovery (WHR)	R245fa
	Solar thermal energy	R245fa (HFC) n-pentane
	Geothermal	n-perfluoropentane & others

For each temperature there is a specific fluid and a specific cycle which allows achieving the best efficiency. Some examples of studies on fluid and cycle selection for different heat sources are presented in Table 3.5.

Table 3.5: List of studies on ORC fluids and cycle selection

Reference	Heat source and temperature range	Considered fluids	Recommended fluids and optimal cycles
Drescher, Brüggemann (2006) **[58]**	Biomass @ 350°C	MDM, Toluene, Ethylbenzene, Propylbenzene, Butylbenzene	AlkylBenzenes: T_{Cond}=90°C* T_{Eva}=250-300°C
Borsukiewicz-Gozdur, Novak (2007) **[59]**	Geothermal @ 80-115°C	Propylene, R227ea, RC318, R236fa, ibutane, R-245fa	Propylene, R227ea, R-245fa: T_{Cond}=25°C T_{Eva}=80-115°C
Zhang, Jiang (2012) **[60]**	Geothermal @ 100-200°C	R134a, R245fa, isobutene, isopentane	T_{brine}=100-150°C: R134a T_{Cond}=35°C T_{brine}=200°C: R245fa T_{Cond}=35°C

Walraven et al. (2012) **[61]**	Geothermal @ 100-150°C	R12, R22, R41, R32, R115, R124, R125, R134a, R142b, R152a, R218, R227ea, R236ea, R236fa, R245fa, R1234yf, R1234ze, RC318, C4F10, C5F12, CF3I, SF6, Ethane, Propane, iso-butane, Propylene, DME, CO_2, N_2O, others.	T_{brine}=125°C, no $T_{limit,Geo}$: R227ea T_{brine}=125°C, $T_{limit,Geo}$=75°C: R1234yf
Badr, O'Callaghan et al. (1990) **[62]**	WHR	R11, R113, R114	R113: T_{Cond}=30-50°C T_{Eva}=120°C
Invernizzi et al. (2007) **[63]**	WHR: MGT flue gas @ 300°C	HFC-43-10mee, R123, n-Pentane, R113, 2-2-Dimethylbutane, 2-3-Dimethylbutane, n-Hexane, Hexafluorobenzene, MM, Pentafluorobenzene, n-Heptane, c-Hexane, MDM, n-Octane, D4, MD2M	MM: T_{Cond}=30°C T_{Eva}=170°C
Lemort et al. (2007) **[64]**	WHR	R245fa, R123, R134a, n-pentane	R123, n-pentane: T_{Cond}=35°C T_{Eva}=60-100°C
Liu, Chien et al. (2004) **[65]**	WHR	R123, iso-pentane, HFE 7100, Benzene, Toluene, p-xylene	Benzene, toluene, R123: T_{Cond}=30°C T_{Eva}=150-200°C
Fahad A. Al-Sulaiman (2013) **[4]**	WHR: steam @ ~100°C	R600, R600a, R134a, R152a, R290, R407c, and ammonia.	R134a: T_{Cond}=35°C T_{Eva}≈90°C
Dai, Wang et al. (2009) **[66]**	WHR: gas @ 145°C	NH_3, butane, isobutene, R11, R123, R141B, R236ea, R245ca, R113, water	R236ea: T_{Cond}=25°C T_{Eva}=87.7°C iso-butane: T_{Eva}=87.1°C
Lakew, Bolland (2010) **[67]**	WHR: air @ 80-200°C	R134a, R123, R245fa, R227ea, n-pentane, propane	T_{ha}=80-160°C: R227ea T_{Cond}=20°C T_{ha}=200°C: R245fa T_{Cond}=20°C

Quoilin, Declaye et al. (2011) **[68]**	WHR: gas @ 180°C with HTF.	R1234yf, R134a, R245fa, HFE7000, SES36, R123, n-butane, n-pentane	R245fa: T_{Eva}=113.5°C R123: T_{Eva}=111.8°C
Schuster et al. (2010) **[42]**	Generic source @ 210°C	Water, R134a, R227ea, R152a, RC318, R236fa, R245fa, isobutene, isopentane, isohexane, cyclohexane, R365mfc	Sup: R365mfc & iso-pentane: T_{Cond}=20°C T_{max}≈180°C Sub: R245fa & iso-butene: T_{Cond}=20°C T_{Eva}≈140°C
Tchanche, Papadakis et al. (2009) **[69]**	Solar: water @ 90°C as HTF	Refrigerants	R134a, R152a, R600, R600a, R290: T_{Cond}=35°C T_{Eva}≈75°C
Façao, Palmero-Marrero et al. (2008) **[70]**	Solar @ 80°C, 100-150°C and 200-250°C	Water, n-pentane, HFE7100, cyclohexane, toluene, R245fa, methanol, ammonia	Cyclohexane: T_{Cond}=45°C T_{Eva}=120-230°C R245fa: T_{Cond}=45°C T_{Eva}=230-250°C
Quoilin, Orosz et al. (2011) **[50]**	Solar: with HTF @ ~150°C	n-pentane, SES36, R245fa, R134a	SES36: T_{Cond}=30°C T_{Eva}=169°C n-pentane: T_{Cond}=30°C T_{Eva}=189°C
** Min temperature of the heat sink instead of condensing temperature*			

3.2.2 ORC fluids used by manufacturers

As mentioned in previous sections, fluid selection studies for different heat sources and applications cover a broad range of working fluids. In fact, only a few fluids are actually used by commercial ORC manufacturers.
ORC manufacturers constructed their first power plants in the beginning of the 80s [44]. The two main ORC manufacturers are Turboden and Ormat, the first one mainly focused on biomass boilers and other high temperature applications, the second one mainly interested on the geothermal market and on machines for remote installations.

It is generally difficult to find out details on the working fluids the ORC manufacturers use in their applications. However, Table 3.6 represents a list of the most famous ORC manufacturers and the related available informations. The fact that the fluids listed are already used in commercial applications, makes them promising candidates for this master thesis, because they are supposed to be available on the market.

Table 3.6: List of the main ORC manufacturers and used working fluids

Manufacturer	Applications	Power range (kWe)	Heat source temperature (°C)	ORC working fluid
Turboden	Biomass-CHP, WHR, Geo.	200-2.000	100-300	Solkatherm (SES36), MDM
Ormat	Geo., WHR, Solar	200-70.000	150-300	Isopentane, n-pentane & co.
Ingeco STG International Electratherm Green machine	WHR, Solar	50	>93	R245fa (HFC)
Verdicorp		30-75	n/a	
Bosch KWK	WHR	65-325	120-150	
Exergy	WHR, Geo., Biomass	n/a	n/a	PP1, isobutene, R245fa
Infinity Turbine Cryostar	WHR, Geo.	n/a	100-400	R134a, R245fa
TriOGen	WHR	160	>350	Toluene

3.3 Suitable organic fluids for DSG

A relatively large group of substances has been considered in this study, comprising fluids both for low and high temperature applications, belonging to families such as linear and aromatic hydrocarbons, refrigerants (HFC) and siloxanes. In particular, the organic fluid that circulates through the solar field must meet basic requirements as safety and technical suitability. In this sense toxic fluids or substances harmful to the ambient should not be taken into consideration. Flammable compounds should also be avoided, even if appropriate safety measures could be provided.

The investigated fluids have been selected in order to deal with different maximum temperature values between 200°C and 400°C, typical values reached from existing CSP systems. There is no optimal fluid that meets all the selection criteria discussed in Section 3.1. Therefore, a trade-off must be made. When the maximum temperature is low, a refrigerant fluid (like R245fa) with a low critical temperature can be used; as the maximum temperature increases, fluids with a higher critical temperature must be used. Among the fluids with an elevated critical temperature found in literature, siloxanes are mentioned as the most promising also due to their environmental friendly characteristics. They allow operating a subcritical ORC with limited pressure. Figure 3.3 reports some thermodynamic data of the selected fluids, showing the different critical temperature and critical pressure and the limited temperature in accordance with the thermal stability.

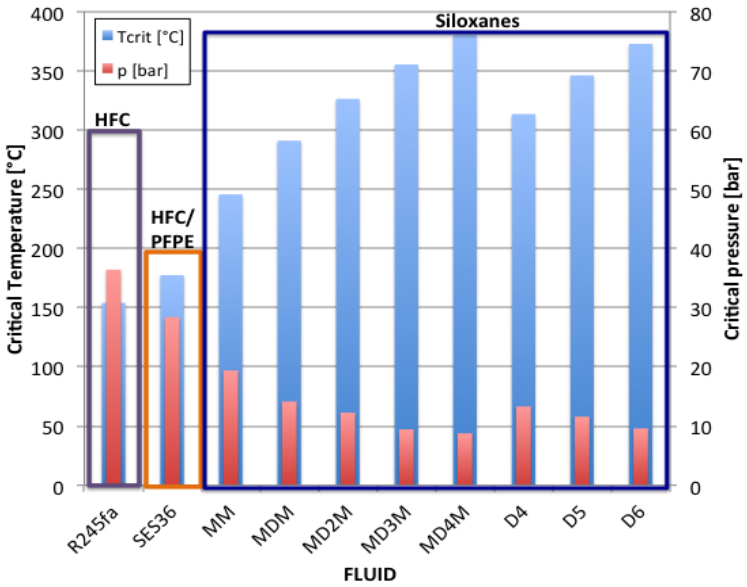

Figure 3.3: Critical temperature and pressure of the selected ORC fluid families

3.3.1 LT fluids: R245fa, SES36

According to the selection criteria mentioned in Section 3.1, two fluids have been selected among the original list of Table 3.2 for a DSG in case of low temperature (< 250°C) applications: R245fa and SES36.

R245fa

R245fa is a HFC also known as pentafluoropropane and by its chemical name 1,1,1,3,3,-pentafluoropropane. From the corresponding T-s diagram, shown in Figure 3.4, it could be considered as an isentropic fluid. Unlike CFC and HCFC, it has no ODP and is nearly non-toxic. Its thermophysical properties and environmental characteristics make it suitable for different applications, such as centrifugal chillers, ORC for energy recovery and power generation, sensible heat transfer in low-temperature refrigeration, heat pumps and passive cooling devices. As well, it has a broad range of applications like foam blowing agent, solvent and aerosol. Although it is intended to remain trapped within the foam insulation, it is practically non bio-degradable with a lifetime of 8.8 years when it eventually does escape into the atmosphere. It has a high GWP of 930, but Honeywell refers to this as acceptable in their literature. Chemical analysis confirmed that the fluid can be considered stable at 300°C [71]. One of the main disadvantages of R245fa is instead the cost. Its actual price is continuously rising, since the fluid is subjected to GWP taxes depending on the country regulations [72].

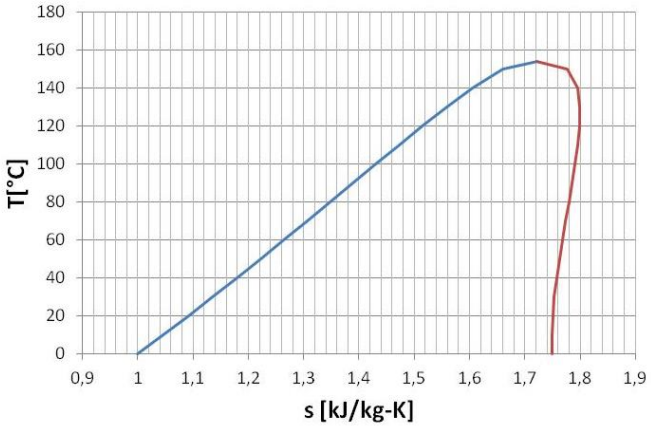

Figure 3.4: T-s diagram of R245fa

Table 3.7: Thermodynamic properties of R245fa

Compound	Molecular Mass, (kg/kmol)	Critical Temp., (°C)	Critical pressure, (bar)	Boiling Temp., (°C)
R245fa	134.05	154.01	36.51	15.3

Solkatherm® SES36

Solkatherm® SES36 is the brand name of an azeotropic binary mixture of 65% of a hydrofluorocarbon, R365mfc and of 35% of a perfluoropoly-ether (PFPE) manufactured by Solvay. A more comprehensive series of thermophysical properties of Solkatherm can be found in [73].
Solkatherm could be a very interesting alternative to the hydrocarbons due to its particular characteristics [74]: high molecular mass combined with favourable transport properties, non-flammable, chemically stable, compatible with the most construction materials and environmentally benign fluid. It is thermally stable and it has been proved in continuous operation conditions up to 190°C (its first decomposition reactions occur in laboratory at 220°C). It boils at a relatively low temperature (36.7°C) and has been successfully adopted for the first time as a working fluid by Turboden, Italy [5] in the case of the low temperature geothermal binary plant of Altheim, Austria. Besides geothermal power plants, other areas where Solkatherm could be used, are local combined heat and power plants, solar-thermal systems, and high temperature heat pumps.

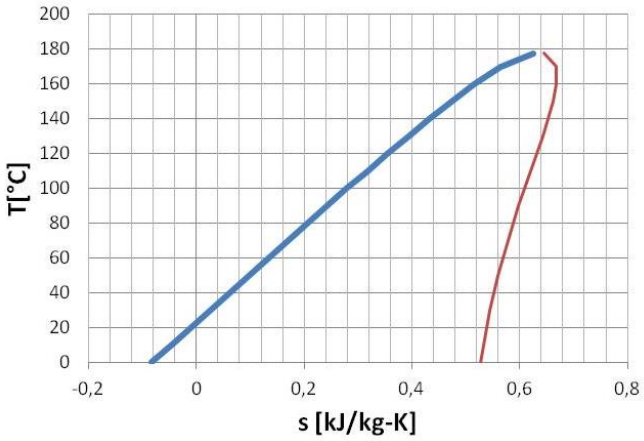

Figure 3.5: T-s diagram of Solkatherm® SES 36

Table 3.8: Thermodynamic properties of Solkatherm® SES36

Compound	Molecular Mass, (kg/kmol)	Critical Temp., (°C)	Critical pressure, (bar)	Boiling Temp., (°C)
SES36	184.45	177.4	28.4	36.7

3.3.2 HT fluids: Siloxanes

For high-temperatures applications, fluids with the highest possible critical temperature should be selected. Among the investigated fluids with a higher critical temperature, siloxanes allow operating a subcritical ORC with limited pressure at high and medium temperatures. Siloxanes are a family of organic compounds that contain silicon, oxygen and hydrocarbon groups. The main advantages of this family of compounds are: low/non-toxicity, limited flammability, good material compatibility, low foul formation over heat transfer surfaces and a good thermal stability. Due to the high molecular complexity, siloxanes are named by their compact units (M unit and D unit) and can be divided in two main groups:

- *Linear siloxanes*

1. **MM** (hexamethyldisiloxane, $C_6H_{18}OSi_2$)
2. **MDM** (octamethyltrisiloxane, $C_8H_{24}Si_3O_2$)
3. **MD2M** (decamethyltetrasiloxane, $C_{10}H_{30}Si_4O_3$)
4. **MD3M** (dodecamethylpentasiloxane, $C_{12}H_{36}Si_5O_4$)
5. **MD4M** (tetradecamethylhexasiloxane, $C_{14}H_{42}O_5Si_6$)

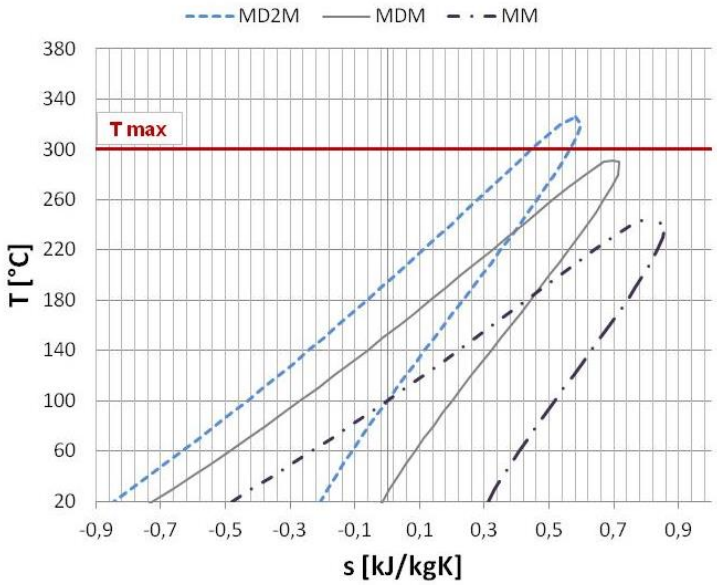

Figure 3.6: T-s diagram and proven thermal stability limit of linear siloxanes [75]

- *Cyclic siloxanes:*

1. **D4** (octamethylcyclotetrasiloxane, $C_8H_{24}O_4Si_4$)
2. **D5** (decamethylcyclopentasiloxane, $C_{10}H_{30}O_5Si_5$)
3. **D6** (dodecamethylcyclohexasiloxane, $C_{12}H_{36}Si_6O_6$)

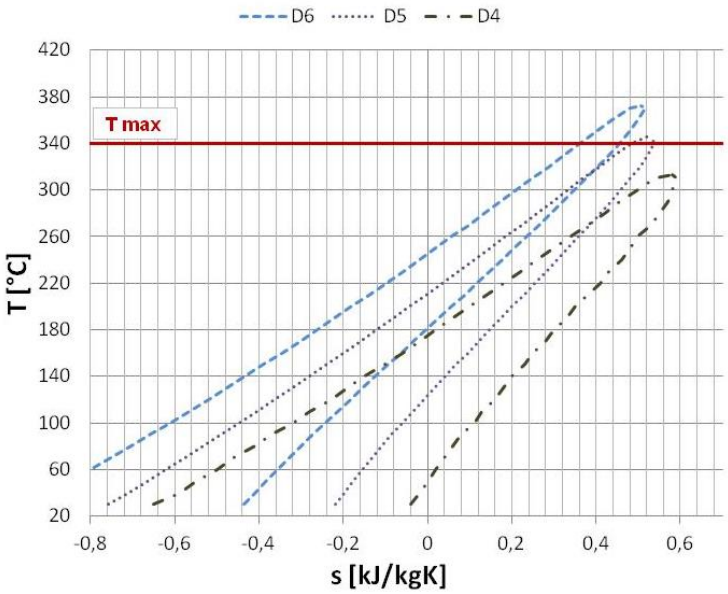

Figure 3.7: T-s diagram and proven thermal stability limit of cyclic siloxanes [75]

At ambient conditions, siloxanes are liquid and appear slightly viscous, odorless, and transparent. Some of their thermodynamic characteristics are summarized in Table 3.9. In principle, siloxanes can all be used as working fluids in ORC turbines depending on the electrical power range [76]. They are already employed as working media in high-temperature ORC applications (turbine inlet temperature = 300°C) for larger power capacities (400 kW_{el} – 2 MW_{el}) and mixture have been successfully adopted as HTF, comprising the CSP industry (Syltherm 800 [77]).

Table 3.9: Thermodynamic properties of siloxanes

Compound	Molecular Mass, (kg/kmol)	Critical Temp., (°C)	Critical pressure, (bar)	Boiling Temp., (°C)
MM	162.38	245.60	19.39	100.25
MDM	236.53	290.94	14.15	152.51
MD2M	310.69	326.25	12.27	194.36
MD3M	384.84	355.21	9.45	229.87
MD4M	458.99	380.05	8.77	260.75
D4	296.62	313.35	13.32	175.35
D5	370.77	346.00	11.60	210.9
D6	444.92	372.63	9.61	244.96

Cyclic siloxanes are more stable than linear siloxanes. In a study of Angelino and Invernizzi [78], it was suggested a thermal limit of cyclic siloxanes near to 400°C, ensuring 340°C by means of an experimental test in the presence of oxygen and humidity. Cyclic stress can accelerate the thermal degradation of siloxanes, although the addition of stabilizing agents may also be considered. In present studies, the maximum temperature of the working fluid in the cycle is usually fixed at 300°C for linear siloxanes and at 340°C for cyclic siloxanes [75].

4 ORC processes analysis

The main objective of this chapter is to evaluate different cycle configurations in order to choose the potential one that could be implemented in a solar field with a feasible TES system. In order to take advantage of the achievable temperatures of the PTCs and in accordance with the research fields of the Line Focus Systems division of DLR, the main interest is set on high temperature processes. Therefore, siloxanes are chosen as working fluids and the following single-pressure level cycles are considered:

- Subcritical saturated regenerative cycle
- Superheated regenerative cycle
- Supercritical regenerative cycle

Useful guidelines to select the most appropriate fluid among the siloxanes and to define the operating parameters have been provided. In accordance with the properties of linear and cyclic siloxanes, the minimum temperatures of the analysed cycles are chosen to ensure a condensing pressure of at least 0.05 bar. This pressure represents a technical limit as explained in Section 4.3. The maximum obtainable temperatures are set well below the stability limit of the selected fluids. After a first thermodynamic optimization of the fluids, the analysis is focused on two particular siloxanes (MM and D4).
The thermodynamic analysis is made using Excel integrated with the CoolProp add-in [79], an open-source library that uses accurate equations of state to provide the thermodynamic and transport properties of 86 pure and pseudo-pure fluids. It includes all significant ORC working fluids, as R245fa and siloxanes (MM, MDM, MD2M, MD3M, MD4M, D4, D5, D6).
Once the cycles with the best performances are selected, a thermodynamic assessment of different storage system integrations is perfomed with the aim of finding the optimum configuration.

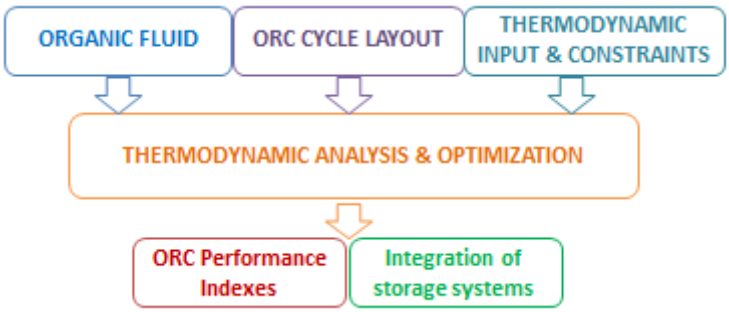

Figure 4.1: Flow chart of the performed analysis

4.1 Regenerative cycles

Three basic configurations are considered: saturated, superheated and supercritical cycles. The non-regenerative cycle configurations are not analysed, because, as mentioned in Chapter 2, regeneration is always convenient in case of organic dry fluids. It was shown that regenerative ORC has higher first and second law efficiencies than basic ORC [80]. Due to the better efficiency, the cycle needs less thermal energy for the same electricity yield. Regarding a solar thermal ORC power plant, the size of the solar field and the overall cost of the plant decrease.

Saturated cycle

In a saturated cycle the working fluid enters the turbine as saturated steam. A representative cycle is shown in the T-s diagram in Figure 4.2. As a general rule, owing to the high molecular complexity of the considered organic fluids, saturated cycles are preferable. In contrast to traditional water steam cycles, superheating is not strictly requested in terms of preventing moisture formation during the expansion in the turbine, as already explained in Chapter 2.

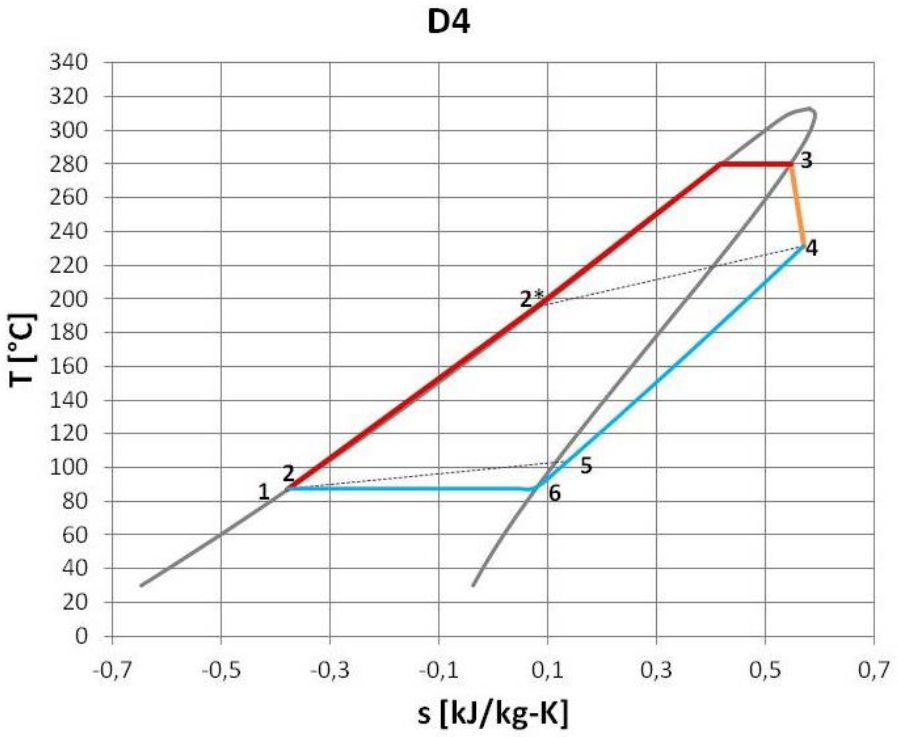

Figure 4.2: Representative T-s diagram of a subcritical saturated cycle

Superheated cycle

In a superheated cycle, after being evaporated the temperature of organic fluid vapour is increased again in order to produce superheated steam before entering the turbine. A simplified representation of the cycle is shown in Figure 4.3. As said before, dry fluids do not need to be superheated in order to avoid the liquid phase at the end of the expansion, but they were also presented in this configuration cycle to obtain more knowledge of their behaviour. The impact of superheating is determined by the rate at which the constant pressure lines diverge [38]. For dry fluids the thermal efficiency of the cycle remains approximately constant when the inlet temperature of the turbine is increased. Moreover, in [80] it is shown that superheating in organic Rankine cycles increases the irreversibility and decreases the second law efficiency. Therefore, organic fluids should be operated at saturated conditions to reduce the total irreversibility of the system.

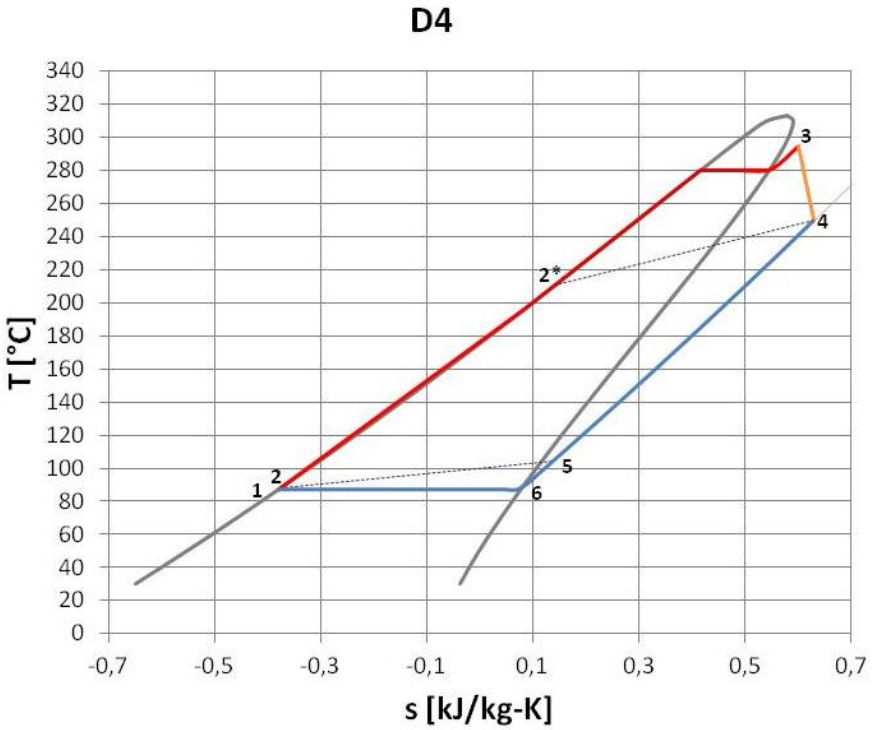

Figure 4.3: Representative T-s diagram of a subcritical superheated cycle

Supercritical cycle

If thermal stability of the fluid allows operation at supercritical temperatures, the working fluid can be compressed directly to a pressure higher than its critical

one (Figure 4.4). Hence, the heating process does not pass through a distinct two-phase region before expansion. Due to their low critical pressures, siloxanes can also be used in supercritical cycles. In order to find the optimum pressure an optimization study should be performed.

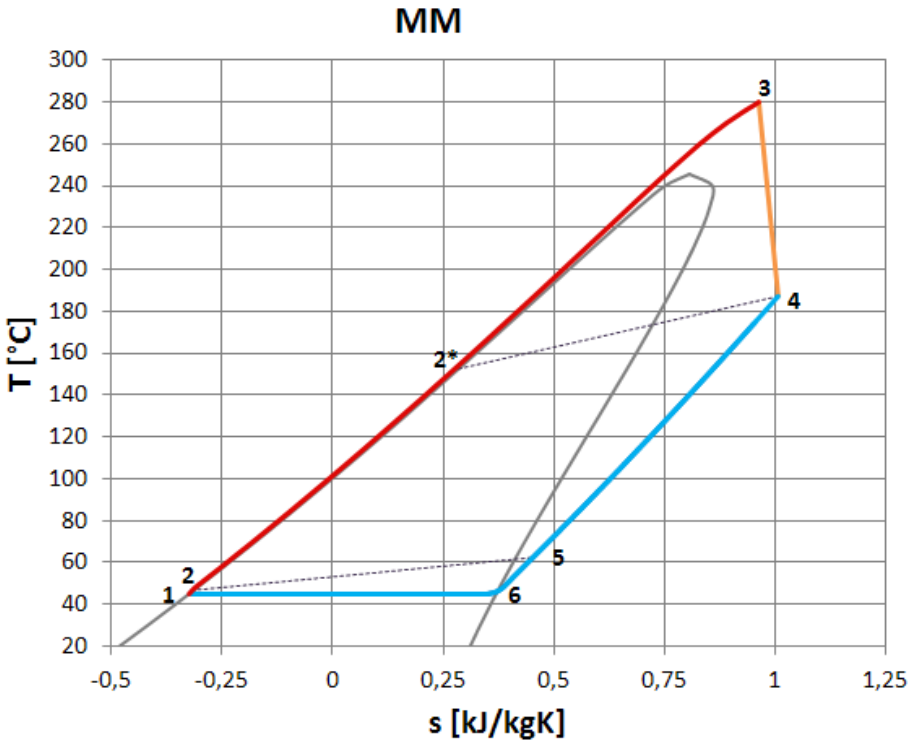

Figure 4.4: Representative T-s diagram of a supercritical cycle

4.2 Basic cycle analysis model

A first model is designed for a rapid screening of potential power cycle configurations. Figure 4.5 shows a schematic representation of the ORC components and the corresponding working fluid state points. Once fixed variables are assigned, all the other thermodynamic points of the cycle can be sequentially calculated. Working fluid enthalpy, temperature, pressure, entropy, and specific volume are calculated for each inlet and outlet of every component by solving mass and energy balances complemented by performance equations. For simplicity, the internal irreversibility and the pressure drops in steam generator, regenerator, condenser and pipes are ignored when the thermodynamic properties are estimated. Each component is considered as a steady-state steady-flow system and is described further.

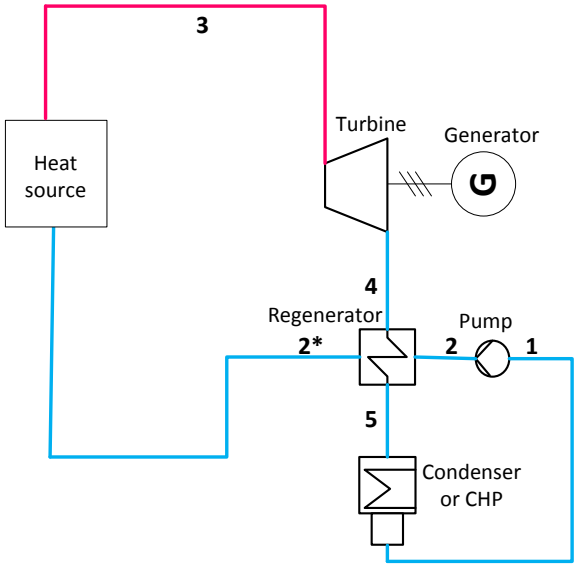

Figure 4.5: Schematic representation of ORC components and working fluid state points

Pump

The pump power can be expressed as

$$\boldsymbol{W_{\mathrm{p}} = \frac{W_{\mathrm{p,ideal}}}{\eta_{\mathrm{is,p}}} = \frac{\dot{m} \cdot (h_{2\mathrm{s}} - h_1)}{\eta_{\mathrm{is,p}}}} \tag{4.1}$$

where $W_{\mathrm{p,ideal}}$ is the ideal power of the pump, $\dot{m}$ is the working fluid mass flow rate, $\eta_{\mathrm{is,p}}$ is the isentropic efficiency of the pump, and h_1 and $h_{2\mathrm{s}}$ are the enthalpies of the working fluid at the inlet and outlet of the pump for the ideal case.

Heat input source

The heat source is equals to the solar thermal energy collected by the solar field. The heat input rate is defined as

$$\boldsymbol{\dot{Q}_{\mathrm{in}} = \dot{m} \cdot (h_3 - h_{2^*})} \tag{4.2}$$

where h_3 and h_{2^*} are the enthalpies of the working fluid at the exit and inlet of the solar field, respectively.

Turbine

The turbine power is given by

$$\boldsymbol{W_t = W_{t,ideal} \cdot \eta_{is,t} = \dot{m} \cdot (h_3 - h_{4s}) \cdot \eta_{is,t}} \tag{4.3}$$

where $W_{t,ideal}$ is the ideal power of the turbine, $\eta_{is,t}$ is the turbine isentropic efficiency, and h_3 and h_{4s} are the enthalpies of the working fluid at the inlet and outlet of the turbine for the ideal case.

Regenerator

The heat rate recovered by the regenerator is

$$\boldsymbol{\dot{Q}_{reg} = \dot{m} \cdot (h_{4s} - h_5) = \dot{m} \cdot (h_{2^*} - h_2)} \tag{4.4}$$

The working fluid temperature at the regenerator outlet T_5 is calculated based on the turbine outlet temperature, the pump outlet temperature, and the regenerator effectiveness. Regenerator effectiveness ε is defined as

$$\boldsymbol{\varepsilon = \frac{\dot{Q}}{\dot{Q}_{max}} = \frac{T_{v,in} - T_{v,out}}{T_{v,in} - T_{l,out}}} \tag{4.5}$$

In accordance with the working fluid state points

$$\boldsymbol{\varepsilon = \frac{T_4 - T_5}{T_4 - T_2}} \tag{4.6}$$

Condenser

The condenser heat rate can be expressed as

$$\boldsymbol{\dot{Q}_c = \dot{m} \cdot (h_5 - h_1)} \tag{4.7}$$

where h_5 and h_1 are the enthalpies of the working fluid at the inlet and outlet of the condenser, respectively.

Net power and performance indexes

Once all components are defined, the net power of the cycle is calculated by

$$\boldsymbol{W_{net} = W_t - W_p} \tag{4.8}$$

Two Performance Indexes are normally introduced as key indicators of the ORC potential. Equation (4.9) defines the thermal (first-law) efficiency as the ratio between the net power of the cycle and the input heat rate.

$$\boldsymbol{\eta_{th} = \frac{W_{net}}{\dot{Q}_{in}}} \tag{4.9}$$

Substituting Equation (4.1), (4.2) and (4.3) the cycle thermal efficiency for a regenerative ORC can be written as

$$\boldsymbol{\eta_{th} = \frac{W_t - W_p}{\dot{Q}_{in}} = \frac{(h_3 - h_{4s}) \cdot \eta_{is,t} - (h_{2s} - h_1) \cdot \eta_{is,p}^{-1}}{h_3 - h_{2^*}}} \tag{4.10}$$

The second performance index is the ORC net specific work (kJ/kg), defined as

$$\boldsymbol{w_{ORC} = \frac{W_{net}}{\dot{m}}} \tag{4.11}$$

4.3 Thermodynamic optimization of siloxanes

The choice of the optimal cycle configuration is strictly related to the considered working fluid, since only a correct selection of both fluid and cycle configuration allows achieving the best system performance [81]. Most of the works published in the literature deal with thermodynamic assessments, i.e. they aim at maximizing the plant efficiency or its power output. However, thermodynamic assessment alone cannot provide exhaustive indications on the optimal working fluid, mainly because of the different thermal and volumetric behaviour of the fluids, which affect the performance, the size and the cost of the plant components [82]. The most important parameters in evaluating the most suitable fluids are the power output of the

system, the condensing pressure and the volume flow ratio in the turbine [83].

First of all, the working fluid selection must account for its consequences on the turbine design. There is a strong relationship between the working fluid properties and the turbine architecture (speed of revolution, number of stages, dimensions) and performance (isentropic efficiency).

In order to select the proper fluid and its related cycle, all eight siloxanes, listed in Table 4.1, are evaluated in according to the following criteria:

- Condensing pressure;
- Maximum temperature;
- Volume flow ratio (V_r).

Table 4.1: Siloxanes data

	Linear siloxanes					Cyclic siloxanes		
Fluids	MM	MDM	MD2M	MD3M	MD4M	D4	D5	D6
T_{crit} (°C)	245.6	290.94	326.25	355.21	380.05	313.35	346	372.63
p_{crit} (bar)	19.39	14.15	12.27	9.45	8.77	13.32	11.6	9.61
T_{max} (°C)	300	300	300	300	300	340	340	340

4.3.1 Condensing pressure

An ORC should operate at the minimum admissible condensing temperature, assuring that the corresponding pressure is not too low. In accordance with previous researches on ORC systems, the lowest technical limit for the condensing pressure is considered to be 0.05 bar [83]. As can be seen in Figure 4.6, MM can be considered as the most suitable candidate in case of electricity production, due to its high condensing pressures for the related low condensing temperatures.

Due to the pressure limit the application of MDM and D4 in power cycles entails relatively high condensing temperatures (66.5°C for MDM and 87.3°C for D4). For that reason both fluids are typically used for combined heat and power systems. With D5 and D6 the condensing temperature would be even higher (> 100°C). For instance, Figure 4.6 shows that the use of D5 and D6, in the considered temperature range leads to very low pressures not feasible for actual condensers. MD2M, MD3M and MD4M are not represented in the figure, but have similar characteristics. While in such cycles the electrical efficiency decreases, rejected heat can be used for applications like CHP, absorption cycles or district heating.

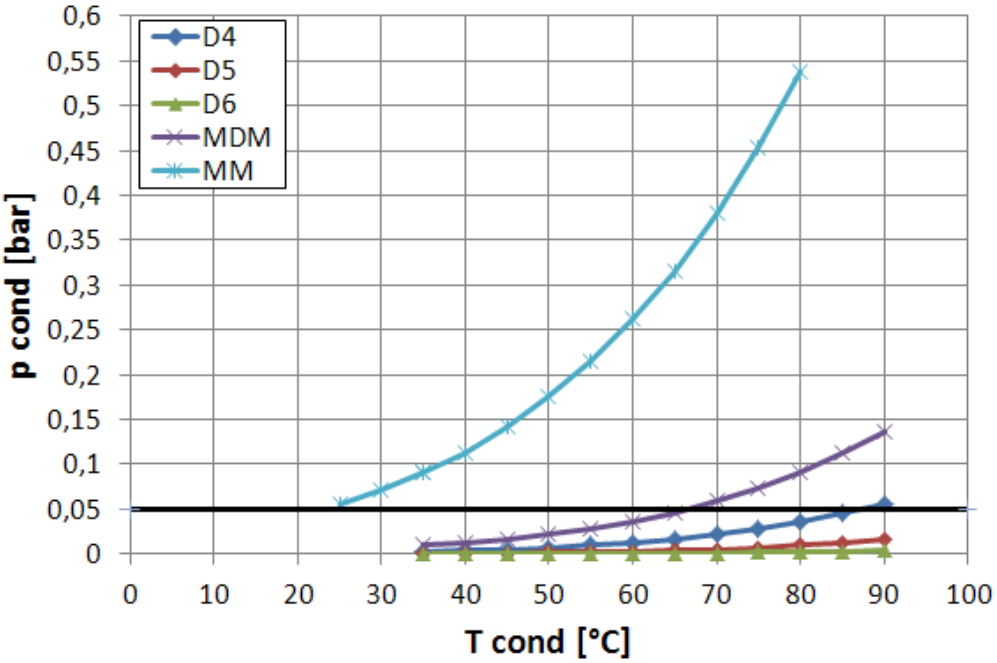

Figure 4.6: Evaluation of condensing pressure and corresponding temperature for siloxanes

4.3.2 Maximum temperature

The maximum temperature is assessed to ensure the thermal stability of siloxanes. In case of saturated cycles a T_{max}/T_{crit} ratio lower than 0.95 is ensured. If the fluid allows a maximum temperature higher than the critical one, supercritical cycles can be realized. According to that, a value of 280°C was chosen as T_{max} in order to perform a saturated process analysis with the fluid D4 and a supercritical process analysis with the fluid MM at the same maximum temperature. The analysis of the following sections refers to these two cycles. A process with fluid MDM is not considered, since at 280°C the ratio T_{max}/T_{crit} is too high, as shown in Table 4.2.

Table 4.2: Reducted temperature for siloxanes MM, MDM and D4 at a maximum temperature of 280°C

Fluids	MM	MDM	D4
T_{max}/T_{crit}	-	0.98	0.94

4.3.3 Volume flow ratio

The use of different fluids implies a wide variation of turbine operating parameters. In order to choose the appropriate working fluid it is necessary to predict the turbine performance and optimize the turbine design variables as e.g. number of stages, speed of revolution and relevant blade geometric parameters. According to similarity rules, the efficiency of a turbine stage is primarily set by its specific speed and specific diameter.

The most important parameters affecting the isentropic turbine efficiency are defined as follows:

• Volume flow ratio (V_r)

$$\boldsymbol{V_r} = \frac{\dot{\boldsymbol{V}}_{\mathbf{out,is}}}{\dot{\boldsymbol{V}}_{\mathbf{in}}} \tag{4.12}$$

• Size parameter (SP)

$$\boldsymbol{SP} = \frac{\sqrt{\dot{\boldsymbol{V}}_{\mathbf{out,is}}}}{\Delta \boldsymbol{h}_{\mathbf{is}}^{\mathbf{1/4}}} = \frac{\boldsymbol{D}}{\boldsymbol{D}_{\mathbf{s}}} \tag{4.13}$$

• Specific speed (N_s)

$$\boldsymbol{N}_{\mathbf{s}} = \frac{\boldsymbol{N}\left(\sqrt{\dot{\boldsymbol{V}}_{\mathbf{out,is}}}\right)}{(\Delta \boldsymbol{h}_{\mathbf{is}})^{\mathbf{3/4}}} \tag{4.14}$$

The isentropic V_r accounts for the effect of the compressibility through the expansion, where $\dot{V}_{out,is}$ and $\dot{V}_{in}$ are respectively the outlet and inlet volume flow rates, evaluated for a multistage machines at the exit of the last stage and at the inlet of the first stage. V_r is variable and strictly dependent on the working fluid considered [63]. Generally speaking, the turbine efficiency decreases by increasing V_r because of the losses related to the occurrence of high Mach numbers and, for reaction turbines, to the negative influence of wide flow area variations across the rotor blades. Moreover, for multistage single-shaft turbines, large V_r prevents operating the various stages at optimum specific speed. In the analyzed case the value of V_r should be below 500 in accordance with the considerations reported in [82].

The *SP* is function solely of the thermodynamic cycle and power output, where Δh_{is} is the isentropic enthalpy drop in the turbine. Furthermore, *SP* is proportional, for a given value of specific diameter D_s to actual turbine dimensions. Low *SP* values penalize turbine efficiency because of large losses caused by the increase of relative blade thickness, clearances and roughness. Since *SP* is defined with reference to the outlet volume flow rate, the contemporary occurrence of high V_r and low *SP* yields leads to very small flow areas in the first portion of the machine with further efficiency penalties [84].

V_r, *SP* and N_s values are calculated for both chosen cycle configurations, under different working conditions. Table 4.3 summarizes the assumed operating parameters. For both configurations, the working fluid, turbine inlet pressure and temperature, condensing temperature and components efficiencies are given as inputs. The maximum temperature of the working fluid at the turbine inlet T_{max} is fixed at 280°C. In case of the subcritical saturated cycle, the turbine inlet pressure $p_{in,t}$ directly depends on this parameter. In case of the supercritical cycle, its critical pressure value is used as $p_{in,t}$. The mass flow rate is equal in both cases to 1 kg/s, in order to systematically compare the different cycles, with fixed normalized mass flow conditions.

Table 4.3: Summary of fixed and parametric conditions used to define the studied cases

Cycle conditions	Saturated cycle with D4	Supercritical cycle with MM
$\dot{m}$	1 kg/s	
T_{max}	280°C	
$p_{in,t}$	8.076 bar	19.394 bar
T_c	Parametric study (25°C - 90°C)	
$\eta_{is,t}$	83%	
$\eta_{is,p}$	70%	
ε	90%	

Figure 4.7 shows the values of V_r for different values of condensing temperature at fixed T_{max} for both analyzed cycles. The value for V_r of the supercritical cycle is far below the allowed maximum of 500. Applying this limit to the saturated cycle with D4, the condensing temperature must be above 70°C. Figure 4.8 and Figure 4.9 shows the values of *SP* and N_s respectively. In order to allow the direct drive of the electric generator without reduction gear, a low speed of rotation *N* of 3000 rpm is assumed.

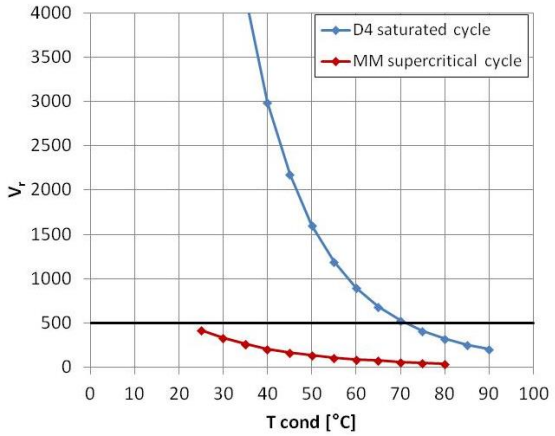

Figure 4.7: Turbine isentropic volume flow ratio for an isentropic expansion as a function of condensing temperature for a maximum cycle temperature of 280°C

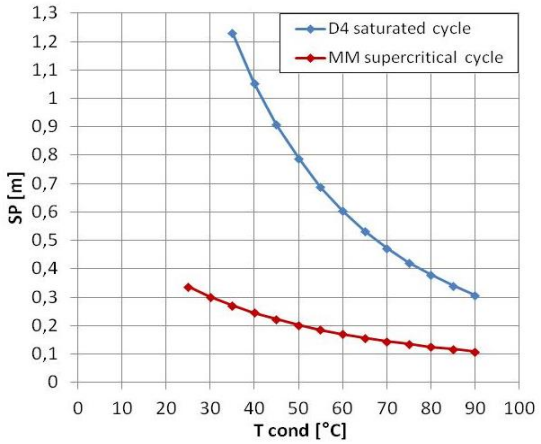

Figure 4.8: Turbine size parameter as a function of condesing temperature for a maximum cycle temperature of 280°C

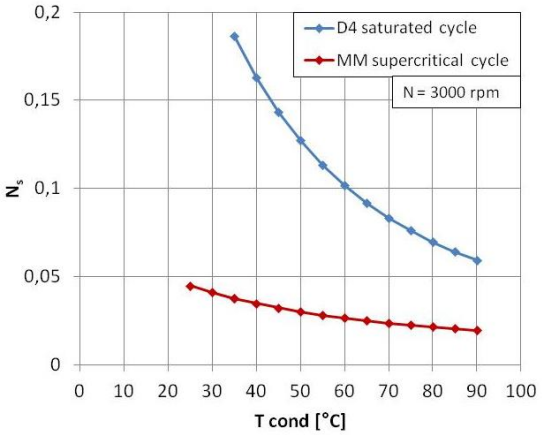

Figure 4.9: Specific speed as a function of the condensing temperature for a maximum cycle temperature of 280°C

4.4 Thermodynamic analysis

The energy analysis based on the first law of thermodynamics is performed and the two performance indexes η_{th} and w_{ORC} are carried out for both chosen cycle configurations.

According to Figure 4.10 and Figure 4.11, adopting a supercritical cycle, in comparison to a saturated one with the same condensing temperature, allows achieving high performances in terms of specific net work, but decreases the cycle efficiency.

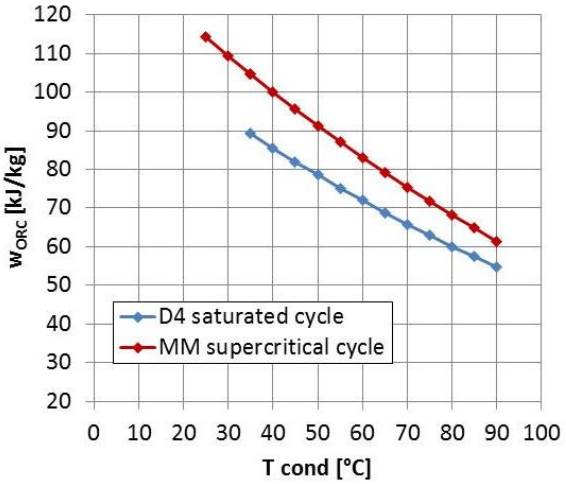

Figure 4.10: Specific net work as a function of condensing temperature in both configurations for a maximum cycle temperature of 280°C

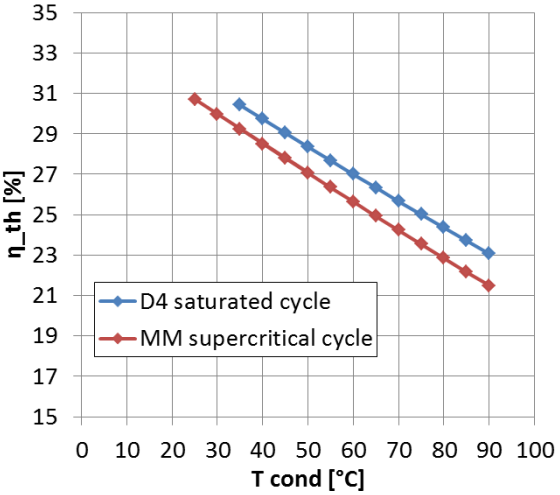

Figure 4.11: Cycle efficiency as a function of condensing temperature in both configurations for a maximum cycle temperature of 280°C

In respect of the previous analysis, a value of condensing pressure p_{cond} of 0.05 bar has to be ensured. Due to the different condensing conditions, the supercritical cycle configuration is considered as a power-only application, while the saturated one as a CHP application. The condensing pressure value p_{cond} is then increased in case of the supercritical cycle configuration with MM to ensure a minimum condensing temperature T_{cond} of 45°C. This value allows operating with air coolers. Table 4.4 reports the performance indexes and the V_r values obtained in both configurations for the two different condensing conditions.

Table 4.4: Different condensing conditions and perfomance indexes for both analyzed configurations

Cycle conditions	**Saturated cycle with D4**	**Supercritical cycle with MM**
T_{cond}	87°C	45°C
p_{cond}	0.05 bar	0.141 bar
Performance Index		
η_{th}	23.413 %	27.786 %
w_{ORC}	56.126 kJ/kg	95.583 kJ/kg
V_r	231.836	171.123

It is important to highlight that the obtained cycle efficiency and specific net work are just two parameters useful for the interpretation of the ORC itself, but cannot be used as optimization parameters. A correct evaluation among the different configurations should always refer to the whole net plant power output, system efficiency or second law efficiency.

In order to evaluate the influence of the turbine inlet pressure on the cycle efficiency for a supercritical cycle with fixed T_{max}, a parametric study of $p_{in,t}$ between 20-35 bar is performed. Figure 4.12 shows the study perfomed on the supercritical cycle at different condensing temperatures. It came out that thermal efficiency reaches its maximum value with a turbine inlet pressure close to the critical pressure value and subsequently decreases slightly for pressures higher than the critical one.

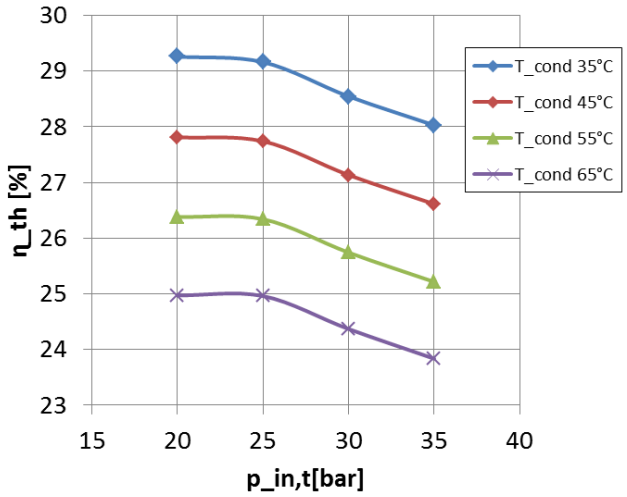

Figure 4.12: Cycle efficiency as a function of turbine inlet pressure for a maximum cycle temperature of 280°C in a supercritical cycle configuration with MM

Figure 4.13 shows in detail the changes of the enthalpy drops of the main components for a condensing temperature of 45°C. Frome here, the following conclusions can be drawn. As the turbine inlet pressure increases at constant temperature, turbine work remains approximately constant, while pump work increases. Energy recovered by the regenerator decreases with increasing turbine inlet pressure. At lower pressures the amount of heat transferred to the power cycle increases while the amount of recoverable heat in the turbine exhaust also increases.

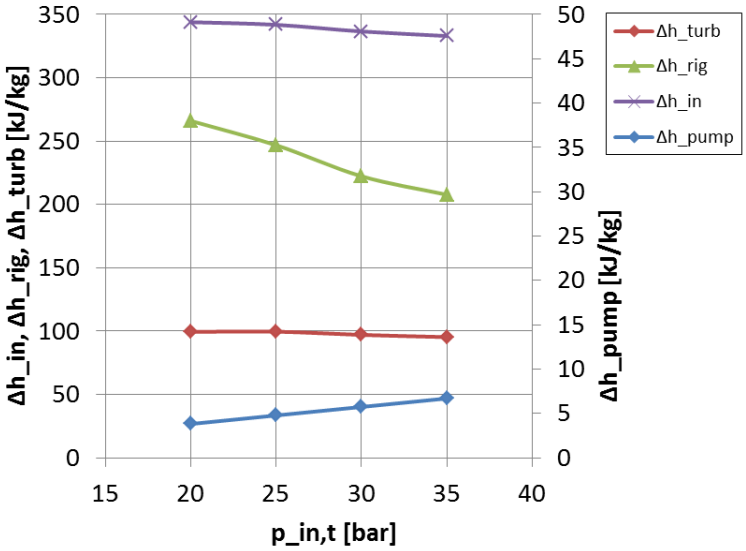

Figure 4.13: Enthalpy drops as a function of the turbine inlet pressure in a supercritical cycle configuration with MM (T_{max} = 280°C and T_{cond} = 45°C)

4.5 Integration of storage: a thermodynamic evaluation

In order to deliver dispatchable electricity a thermal energy storage system is indispensable for solar thermal power plants. As mentioned in Chapter 1, many different energy storage concepts have been proposed to be applicable for DSG solar thermal power plants considering the phase change in the used water-steam-cycle. The most promising concepts have been thermodynamically evaluated and are here extended to ORC processes using siloxanes.
In Table 4.5 a list of possible configurations is presented.

Table 4.5: Possible configurations of a DSG ORC coupled with a TES system

SCHEME OPTIONS		
Configuration	**TES Systems**	
	Indirect Two-Tank	**PCM**
Subcritical saturated cycle with D4	**X**	
	X	**X**
Supercritical cycle with MM	**X**	

Subcritical saturated cycle with D4

The first possible configuration, shown in Figure 4.14, analyses the integration with an indirect two-tank molten salt storage system, since it is the most commercially acceptable thermal storage design in today's CSP plants. As discussed in Section 1.2.3, the recirculation mode is the preferred operation mode for DSG collector fields. Therefore, this concept is applied for the saturated configuration and it requires a liquid-steam separator at the end of the evaporation section of the collector loop.

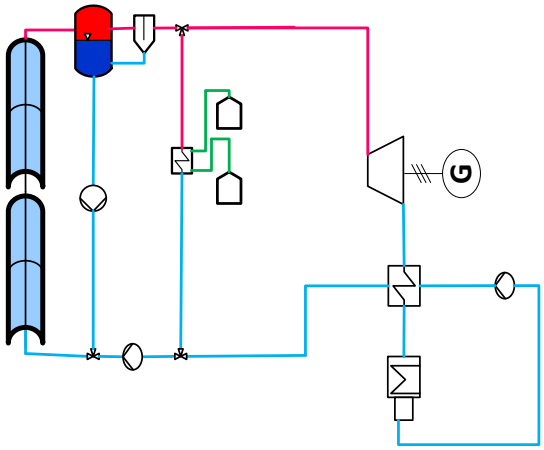

Figure 4.14: Integration of an indirect two-tank storage system in a parabolic trough power plant with a saturated ORC direct steam generation

Figure 4.15 shows a T-Q diagram of the charging process, using as well latent and sensible heat. It can be seen that all the available heat can be transferred to the molten salt. The trend of the molten salt heating curve is defined by the lower limit temperature of the molten salt and the pinch point, the point where the temperature difference is minimal. The value of the pinch point depends on the heat exchanger design and must always be positive, in order to make the heat exchange possible. The necessity to store as well sensible as latent heat leads to a higher decrease of the steam parameters between charging and discharging processes compared to a case with only sensible heat. The temperature in the discharge process is lower. In order to maintain a saturated configuration, the pressure is also lower. A lower pressure leads to lower mass flow rate in the turbine, decreasing the power output. Due to part-load operating points, the efficiency is also lower. For this reason, the gap between the steam parameters in the solar field and the steam parameters in the power block during storage operation has to be minimised. In terms of overall efficiency it is aspired to achieve high temperature levels in the storage medium, in order to reach highly efficient operation conditions in the power block during the discharging process [85]. Nevertheless, these new operation conditions are subjected to respect a new pinch point, as shown in Figure 4.16.

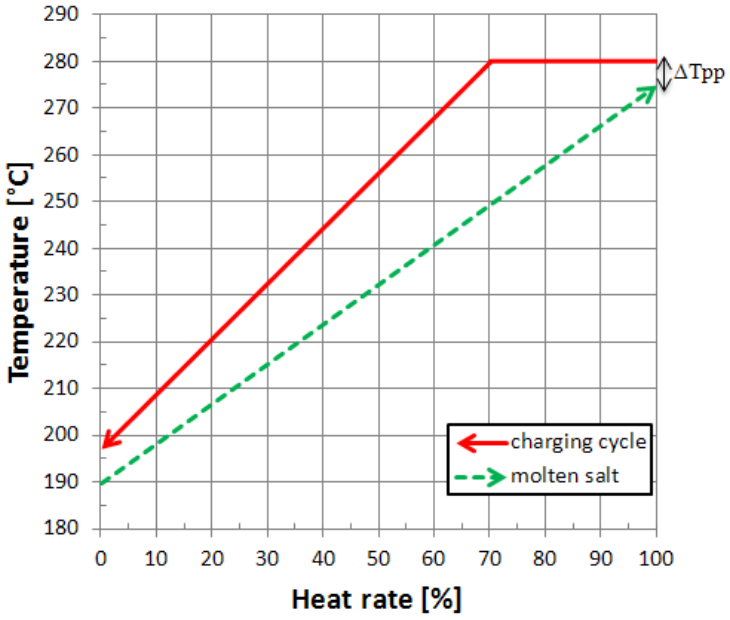

Figure 4.15: T-Q diagram of the charging process of an indirect two-tank storage system in case of a saturated cycle

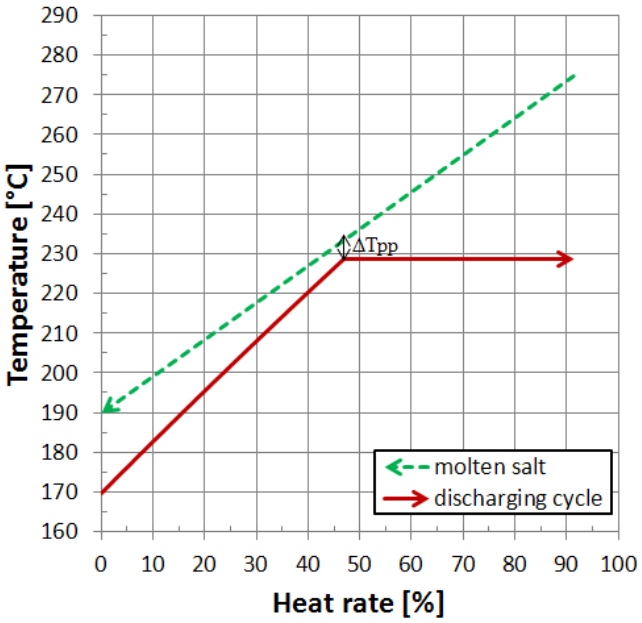

Figure 4.16: T-Q diagram of the discharging process of an indirect two-tank storage system in case of a saturated cycle

Figure 4.17 shows a configuration that couples a sensible heat with a latent heat storage based on PCMs. During the charging process, heat from the condensing steam is transferred to the melting PCM. During the discharging process, heat from the solidifying PCM is used to generate steam. As represented in the T-Q diagram of Figure 4.18, in these sections the temperature in the PCM remains constant.

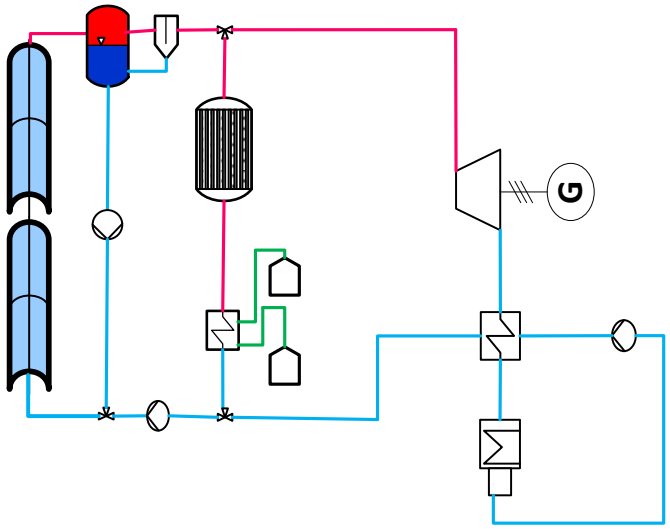

Figure 4.17: Integration of an indirect two-tank and a PCM storage system in a parabolic trough power plant with saturated ORC direct steam generation

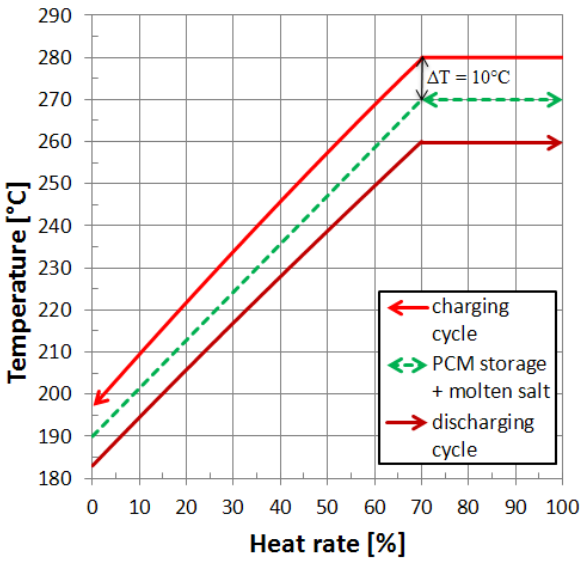

Figure 4.18: T-Q diagram of the charging and discharging process of a PCM and indirect two-tank storage system in case of a saturated cycle

In case of siloxanes the two phase-change is relatively small. Only a low amount of the available heat from the ORC cycle can be utilized for PCM storage use. Due to the limited experience in this temperature range and to the low thermal conductivity in the solid phase, storage concepts with PCMs are still in development to become cost-effective [86].

Supercritical cycle

In case of a supercritical cycle the only possible configuration is the indirect two-tank molten salt storage system (Figure 4.19).

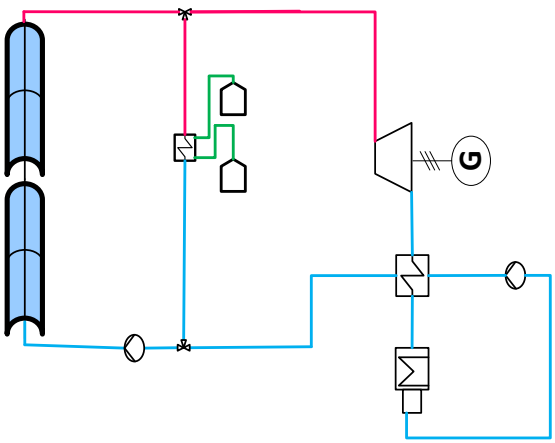

Figure 4.19: Integration of an indirect two-tank storage system in a parabolic trough power plant with a supercritical ORC direct steam generation

The T-Q diagram of the charging and discharging process is similar to the one in case of saturated cycle. Due to the pinch-point limitation, the main difference is that the supercritical cycle can obtain in the discharging process a better thermal match with the heat source than the saturated one, as reported in Figure 4.20.
Hence, it can be noted that the gap between the steam parameters in the solar field and the steam parameters in the power block during storage operation is minimised.

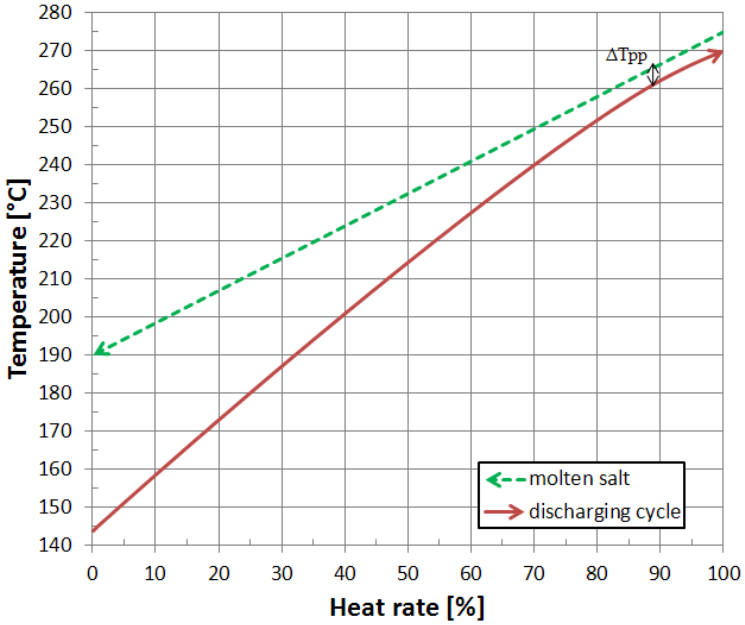

Figure 4.20: T-Q diagram of the discharging process of an indirect two-tank storage system in case of a supercritical cycle

5 Solar thermal ORC power plant Modelization

In order to assess solar thermal ORC power plant configurations, thermodynamic models in the simulation environment EBSILON®Professional have been established. The plant model consists of three major components which are described here in this chapter:

- Solar field (SF)
- Thermal Energy Storage System (TES)
- Power block (PB)

The simulation study is perfomed for both the chosen cycle configurations of Chapter 4 and is then divided into three phases:

1. Choice of the thermodynamic parameters of the cycle at design point;
2. Off-design analysis, which corresponds to the operating conditions which vary from the nominal point at different DNI;
3. Evaluation of simulation data.

5.1 Preliminary Sizing

In the simulation of both cycles the solar field is assumed to be equal. The solar field is characterized by its aperture area, type and number of collectors. In order to determine the total aperture area A_{eff} and the number of collectors, a preliminary sizing for an effective direct normal irradiation $\mathrm{DNI_{eff}}$ of 850 $\mathrm{W/m^2}$ is made. The following assumptions are considered:

1. The chosen type of collectors is the Eurotrough ET150 with the Schott receiver PTR70.

2. The proposed power plant is equipped with a TES system of 4 hours of full-load capacity. Thus, the solar field compared to the power block must be oversized. The solar multiple *SM* represents the solar field size related to the power block, in terms of nominal thermal power. In this case a *SM* equal to 1.5 is fixed [87].

3. The gross electrical power of both plants $W_{\mathrm{PB,nom}}$ is set to be 1 $\mathrm{MW_{el}}$, while

the nominal cycle efficiency $\eta_{\mathrm{th,nom}}$ is assumed to be approximately 25%.

4. The nominal solar field efficiency $\eta_{\mathrm{th,SF}}$ is assumed to be equal to 75%. In fact this value is overestimated in order to balance the assumed $\eta_{\mathrm{th,nom}}$.

Table 5.1 summarizes the data used for the preliminary sizing.

Table 5.1: Assumed parameters for the sizing of both solar power plants

Parameters	
Solar field technology	Eurotrough ET150 + Schott PTR 70
Thermal storage capacity	4 h
$\boldsymbol{W_{\mathrm{PB,nom}}}$	1 MW_{el}
$\boldsymbol{\eta_{\mathrm{th,nom}}}$	25 %
$\boldsymbol{SM}$	1.5
$\mathbf{DNI_{eff}}$	850 W/m^2
$\boldsymbol{\eta_{\mathrm{th,SF}}}$	75 %

The sizing process is now described as follows.
The total aperture area is determined using the design-point power cycle rating, the solar field efficiency $\eta_{\mathrm{th,SF}}$ and the desired solar multiple *SM*.
Since *SM* is defined as the ratio between the thermal power produced by the solar field at the design point $\dot{Q}_{\mathrm{SF,nom}}$ and the thermal power required by the power block at nominal conditions $\dot{Q}_{\mathrm{PB,nom}}$

$$\boldsymbol{SM} = \frac{\boldsymbol{\dot{Q}_{\mathrm{SF,nom}}}}{\boldsymbol{\dot{Q}_{\mathrm{PB,nom}}}} \tag{5.1}$$

the solar field thermal output at design $\dot{Q}_{\mathrm{SF,nom}}$ is calculated according to the following equation

$$\boldsymbol{\dot{Q}_{\mathrm{SF,nom}}} = \frac{\boldsymbol{W_{\mathrm{PB,nom}} \cdot SM}}{\boldsymbol{\eta_{\mathrm{th,nom}}}} \tag{5.2}$$

Hence, the total incident thermal energy $\dot{Q}_{\mathrm{inc,nom}}$ can be determined by dividing the total thermal energy output by the solar field efficiency, as shown in Equation (5.3).

$$\dot{Q}_{\mathbf{inc,nom}} = \frac{\dot{Q}_{\mathbf{SF,nom}}}{\eta_{\mathbf{th,SF}}} \tag{5.3}$$

Therefore, the effective aperture area is given by

$$A_{\mathbf{eff}} = \frac{\dot{Q}_{\mathbf{inc,nom}}}{\mathbf{DNI_{eff}}} \tag{5.4}$$

Therefore, the effective number of collectors is calculated by

$$n_{\mathbf{coll}} = \frac{A_{\mathbf{eff}}}{A_{\mathbf{coll}}} \tag{5.5}$$

By rounding off this value and estimating to an even number so as to obtain the symmetry of the collectors in each loop, the chosen number of collectors is equal to 12. In all, the gross aperture area A_{gross} is 10386 m².

5.2 EBSILON®Professional

The software used in this thesis to model the solar thermal power plant and to run thermodynamic calculation on the cycle conditions is EBSILON®Professional 10.05 (referred to as EBSILON in this thesis), a commercial simulation software developed by STEAG Energy Services GmbH. EBSILON is the abbreviation for "energy balance and simulation of the load response of power generating or process controlling network structures". It is a Windows-based modeling tool with a graphical user interface that allows the drag-and-drop arrangement of multiple pre-built components connected by material and logic lines to simulate thermodynamic cycle processes for power plants in the steady state.
As shown in Figure 5.1, the basic control elements and tool bars are:

- Standard toolbar
- Component bar, for selecting a component from a category
- Component wizard bar, for accessing components classified by numbers
- Ebsilon bar, for starting simulations
- Zoom bar, for zooming in the model and finding objects

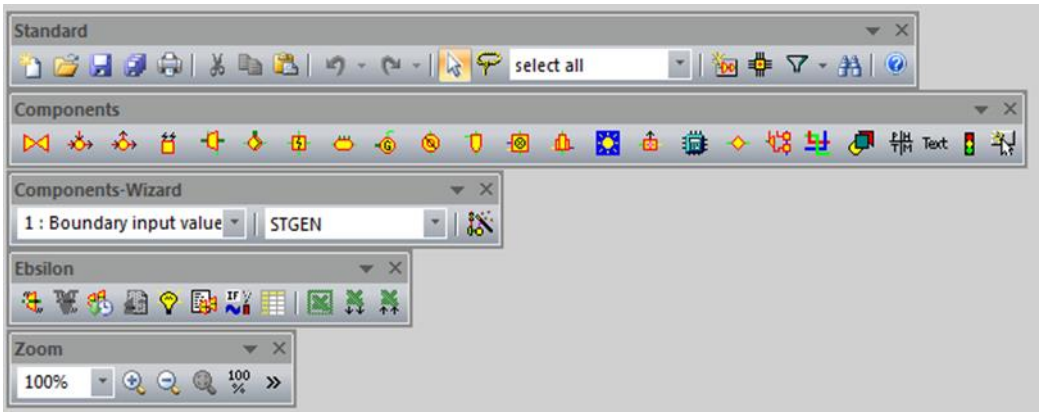

Figure 5.1: EBSILON control elements and tool bars

After defining the design of the cycle, it is necessary to define the values that characterize it. There are two ways of doing that:

1. Some components can be defined directly in their component properties window, like e.g. the Sun (Component 117), as shown in Figure 5.2

2. The other possibility is to set a value (e.g. mass flow, temperature or pressure) directly on a pipe of the cycle using the "Measured/General value input" (Component 46 or 33), as shown in Figure 5.3.

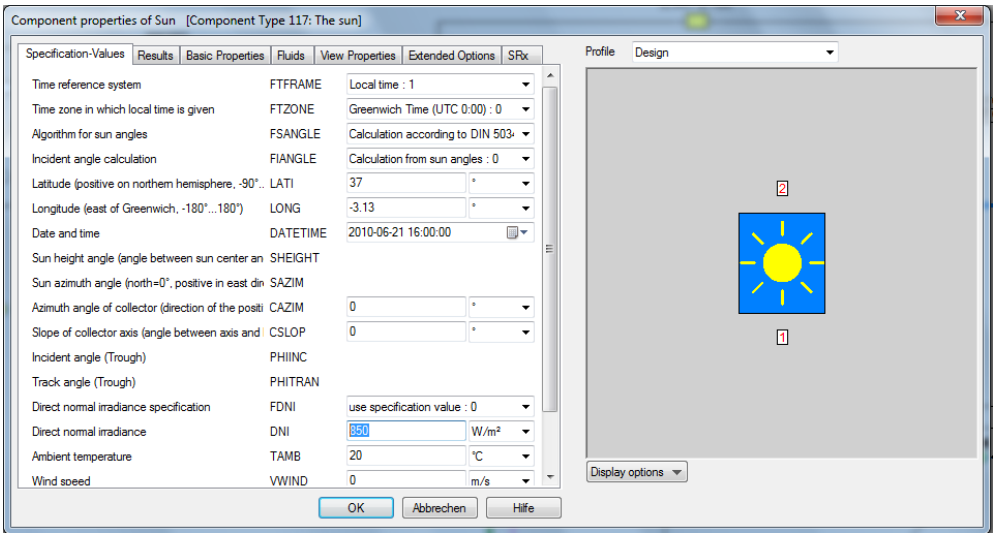

Figure 5.2: Defining data of a component in EBSILON

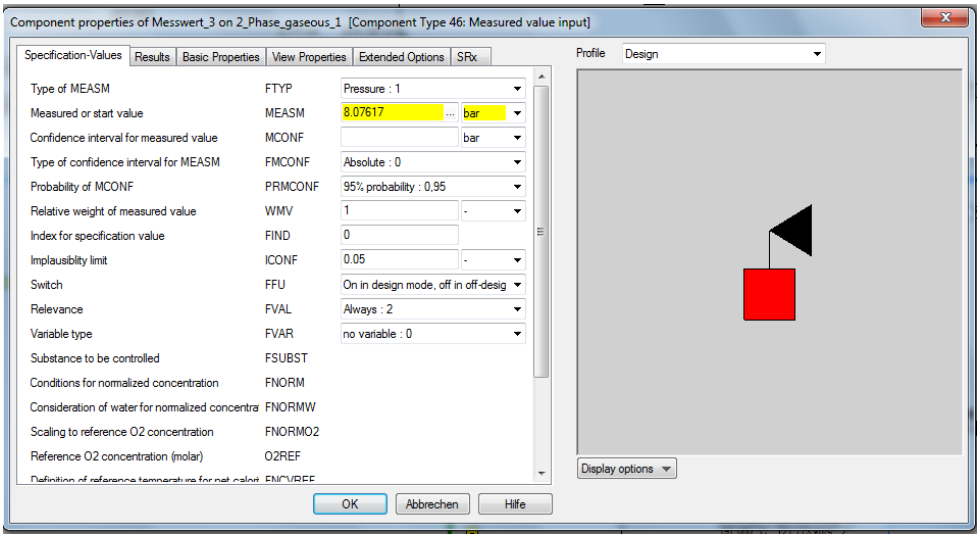

Figure 5.3: Defining data of a pipe in EBSILON

A variety of fluids, such as water, gases, heat transfer fluids, and combustibles are implemented in EBSILON. Additionally, fluid properties from the REFPROP library, distributed by NIST [88], can be used. The present thesis makes use of the fluid properties of the siloxanes MM and D4.

Only if all necessary values have been supplied, and the system is completely determined, a power plant process simulation can be successfully computed.

EBSILON is composed of two calculation modes:

• Design Calculation ("full load")
• Off-design Calculation ("part load")

In the design mode, the calculation runs using the user defined specification values for all components for a nominal operating point in order to store the results as reference values for off-design and allow the components to be sized. In off-design mode components are then fixed and simulations can be performed for different sets of input data. In all standard EBSILON components correlations for the calculation of off-design operating-points are implemented. EBSILON offers the possibility of handling different cycle cases in "profiles" in a tree-like hierarchy. Profiles help the user to manage several variations of one cycle within one document. This is especially useful for handling design and off-design calculations as well as property data variation. The root of this tree is always the design case. An example of such a hierarchy scheme is shown in Figure 5.4.

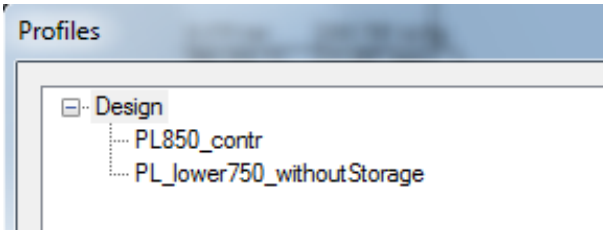

Figure 5.4: Hierarchy tree in EBSILON

The subprofiles inherit all properties, such as the specification values and characteristics of all components, from its parent. In this thesis the parent profile is always the design case, so that nearly all parameters values are assigned in the root profile. In the respective subprofiles the analysed parameter (e.g. DNI) and the operational parameters can be defined or changed in order to meet the plant control strategies.

5.3 Solar field

The modeling of the main components of the solar field (e.g. the sun, line focusing collectors, piping and headers) is carried out taking advantage of the add-on EbsSolar library [89], developed in cooperation with the DLR.

5.3.1 The sun

In EBSILON, the sun is represented by Component 117. According to DIN 5034 [90], the solar azimuth (γ_s) and solar height angle (α_s), both shown in Figure 5.5, are calculated using the inputs of local time, latitude, and longitude.

Assuming that the PTC is not built on a slope and the collector axis is oriented north-south ($\gamma_c = 0$), the tracking angle (ρ) and the incident angle (θ_i) can be calculated with equations (5.6) and (5.7).

$$\tan\rho = \frac{\sin\gamma_s}{\tan\alpha_s} \tag{5.6}$$

$$\cos\theta_i = \sqrt{1 - \cos^2\alpha_s \cos^2\gamma_s} \tag{5.7}$$

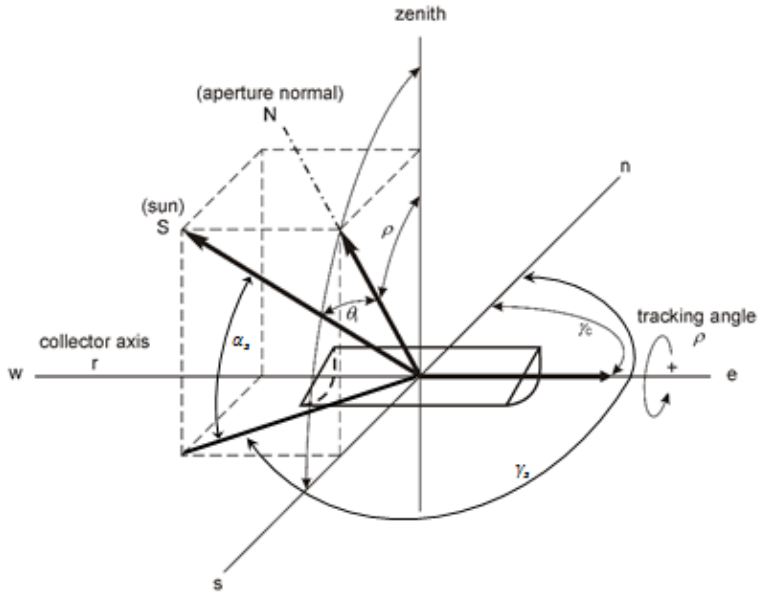

Figure 5.5: The angles of a parabolic trough collector in relation to the sun adapted from [91]

5.3.2 Parabolic trough collector

For the simulation the EuroTrough collector with the Schott PTR70 receiver has been chosen. The selected PTC is modelled in EBSILON by Component 113, represented in Figure 5.6. Equations for heat balance and pressures drops are implemented in this component and are described in detail in the following subsections.

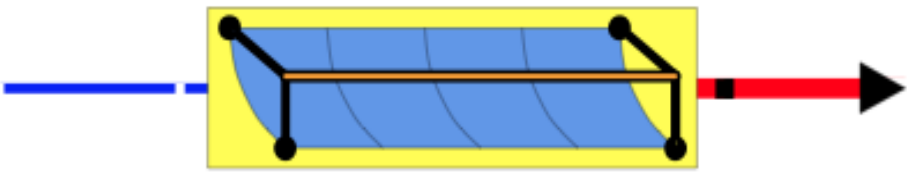

Figure 5.6: Representation of the parabolic trough collector model in EBSILON

Heat balance

The effective heat transferred to the fluid flow is calculated by the difference between the incoming optical thermal power $\dot{Q}_{\text{solar}}$ and the total heat losses that occur in the receiver $\dot{Q}_{\text{loss}}$, as shown in Equation (5.8).

$$\dot{\boldsymbol{Q}}_{\mathbf{col,eff}} = \dot{\boldsymbol{Q}}_{\mathbf{solar}} - \dot{\boldsymbol{Q}}_{\mathbf{loss}} = \\ = \mathbf{DNI} \cdot \mathbf{cos}(\boldsymbol{\theta_i}) \cdot \boldsymbol{A}_{\mathbf{eff}} \cdot \boldsymbol{\eta}_{\mathbf{opt,0}} \boldsymbol{\eta}_{\mathbf{clean}} \boldsymbol{\eta}_{\mathbf{shad}} \boldsymbol{\eta}_{\mathbf{end}} \mathbf{IAM}(\boldsymbol{\theta_i}) \cdot \boldsymbol{f}_{\mathbf{tr}} - \dot{\boldsymbol{Q}}_{\mathbf{loss}} \tag{5.8}$$

with:

- $\eta_{\mathrm{opt,0}}$: optical peak efficiency;
- η_{clean} : reflecting mirror cleanliness factor;
- η_{shad} : shading loss factor;
- η_{end} : end loss factor;
- $\mathrm{IAM}(\theta_i)$: incident angle modifier as a function of θ_i in degree;
- f_{tr} : focusing state of the collector;
- $\dot{Q}_{\mathrm{loss}}$: thermal losses of the receiver.

In the simulation of on-design conditions (with incidence angle set to 0°), $\eta_{\mathrm{opt,0}}$ and η_{clean} are set respectively to 0.75 and 1 [87]. For a further explanation of these efficiency factors see Appendix. With an incidence angle of 0°, reciprocal shading effect and endlosses effect do not occur.

The incident angle modifier (IAM) accounts for optical losses and spillage of solar radiation with increasing incident angle. The IAM is described by a second-order polynomial correlation:

$$\mathbf{IAM}(\boldsymbol{\theta_i}) = \mathbf{max}\left(\mathbf{0}, \left(\mathbf{1} + \frac{\boldsymbol{a_1} \cdot \boldsymbol{\theta_i}}{\boldsymbol{cos\theta_i}} + \frac{\boldsymbol{a_2} \cdot \boldsymbol{\theta_i^2}}{\boldsymbol{cos\theta_i}}\right)\right) \tag{5.9}$$

where a_1 and a_2 are two empiric parameters. The measured parameters of the EuroTrough collector are the following [92]:

a_1 = 0.00010596;
a_2 = -0.00017091.

Figure 5.7 shows the graphical representation of the IAM correlation.

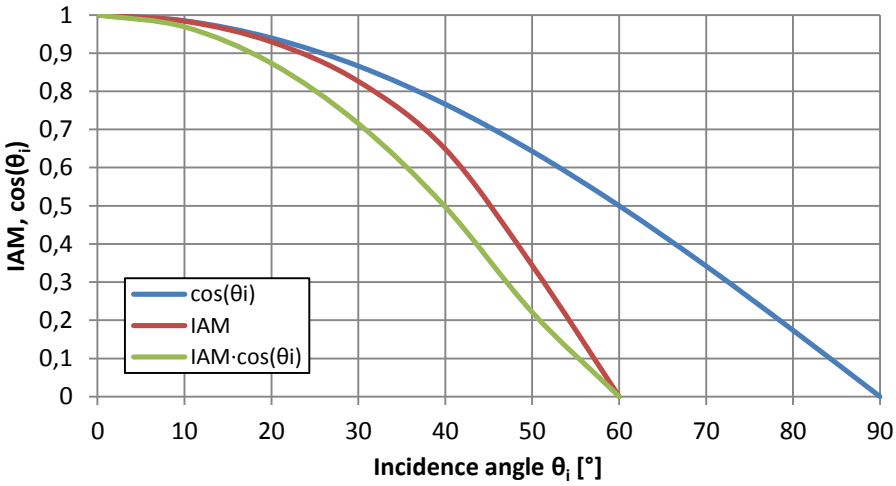

Figure 5.7: IAM correlation of the Eurotrough collector

The focusing state of the collector (f_{tr}) is a parameter that simulates the defocusing of the PTCs. It can assumed a value between 0 and 1, with 0 being a completely defocused state and 1 being normal.

The total heat losses in the receiver $\dot{Q}_{\mathrm{loss}}$ are due to convection, radiation and conduction in and around the receiver, as shown in Figure 5.8 [93]. In order to specify all the heat transfers, the nomenclature is specified in Table 5.2.

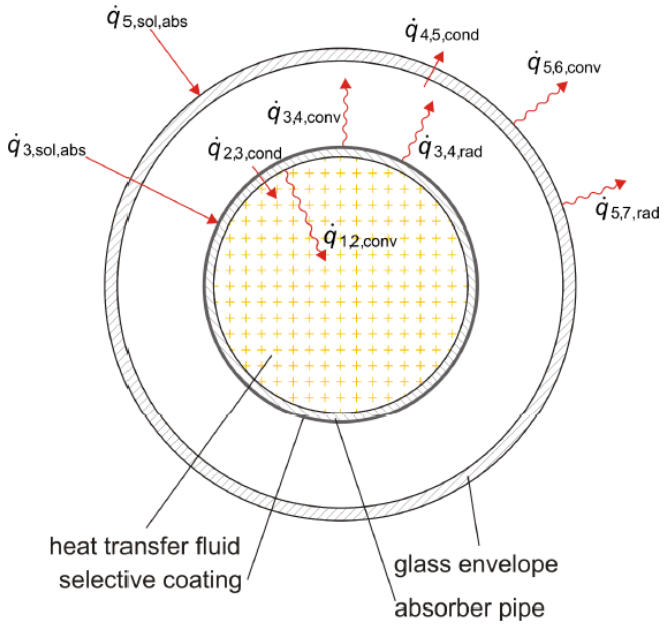

Figure 5.8: One-dimensional heat balance of a receiver [91]

Table 5.2: Nomenclature for 1-dimensional heat balance of a receiver

Heat flux [W/m]	Heat Transfer type	From	to
$\dot{q}_{1,2,conv}$	Convection	Absorber inner surface	Heat transfer fluid
$\dot{q}_{2,3,cond}$	Conduction	Absorber outer surface	Absorber inner surface
$\dot{q}_{3,sol,abs}$	Radiation	Sun	Absorber outer surface
$\dot{q}_{5,sol,abs}$	Radiation	Sun	Glass envelope outer surface
$\dot{q}_{3,4,conv}$	Convection	Absorber outer surface	Glass envelope inner surface
$\dot{q}_{3,4,rad}$	Radiation	Absorber outer surface	Glass envelope inner surface
$\dot{q}_{4,5,cond}$	Conduction	Glass envelope inner surface	Glass envelope outer surface
$\dot{q}_{5,6,conv}$	Convection	Glass envelope outer surface	Surrounding air
$\dot{q}_{5,7,rad}$	Radiation	Glass envelope outer surface	Sky

At high temperatures, as well as in this case, conduction can be neglected [91]. The convective heat losses can be defined as

$$\dot{Q}_{conv} = h_{conv} \cdot A_{abs} \cdot (T_{abs} - T_{amb}) \tag{5.10}$$

where h_{conv} is the heat transfer coefficient for convection due to the wind, A_{abs} the absorber surface area, T_{abs} the absorber temperature and T_{amb} the ambient temperature.

The radiation losses can be approximated by Stefan's law and are defined as

$$\dot{Q}_{rad} = A_{abs} \cdot \varepsilon \cdot \sigma \cdot \left(T_{abs}^4 - T_{amb}^4\right) \tag{5.11}$$

where ε is the emissivity of the receiver and σ is Stefan's constant equal to $5.67 \cdot 10^{-8}$ W/m^{2}K^4.

Thus, the total heat losses are given by Equation (5.12) and are usually expressed as length-based values in W/m.

$$\begin{aligned} \dot{q}_{loss} &= \dot{q}_{5,6,conv} + \dot{q}_{5,7,rad} = \\ &= h_{conv} \cdot \pi D_{abs} \cdot (T_{abs} - T_{amb}) + \pi D_{abs} \cdot \varepsilon \cdot \sigma \cdot \left(T_{abs}^4 - T_{amb}^4\right) \end{aligned} \tag{5.12}$$

In practice, manufacturers usually provide an approximating fourth order polynomial correlation for their receiver heat losses. The length-specific heat

loss of the receiver tube Schott PTR70 is given in Equation (5.13) and the resulting curve is shown in Figure 5.9 [94].

$$\dot{q}_{\mathbf{loss}} = \mathbf{0,141} \cdot T_{\mathbf{abs,°C}} + \mathbf{6,48} \cdot \mathbf{10^{-9}} \cdot T^{\mathbf{4}}_{\mathbf{abs,°C}} \tag{5.13}$$

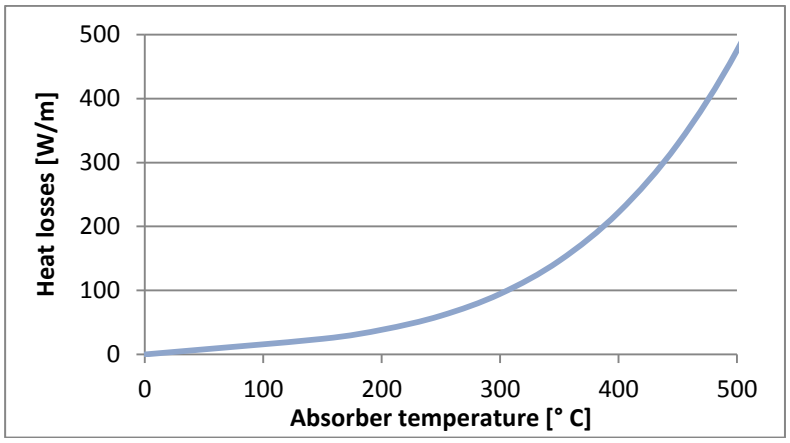

Figure 5.9: Heat loss curve of Schott PTR70 [94]

The receiver temperature and the fluid temperature are considered almost equal and Equation (5.13) is used for the EBSILON model.

Table 5.3 summarizes the parameters used as input in EBSILON.

Table 5.3: Parameters of the PTC EuroTrough ET150 + Schott PTR70 receiver

Property	EuroTrough ET150 + PTR70
Outer diameter	0.07 m
Inner diameter	0.0654 m
Focal length	1.71 m
Gross aperture width	5.77 m
Length	150 m
Optical active portion of aperture	0.9461
Row spacing (absolute)	17.28 m (*)
Pipe wall roughness	10^{-6} m
Peak optical efficiency	75 %
Mirror cleanliness factor	100 %
Parameter IAM long (const. term)	1
Parameter IAM long (lin. term)	0.00010596
Parameter IAM long (quad. term)	-0.00017091
Heat loss (lin. term in T)	0.141
Heat loss (^4 term in T)	$6.48 \cdot 10^{-9}$
(*) see Appendix	

Pressure drops

Pressure drops that occur in the absorber tube of the collector are composed of two parts, the frictional pressure drops $\Delta p_{\mathrm{frict}}$ and the momentum pressure drops (acceleration) Δp_{mom}.

$$\boldsymbol{\Delta p_{tot} = \Delta p_{frict} + \Delta p_{mom}} \tag{5.14}$$

Both pressure drops are calculated based on state-of-the-art correlations already implemented in EBSILON. The correlations used differ depending on whether the flow is single-phase or two-phase.

For a single-phase flow, the frictional pressure drop is calculated with the Darcy-Weisbach equation (5.15), with the coefficient of friction determined in case of turbulent flow by the Colebrook equation (5.16):

$$\boldsymbol{\Delta p_{frict} = f \cdot \frac{\Delta L}{D_{abs}} \cdot \rho \cdot \frac{v^2}{2}} \tag{5.15}$$

with

$$\boldsymbol{\frac{1}{\sqrt{f}} = -2 \cdot \log_{10}\left(\frac{\frac{\varepsilon}{D_{abs}}}{3.7} + \frac{2.51}{Re_{D_{abs}} \cdot \sqrt{f}}\right) \rightarrow Re_{D_{abs}} > 2300} \tag{5.16}$$

$$\boldsymbol{f = \frac{64}{Re_{D_{abs}}} \rightarrow Re_{D_{abs}} < 2300} \tag{5.17}$$

where:

f	:	coefficient of friction
$Re_{D_{\mathrm{abs}}}$	:	Reynolds number
D_{abs}	:	absorber pipe inner diameter (m)
ε	:	absolute internal pipe roughness (m)
ρ	:	mean density (kg/m^3)
v	:	mean velocity (m/s)

The momentum pressure drop reflects the change in kinetic energy of the flow and is calculated for a single-phase flow according to Equation (5.18).

$$\Delta p_{mom} = \rho_{out} \cdot \frac{v^2_{out}}{2} - \rho_{in} \cdot \frac{v^2_{in}}{2} \tag{5.18}$$

Two-phase pressure drops, as needed for direct steam generation applications, can be calculated with the empirical correlation of Friedel [95]. This correlation is also implemented in the collector models in EBSILON.
In order to evaluate the two-phase frictional pressure drop, the single liquid-phase pressure drop is multiplied with a two-phase multiplier [25]:

$$\Delta p_{frict,two-phase} = \Delta p_{frict,liq} \cdot \Phi_l^2 \tag{5.19}$$

The two-phase multiplier is calculated by Equation (5.20), which is valid for viscosity ratios of $\frac{\mu_g}{\mu_l} \leq 1500$.

$$\Phi_l^2 = (1-x)^2 + x^2 \frac{f_g}{f_l} \cdot \frac{\rho_l}{\rho_g} + 3.43 \cdot x^{0.69} \cdot (1-x)^{0.24} \cdot \cdot \left(\frac{\rho_l}{\rho_g}\right)^{0.8} \cdot \left(\frac{\mu_g}{\mu_l}\right)^{0.22} \cdot \left(1 - \frac{\mu_g}{\mu_l}\right)^{0.89} \cdot Fr_l^{-0.047} \cdot We_l^{-0.033} \tag{5.20}$$

where:

x : vapor quality
f_g : coefficient of friction for the singles gas-phase
f_l : coefficient of friction for the single liquid-phase

Weber and Froude number are calculated as follows:

$$We_l = \frac{16 \cdot \dot{m}^2}{\sigma \cdot \rho_l \cdot \pi^2 \cdot d^5} \tag{5.21}$$

$$Fr_l = \frac{16 \cdot \dot{m}^2}{g \cdot \rho_l^2 \cdot \pi^2 \cdot d^5} \tag{5.22}$$

where:

σ : surface tension (N/m)
g : gravitational acceleration (m/s^2)

The two-phase momentum pressure drop is given by

$$\Delta p_{\mathrm{mom}} = \dot{G}^2 \left\{ \left[\frac{(1-x)^2}{\rho_{\mathrm{l}}(1-\varepsilon)} + \frac{x^2}{\rho_{\mathrm{g}}\varepsilon} \right]_{\mathrm{out}} - \left[\frac{(1-x)^2}{\rho_{\mathrm{l}}(1-\varepsilon)} + \frac{x^2}{\rho_{\mathrm{g}}\varepsilon} \right]_{\mathrm{in}} \right\} \tag{5.23}$$

where $\dot{G}$ is the mass velocity (kg/m^{2}s) and ε is the void fraction calculated as follows:

$$\varepsilon = \frac{x}{\rho_{\mathrm{g}}} \left[(1 + 0.12(1-x))\left(\frac{x}{\rho_{\mathrm{g}}} + \frac{1-x}{\rho_{\mathrm{l}}}\right) + \frac{1.18(1-x)\left[g\sigma(\rho_{\mathrm{l}} - \rho_{\mathrm{g}}\right]^{0.25}}{\dot{G}^2 \rho_{\mathrm{l}}^{0.5}} \right]^{-1} \tag{5.24}$$

5.3.3 Layout

The solar field consists of:

- A cold distributing header, where the mass flow coming from the power block is split into several collector loops;
- A number of loops consisting of 2 or more PTCs connected in series trough a "U" configuration;
- A hot collecting header, that collects the fluid from the loops to the power block.

The solar field can be arranged in different layouts. For traditional solar thermal plants working with HTF, two field layouts are usually adopted: an 'H' field layout for collector field areas greater than 400000 m^2, and an 'I' field layout for areas less than 400000 m^2 [96]. Other layouts have been proposed for specific class of power plant. As shown in Figure 5.10, the chosen solar field's layout for the small-scale DSG-ORC power plant consists of 6 collector loops, each consisting of 2 Eurotrough ET150 collectors.

In order to minimize the mutual shading phenomenon (Appendix) and to ensure accessibility to the collector loops, an optimum value for the distance between the rows of collectors (d_{row}) is used. A trade-off between land-use and shading phenomenon suggests adopting a value equal to approximately 3 times the collector width [91]. According to state-of-the-art row distance, a value of 17.28 m has been set.

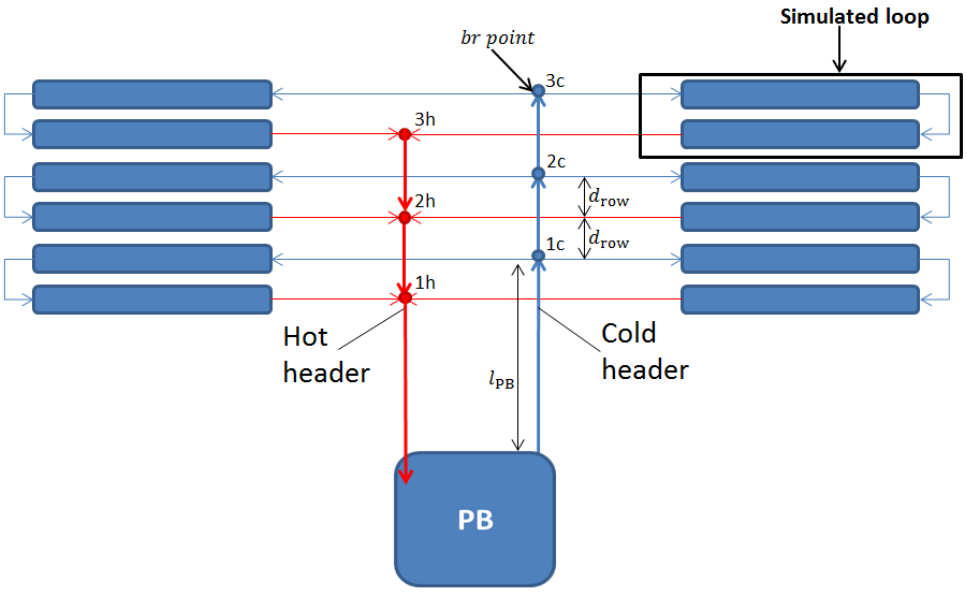

Figure 5.10: Solar field layout, consisting of 6 collector loops with 2 collectors per loop

In case of the saturated configuration, the recirculation mode is applied. For compact water-steam separators in DSG systems, the inlet steam quality is normally set between 0.7-0.8 [26]. In this case the two-phase flow exits the solar field with an imposed vapor quality x of 0.5 [87], in order to be more conservative. Downstream of the solar field, the liquid phase is separated and recirculated while saturated steam (with $x = 1$) is flows to the turbine.

The simulation in EBSILON models only one representative PTC loop. Thus, in order to consider the whole solar field, the mass flow rate of the fluid is increased by a factor of six after the loop.

Piping and headers

As mentioned before, headers are installed for distributing and collecting the working fluid in the collector field. In both headers heat and pressure losses occur.

In order to identify the piping heat losses, a heat loss factor $q_{\mathrm{loss,H\&P}}$ of 10 W/m^2 found in literature [97] has been used. The total heat losses of headers and piping are then calculated according to Equation (5.25).

$$\dot{Q}_{\mathrm{loss,H\&P}} = q_{\mathrm{loss,H\&P}} \cdot A_{\mathrm{gross}} \tag{5.25}$$

In order to identify the piping pressure drop, the pressure drop in the flow to the outermost loop should be calculated. In fact, it defines the pressure drop in the flows through all of the loops. The pressure drop in the inner loops is set equal to the pressure drop in the last loop by the throttling action of valves in the inner loops. A simplified scheme of this hydraulic analysis is represented in Figure 5.11.

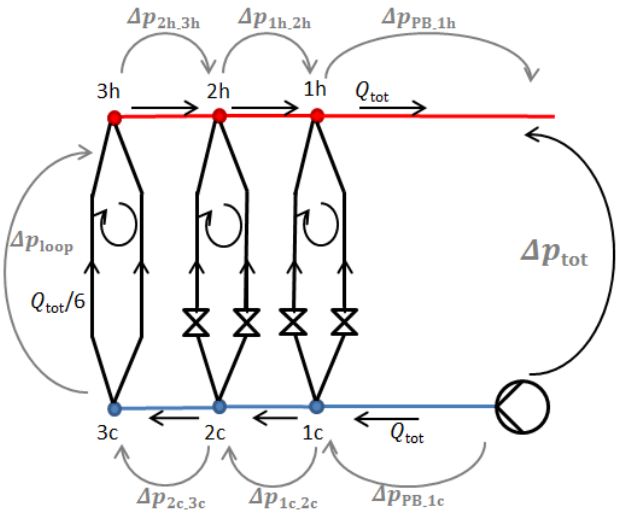

Figure 5.11: Simplified scheme of hydraulic analysis pipe network

In order to approximate the frictional pressure drop, the correlations described previously for the collector are still valid and a simple model has been run in EBSILON. Firstly, lengths and inner diameters of both header pipes have to be sized. Referring to Figure 5.10, the total length of one header (l_h) depends on the number of branches (n_{br}), on the row distance between the collectors (d_{row}) and on the distance from the PB to the first loop (l_{PB}):

$$\boldsymbol{l_h = (n_{br} - 1) \cdot d_{row} \cdot 2 + l_{PB}} \tag{5.26}$$

The chosen sizing for the inner diameter is based on maintaining constant the fluid velocity along the pipe length. This characteristic involves a theoretical pipe diameter modification every time the mass flow changes. Cold header pipe diameter decreases as the distance from the power block increases (Figure 5.12), whereas hot header pipe diameter increases as the distance to the power block decreases.

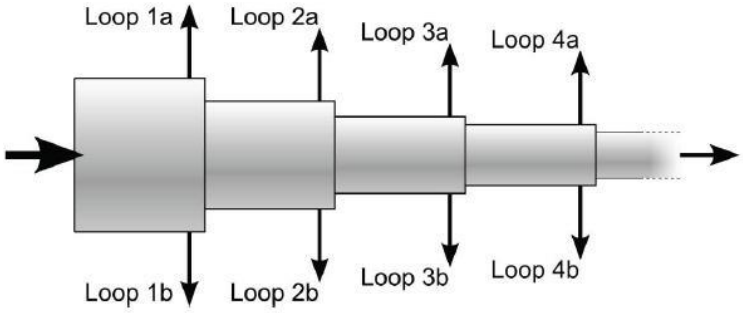

Figure 5.12: Schematic representation of a cold header

In order to determine the optimum diameter of each header section, the design velocity has been set to 2 m/s for the liquid flow in the cold heater and to 10 m/s for the vapour flow in the hot header [87]. Once the diameters are selected, the frictional pressure drops are carried out.

Hence, the total pressure drops for both configurations can be calculated for each header. For simplicity, pressure drops through the pipe fittings (e.g. elbows or tees) are neglected.

5.4 Thermal storage system

The thermal storage system consists of a hot and a cold tank. In respect of the temperature range of the cycle (195°C-280°C), and of its availability in EBSILON, the chosen storage media is HITEC molten salt. Its characteristics are compared with the ones of the thermal oil and other types of molten salt in Table 5.4.

Table 5.4: Molten salt and Therminol VP-1 properties

Salt	Solar Salt	HITEC	HITEC XL	Therminol VP-1
Composition (%)				biphenyl/diphenyl
$NaNO_3$	60	7	7	
KNO_3	40	53	45	
$NaNO_2$		40		
$Ca(NO_3)_2$			48	
Maximum temperature (°C)	600	535	500	400
Melting temperature (°C)	220	142	120	13
Density @ 300°C (kg/m^3)	1899.2	1864.8	1992	815
Heat capacity @ 300°C (J/kgK)	1391.4	1561.7	1447	2319
Nominal cost ($/kg)	0.49	0.93	1.19	2.2

The thermal storage system is then modelled using a simple energy balance approach that includes charging and discharging energy rates, thermal losses and

general sizing inputs. As shown in Figure 5.13, the solar field circuit and the storage tank circuit are connected with a heat exchanger. Component 118 represents a tank equipped with two connections, one for an inflow and one for an outflow. The concept of two connections is chosen, because in EBSILON modeling flow reversal is not feasible. In EBSILON the storage model itself is not responsible for keeping the load state within tolerated limits "empty" or "full". This task as well as supervising consistence with minimum and maximum mass flow rates during charge or discharge operation has to be solved by use of control or limiter components.

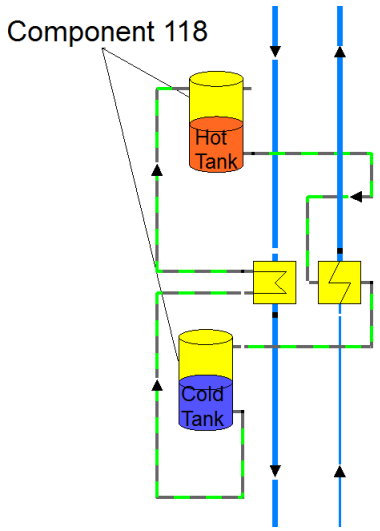

Figure 5.13: Representation of the indirect two-tank storage system in EBSILON

The organic working fluid in both cycle configurations leaves the solar field at approximately 280°C and is then pumped directly to the turbine or, in storage system charging mode, to the heat exchanger. There, the HITEC solar salt coming from the cold tank at $T_{\mathrm{TES,cold}}$ (190°C) is heated up to $T_{\mathrm{TES,hot}}$ (275°C), the design temperature level of the hot tank. The design temperature value of the cold tank is chosen in order to avoid the melting temperature of the salt, while the one of the hot tank in order to ensure a ΔT_{pp} of 5°C during the charging process. Hence, for storage system charging mode, three temperature boundary conditions are already given. The remaining free variable is either the organic working fluid outlet temperature or one of the two fluid mass flow rates. In this study the design mass flow rate of the organic fluid in charging mode is assumed to be approximately 8.44 kg/s in case of D4 and 8.53 kg/s in case of MM. The corresponding mass flow rate of the molten salt and the organic fluid outlet temperature (solar field return temperature) is calculated for steady state.
For storage system discharging mode, the HITEC salt feed and drain temperatures are given as well. Here, the hot salt at 275°C is pumped from the

hot tank, through the heat exchanger, and fed into the cold tank at 190°C. The organic fluid inlet temperature corresponds to the regenerator exit temperature. The remaining free variable is either the organic fluid outlet temperature or one of the two fluid mass flow rates. In contrast with the charging mode, this kind of approach is valid only in case of MM (supercritical cycle). Here, the HITEC mass flow rate is set and the corresponding mass flow rate of the organic fluid and its outlet temperature (turbine inlet temperature) are calculated for steady state. In case of D4, due to the saturated cycle configuration, remaining free variables are not allowed and only one possible charging mode exists. As we will see in next chapter, this charging mode has to be determined performing a pinch-point analysis in the heat exchanger. Figure 5.14 shows a simplified scheme of the charging and discharging modes in an indirect two-tank storage system.

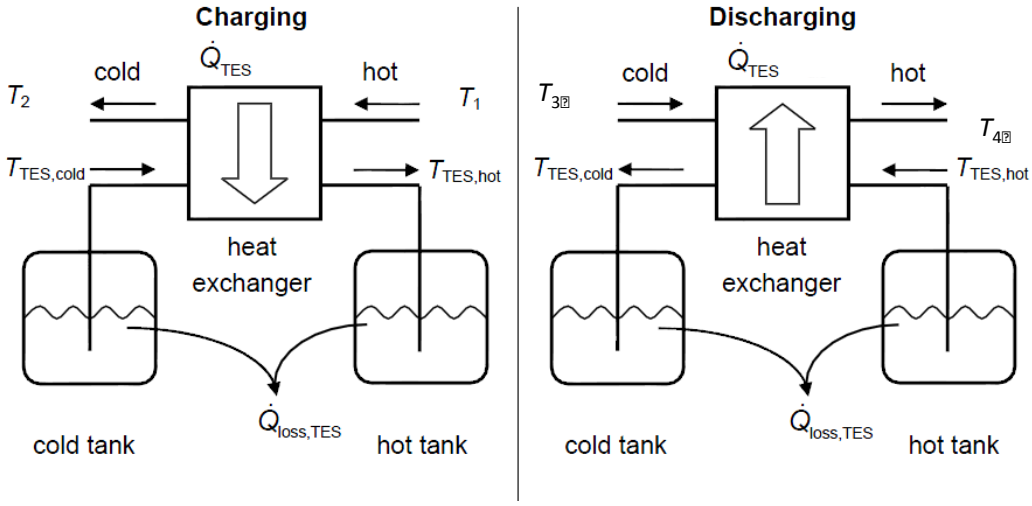

Figure 5.14: Scheme of charging and discharging modes in an indirect two-tank storage system adapted from [91]

The thermal capacity of the storage is evaluated with Equation (5.27), assuming 4 hours of full-load operation (power block in storage-only mode).

$$\boldsymbol{Q_{storage} = \frac{W_{PB,nom}}{\eta_{th,nom}\eta_{dis}} \cdot \Delta t = m_{salt} \cdot \bar{c}_p \cdot (T_{TES,hot} - T_{TES,cold})} \qquad (5.27)$$

where η_{dis} is the discharge efficiency due to the heat losses in the heat exchangers.

Each storage tank has the same volume calculated as follow

$$\boldsymbol{V_{\text{storage}} = \frac{Q_{\text{storage}}}{\overline{\rho c_{\text{p}}} \cdot \Delta T_{\text{TES}}}} \tag{5.28}$$

The evaluated tank capacity is then increased taking into account the thermal losses and a security gap.

In this study the dependence of the heat losses from the salt temperature and from the fill level of each tank has been neglected. Heat losses $\dot{Q}_{\text{loss,TES}}$ are expressed as function of the capacity Q_{storage} with an empiric factor *a*:

$$\boldsymbol{\dot{Q}_{\text{loss,TES}} = a \cdot Q_{\text{storage}}} \tag{5.29}$$

A maximal heat loss of 1% of the storage capacity per 12 hours corresponds to an *a* value of $2.3148 \cdot 10^{-11}$ 1/s [91].

Table 5.5 summarizes the specific data of the storage system used as input in EBSILON. Pressure drops in the heat exchangers are neglected.

Table 5.5: Specific data of the TES system used in EBSILON

	Cold TES	Hot TES
Diameter	9.5 m	9.5 m
Height	3.5 m	3.5 m
Mass at full state	460 t	460 t
Temperature in storage	190°C	275°C
Pressure in storage	1.5 bar	1.5 bar

5.5 Power block

As mentioned before, the PB's gross electrical power is approximately 1 MW, and a turbine inlet temperature of 280°C is chosen for both the saturated and the supercritical cycles. For the construction of the PB in EBSILON, proper components available in its standard library have been selected. All the data assumed to characterize each component are reported in details in the following sub-sections, while the equations to define their performances can be found in Chapter 4, Section 4.2.

5.5.1 ORC Turbine

The ORC turbine is designed with Component 6 (Figure 5.15) and is then connected to a generator (Component 11) with a generator efficiency η_{gen} of 0.96. In nominal conditions, the turbine is defined by several parameters as the isentropic efficiency ($\eta_{\mathrm{is,T}}$ = 0.83) and the mechanical efficiency ($\eta_{\mathrm{o\&}m}$ = 0.998) [98]. The nominal inlet pressure is set by using a "general input value" in accordance with the chosen values.

For the supercritical cycle, the value of the turbine inlet pressure has been analysed from a thermodynamic point of view in Chapter 4. Even if a value close to the critical pressure leads to slightly higher cycle performances, in the simulation model a higher pressure value is used. As explained further, in this case a turbine inlet pressure of 30 bar is used in order to avoid the two-phase region in off-design mode.

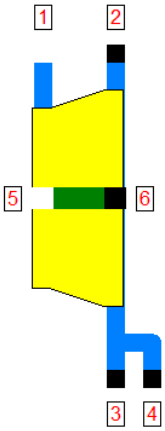

Figure 5.15: Representation of the turbine in EBSILON

In order to perform off-design simulations, the turbine operates usually in sliding pressure (see Section 6.2) following the Stodola's Cone Law [99]. Once the design parameters are given, the law determines the relationship between the turbine inlet and outlet pressure and the mass flow through the turbine.
Figure 5.16 shows this dependence in a 3-dimensional diagram that has the shape of a degenerate quadric surface, the cone directrix being an ellipse.

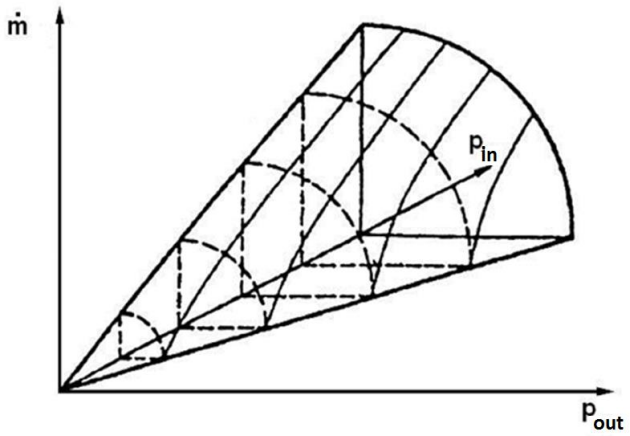

Figure 5.16: Graphic representation of Stodola's cone law

Considering an ideal gas, the Stodola's Cone law equation can be simplified to [100]:

$$\frac{\dot{m}}{\dot{m}_N} = \frac{p_{in}}{p_{out}} \cdot \sqrt{\frac{1 - \left(\frac{p_{out}}{p_{in}}\right)^2}{1 - \left(\frac{p_{out,N}}{p_{in,N}}\right)^2}} \cdot \sqrt{\frac{T_{in,N}}{T_{in}}} \tag{5.30}$$

where "$\dot{m}$" is the mass flow rate, "p" the pressure and "T" the temperature in the turbine respectively. The sub-index "in" stands for the inlet value, "out" for the outlet value and "N" for the design values.

Thus, from a given mass flow the corresponding turbine inlet pressure required by the turbine nozzle area can be calculated in according to Equation (5.31):

$$p_{in} = \sqrt{p_{out}^2 + \left(\frac{\dot{m}}{\dot{m}_N}\right)^2 \cdot (p_{in,N}^2 - p_{out,N}^2) \cdot \frac{T_{in}}{T_{in,N}}} \tag{5.31}$$

The other important parameter that changes when simulating in off-design conditions is the turbine isentropic efficiency $\eta_{is,T}$. In fact, it is influenced by many design parameters as blade construction and operation points, reaching its maximum value at full load. Most of the documentation available refers $\eta_{is,T}$ as a function of the ratio between the actual enthalpy drop and the design enthalpy drop, in accordance with [101]. In EBSILON such a function could not be implemented. Hence, the final solution was adapting it as a function of the mass/volume flow rate.

5.5.2 Regenerator

Component 26 is used to model a regenerator that operates in counter-current flow without pressure drops. In design mode, the cycle parameters are set in order to permit the calculation of the proper T_2 and T_4 (indicated in Figure 5.17) by the component using an effectiveness ε of 0.9 [102].

$$\boldsymbol{\varepsilon = \frac{T_3 - T_4}{T_3 - T_2}} \tag{5.32}$$

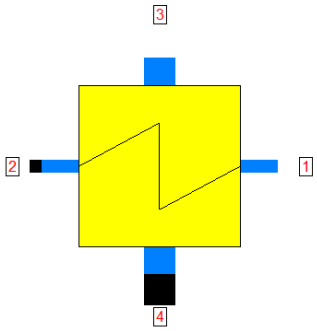

Figure 5.17: Representation of the regenerator in EBSILON

The total *UA* parameter, which gives a reasonable indication of the heat exchanger dimension, is calculated according to the following formula:

$$\boldsymbol{UA = \frac{\dot{Q}_{reg}}{\Delta\vartheta_{ml}}} \tag{5.33}$$

where $\Delta\vartheta_{ml}$ is the logarithmic mean temperature difference defined as

$$\boldsymbol{\Delta\vartheta_{ml} = \frac{\Delta\vartheta_1 - \Delta\vartheta_2}{ln\frac{\Delta\vartheta_1}{\Delta\vartheta_2}}} \tag{5.34}$$

with

$$\boldsymbol{\Delta\vartheta_1 = T_{cold,in} - T_{hot,out} = T_1 - T_4} \tag{5.35}$$

$$\boldsymbol{\Delta\vartheta_2 = T_{cold,out} - T_{hot,in} = T_2 - T_3} \tag{5.36}$$

In off-design mode, it is assumed that the performance of the component (i.e. *UA* as a function of other influencing parameters) is known and is either specified as a characteristic line.

5.5.3 Condenser and cooling system

Condensers operate by removing heat from a vapor to a liquid state. The three main types used in power plants are water-cooled condensers, cooling towers and air-cooled condensers.

- In the first type of condensers, the steam flow is sent to a heat exchanger in which the condensation occurs using cooling water as a refrigerant fluid. The cooling water can be provided from a river or the sea, from where it is pumped to the condenser. The condenser consists of a pipe bundle through which the cooling water is heated while the steam outside the pipes is condensed. These condensers are realized as shell-and-tube or tube-and-tube type. The application of this type of condenser is limited to those facilities that have easy access to water sources. Therefore they are not recommended for CSP applications that are normally built in desert areas.

- Cooling towers are heat exchangers in which two fluids, water and cooling air, are put in contact to transfer heat. The cooling is therefore possible through the exchange of heat and mass between the two fluids. There are two main types of cooling towers: open circuit and closed circuit. In an open circuit the hot water from the condenser is sprayed into a rain-like pattern, through which the ambient air is induced directly by fans. A closed circuit works through the same physical principle of heat exchange, but without a direct contact between the condensing water and the air. Cooling towers are the most used types of condensers in large-scale CSP plants.

- Air-cooled condensers are used in places where it is difficult to find a source of cooling water. In this case the steam flow is condensed into thinned tubes by ambient air moved by axial fans. One of the disadvantages of this type of condenser is that the heat transfer coefficient of the air is substantially lower than that of water, and, in order to improve the heat exchange, there is the need to increase the surface area of the condenser. In addition, the dry-bulb temperature is higher than the wet-bulb one. Thus, in comparison with cooling towers, air coolers reject heat at a higher temperature. Although air-cooled condensers require less maintenance, they produce more noise, as well as

power consumption, due to the air exchange forced by fans. The growing attention to minimize the consumption of water makes this type of condensers an attractive option for CSP plants (e.g. Ivanpah plant [11]).

Therefore, in case of the supercritical configuration with MM, an air-cooled condenser is chosen and it is modeled in EBSILON with Component 7 (Figure 5.18). Pressure drops in this component are neglected.

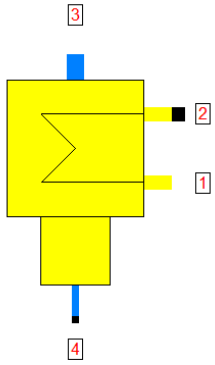

Figure 5.18: Representation of the air-cooled condenser in EBSILON

The amount of steam to be condensed, the steam enthalpy, the air inlet temperature and its pressure are specified. In design mode, the temperature rise of the cooling air is provided, giving as input the air inlet temperature $T_{\mathrm{AIR,in}}$, the approach-point ΔT_{AP} and the pinch-point ΔT_{PP} (Table 5.6). EBSILON then calculates the nominal cooling air flow rate and the nominal value for *UA*. The *UA*-value of the off-design calculation results from the *UA*-value of the design calculation multiplied by a correction factor that is determined by a default characteristic line. In case the cooling air outlet temperature is specified, EBSILON then calculates a new value for the cooling air flow rate. In this model heat losses to the surroundings are not taking into account.

Table 5.6: Parameters for the calculation of the temperature rise in the condenser

$\boldsymbol{T_{\mathrm{AIR,in}}}$	30°C
$\boldsymbol{\Delta T_{\mathrm{AP}}}$	15°C
$\boldsymbol{\Delta T_{\mathrm{PP}}}$	1°C

As analysed in Chapter 4, the desired condensing pressure should not be lower than 0.05 bar. In case of the fluid D4, this leads to a relatively high condensing temperature (87.3°C). In order to take advantage of the heat reject at this condensing temperature (e.g. absorption chillers), for the saturated cycle with D4, the condenser is replaced with a Heat Consumer (Component 35 in Figure 5.19).

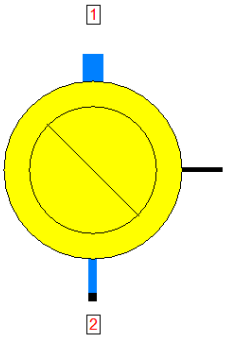

Figure 5.19: Representation of the heat consumer in EBSILON

5.5.4 Pump

The task of the pump is to raise the pressure of the fluid from a low to a high value. In EBSILON, Component 83 (represented in Figure 5.20) is used to model a multistage centrifugal pump with variable speed. A nominal hydraulic efficiency $\eta_{\mathrm{is,p}}$ of 0.7 [98] and a mechanical efficiency $\eta_{\mathrm{o\&}m}$ of 0.998 are defined. In fact, the model calculates the enthalpy at the outlet, based on this efficiency, with the volume flow and pressure head being imposed by measuring points at the inlet and outlet of the pump. The pump is then coupled with a motor (Component 29), characterized by a nominal electrical efficiency $\eta_{\mathrm{o\&}e}$ of 0.85.

In both configurations two pumps are normally used: one condensate pump and one feed pump before the solar field. Due to the recirculation mode, in case of the saturated configuration, an extra recirculation pump is used. All of them have the same assumed parameters.

In off-design mode the performance of each pump is given by an efficiency characteristic line already implemented in EBSILON.

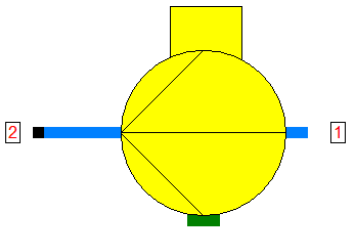

Figure 5.20: Representation of the pump in EBSILON

5.6 Reference systems

As mentioned in the previous sections, both power plant configurations consists of 6 collector loops of the model Eurotrough ET150 with a total net collector area of 9826 m^2. The storage capacity sums up to 4 full load hours.
The most important technical parameters are summarized in Table 5.7.

Table 5.7: Technical specifications of the reference systems

Description	Symbol	Supercritical configuration with MM	Saturated configuration with D4
Parameters for solar field and storage system			
Solar multiple	SM	1.5	
Gross aperture area of the solar field	A_{gross}	10386 m^2	
Net aperture area of the solar field	A_{net}	9826 m^2	
Number of full load hours in storage	h_{n}	4 h	
Storage capacity	Q	16 MWh	
Storage efficiency charging and discharging	$\eta_{\text{cha}},\eta_{\text{dis}}$	95%	
Parameters for the PB at design point			
Turbine inlet temperature	$T_{\text{in,t}}$	280°C	
Turbine inlet pressure	$p_{\text{in,t}}$	8.076 bar	30 bar
Isentropic turbine efficiency	$\eta_{\text{is,T}}$	83%	
Generator efficiency	η_{gen}	96%	
Regenerator effectiveness	ε	90%	
Isentropic pump efficiency	$\eta_{\text{is,p}}$	70%	
Motor pump efficiency	$\eta_{\text{o\&}e}$	85%	
Condensing pressure	p_c	0.141 bar (Air-coolers)	0.05 bar (CHP)

5.7 Simulation layouts

In Figure 5.21 and Figure 5.22 the simulation layout for both configurations is presented as displayed in EBSILON. The plant operates as follows. The cold liquid at the solar field inlet (state 3) is heated by the solar field to state 4. Here, a part of the hot fluid enters the TES system circuit, while the remaining fraction is sent to the PB. Both streams are then mixed up again before the feed pump.
It must be noted, that the specific properties of the chosen ORC fluids lead to numerical instabilities in EBSILON. Therefore, in order to make the simulations successfully converge, some pipes in the layout model are physically decoupled. For simplicity, in these cases the boundary conditions have been set properly on the pipes using transmitter elements.

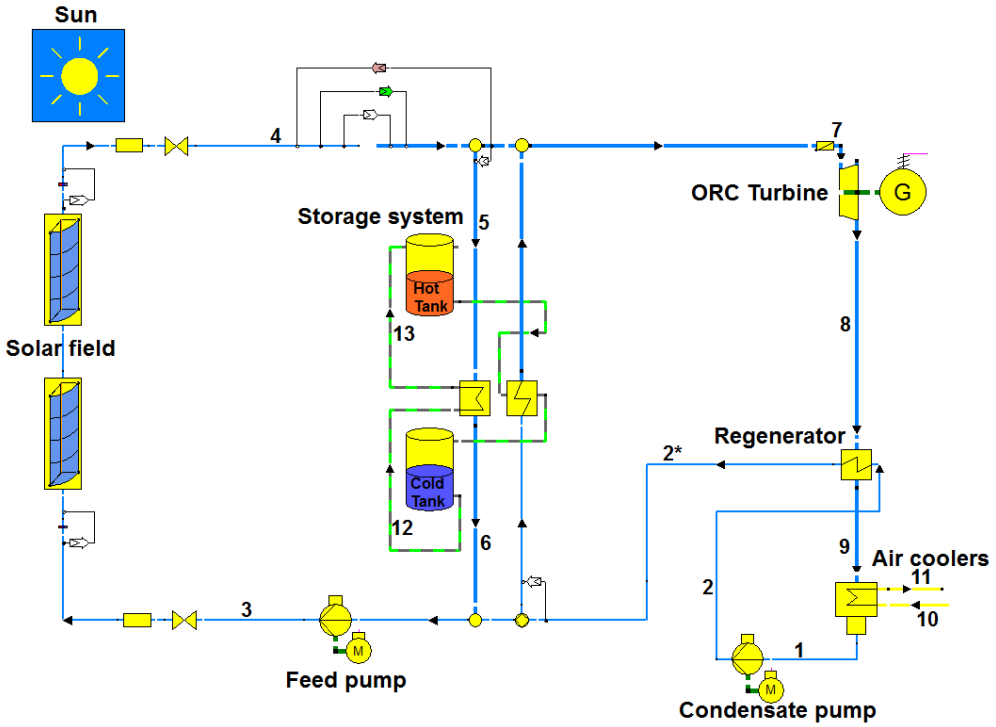

Figure 5.21: Simulation layout of the supercritical cycle configuration in EBSILON

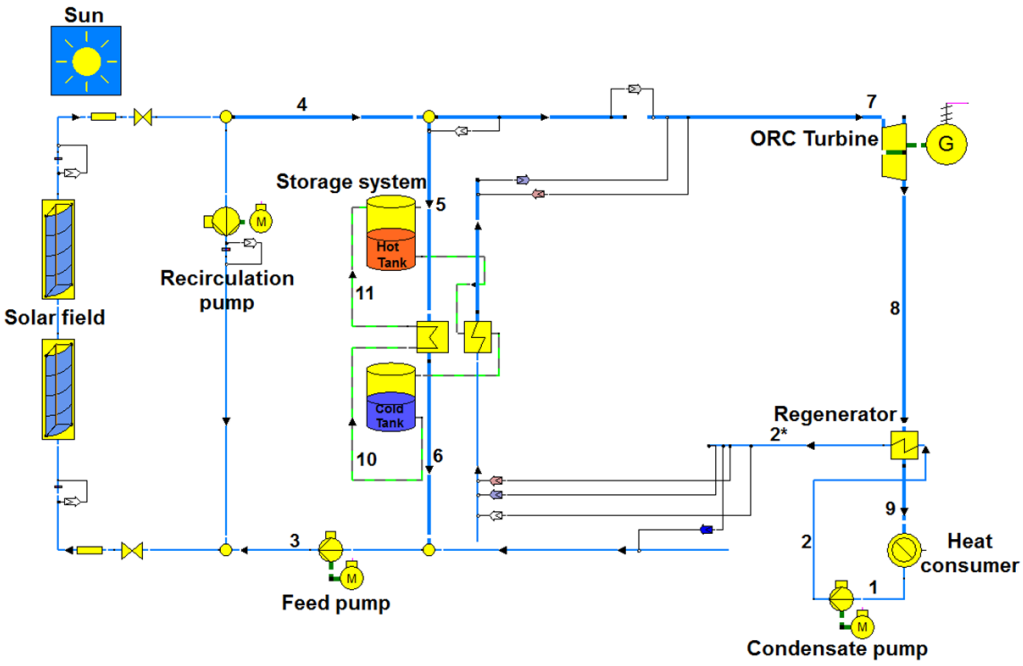

Figure 5.22: Simulation layout of the saturated cycle configuration in EBSILON

A simulation has been run for both configurations in order to assess how the whole system works under nominal conditions, thus with a DNI_{eff} of 850 W/m^2. For each cycle point the following data are carried out. Table 5.8 refers to the supercritical configuration (MM), while Table 5.9 to the saturated one (D4).

Table 5.8: Cycle parameters obtained in EBSILON at nominal conditions for the supercritical configuration

Point	Fluid	$\dot{m}$ (kg/s)	T (°C)	p (bar)	h (kJ/kg)	s (kJ/kgK)
1	MM	12.1	44.9	0.141	-112.128	-0.324
2	MM	12.1	46.7	30	-106.381	-0.319
2*	MM	12.1	152	30	113.432	0.273
3	MM	20.6	170.6	34.654	155.479	0.368
4	MM	20.6	280	30	452.75	0.963
5	MM	8.5	280	30	452.75	0.963
6	MM	8.5	195	30	212.49	0.495
7	MM	12.1	280	30	452.75	0.963
8	MM	12.1	187.2	0.141	355.608	1.001
9	MM	12.1	62.4	0.141	135.795	0.453
10	AIR	189.8	30	1	30.155	6.885
11	AIR	189.8	45.7	0.99875	45.963	6.936
12	HITEC salt	15.4	190	1	296.719	0.825
13	HITEC salt	15.4	275	1	429.461	1.088

Table 5.9: Cycle parameters obtained in EBSILON at nominal conditions for the saturated configuration

Point	Fluid	$\dot{m}$ (kg/s)	T (°C)	p (bar)	h (kJ/kg)	s (kJ/kgK)
1	D4	17.1	87.3	0.05	-152.838	-0.378
2	D4	17.1	87.9	8.076	-151.524	-0.377
2*	D4	17.1	195.9	8.076	38.59	0.082
3	D4	25.6	196.4	16.104	39.546	0.082
4	D4	25.6	280	8.076	280.785	0.545
5	D4	8.4	280	8.076	280.785	0.545
6	D4	8.4	195	8.076	36.810	0.078
7	D4	17.1	280	8.076	280.785	0.545
8	D4	17.1	231.1	0.05	223.345	0.569
9	D4	17.1	104	0.05	33.231	0.137
10	HITEC salt	15.5	190	1	296.719	0.825
11	HITEC salt	15.5	275	1	429.461	1.088

5.8 Plant operation management

The advantage of a CSP power plant coupled with a TES system is the ability to store heat energy for short periods of time and thus have a “buffering” capacity that allows it to smooth electricity production considerably.
Various plant operation modes can be outlined. For instance, the system may operate according to the following operation modes:

1. Start and stand-by operation mode;
2. Solar operation and charging mode;
3. Defocus mode;
4. Solar operation and discharging mode;
5. Storage-only operation mode.

5.8.1 Start and stand-by operation mode

The start and stand-by operation is a solar part-load operation that occurs when the solar irradiation is not high enough to run the power block at full load (e.g. in the early morning) and the storage system is empty (Figure 5.23). According to the chosen control logic, the outlet field temperature is maintained fixed at the design vaue of 280°C. Thus, a lower mass flow rate is heated up. The solar field provides all the thermal energy directly to the PB, avoiding the accumulation phase in the storage system.

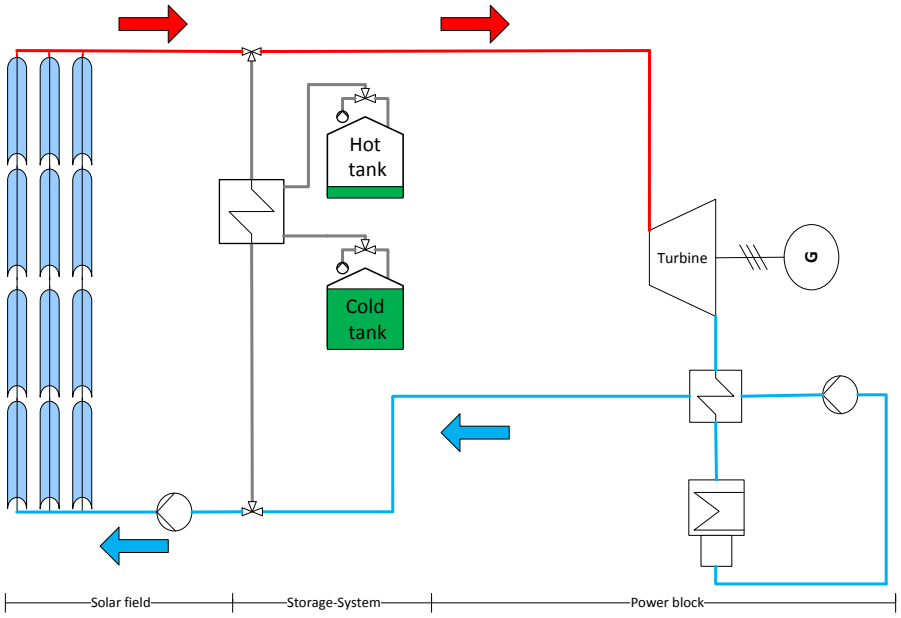

Figure 5.23: Simplified representation of the start and stand-by operation mode

5.8.2 Solar operation and charging mode

The middle of the day, especially during summer, is usually characterized by high DNI values. Here, the solar field can provide a thermal energy to the PB even higher than that required to run it at full load. In this case the heat rate in excess is stored in the TES system. As shown in Figure 5.24, the fluid passes through a heat exchanger in the TES circuit and transfers its heat to the molten salt. The molten salt is pumped from one tank to another, from a temperature of 190°C to 275°C. To ensure reliable operation of the heat exchanger a margin on the minimum mass flow rates that flow in the heat exchanger should be set. Thus, the inlet temperature to the SF is given by mixing the fluid coming from the heat exchanger of the storage system with the fluid coming from the PB (regenerator outlet).

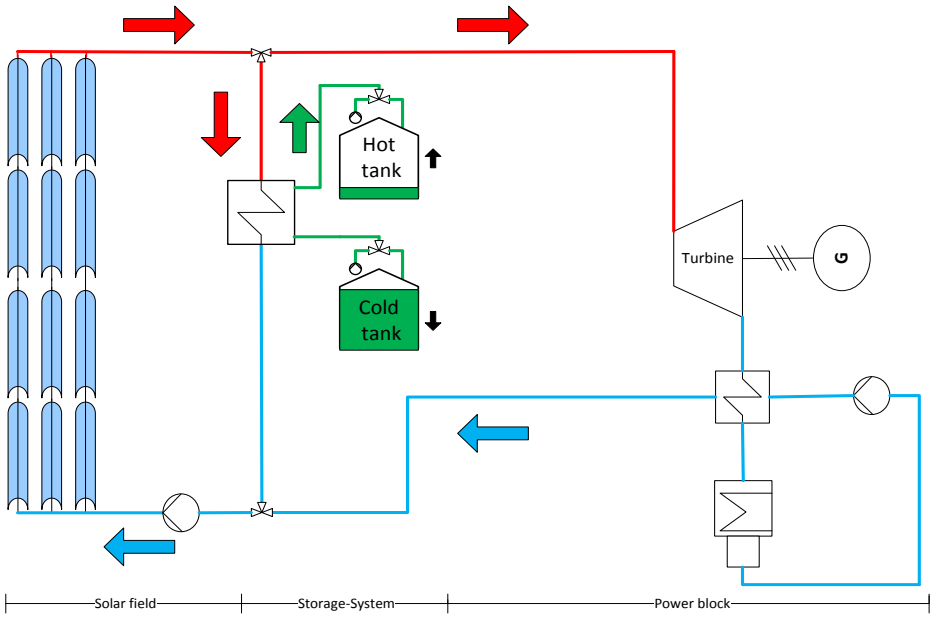

Figure 5.24: Simplified representation of the solar operation and charging mode

5.8.3 Defocus mode

As explained in Section 5.1, the solar thermal ORC plant has been sized with a DNI_{eff} of 850 W/m^2. When the effective DNI exceeds the design value, there is an overproduction of heat in the solar field. According to the adopted control strategy, the mass flow rate of the organic fluid is greater than that produced in nominal conditions. Hence, when the storage system is full, the turbine capacity increases. Some collectors must be defocussed in order to avoid that the

maximum turbine capacity is exceeded (in our case 110% of the design capacity). This value represents a limit for the operation of the turbine.

5.8.4 Solar operation and discharging mode

This mode of operation provides the simultaneously generation phase from both the SF and the TES system (Figure 5.25). It occurs during the day when the thermal energy produced by the SF is not sufficient to meet the electricity demand and, therefore, must be complemented by taking the portion missing from the TES system. Part of the fluid from the regenerator passes through the TES system circuit and is heated in the heat exchanger, while the other passes in the SF. Both flows have a significant pressure difference depending on the operating points. To mix up both flows together in front of the turbine, the pressure of the stream from the solar field has to be throttled in order to be at least equal to the storage discharge pressure. Hence, if stream is taken from both the solar field and the storage, the system operates in sliding pressure mode. Due to this mode, with this plant configuration the design power cannot be maintained during long low-irradiance periods by means of the storage.

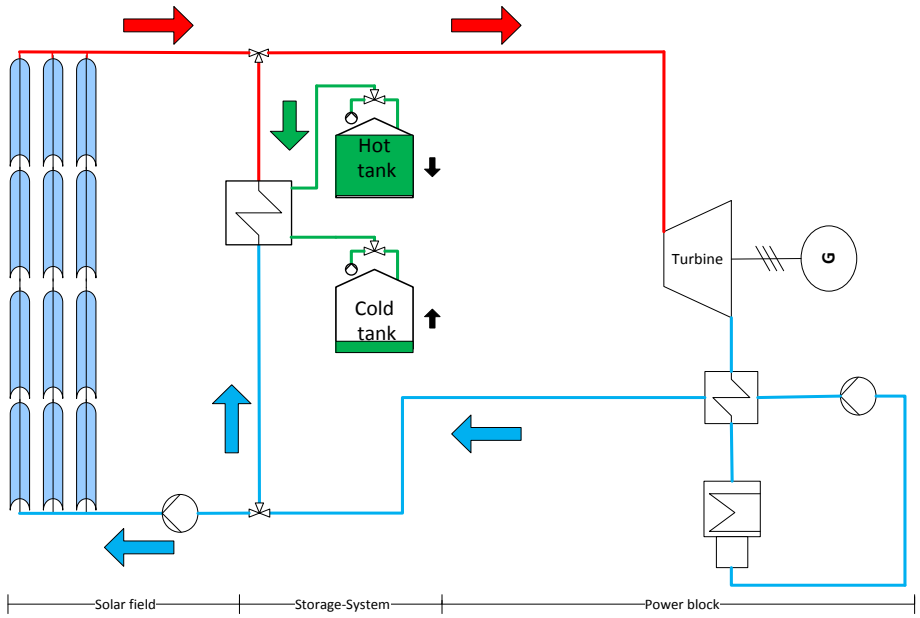

Figure 5.25: Simplified representation of solar operation and discharging mode

5.8.5 Storage-only operation mode

The storage-only operation mode may be perfomed during bad weather periods or during the night. Here, only the stored heat from the TES system is used to operate the ORC cycle (Figure 5.26). The discharging process of the TES system should be represented in a T-Q diagram in order to evaluate the feasibility of the heat exchange in accordance with the preliminary study conducted in Chapter 4, Section 4.5. It is important to remember that a main difference arises in the heat exchange when using a supercritical configuration instead of a saturated one, as a consequence of the different thermal match in the heat exchanger.

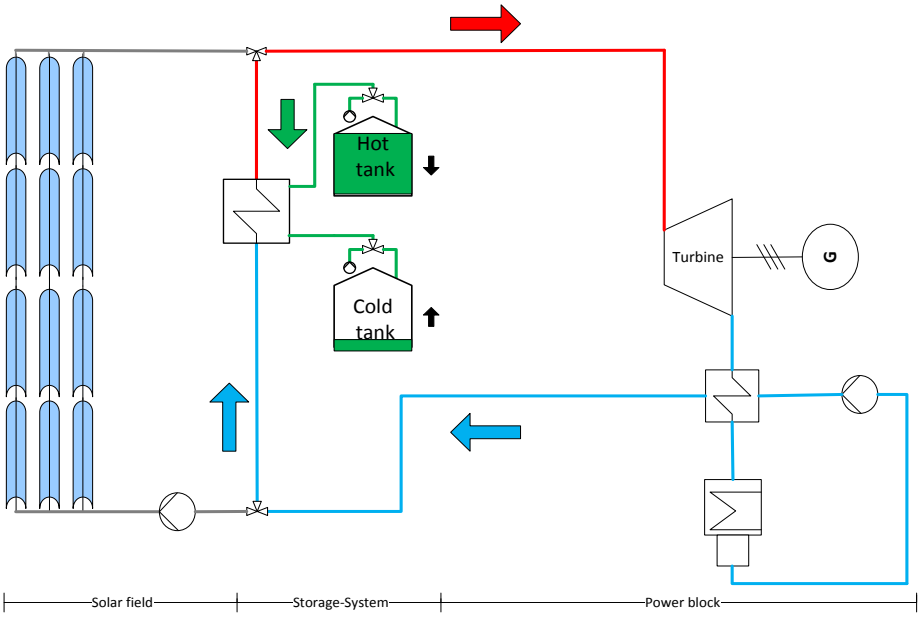

Figure 5.26: Simplified representation of storage-only operation mode

6 Evaluation of simulation data

In order to characterize the performance of the systems in design, off-design and storage-only operation modes, the net electric power and the system efficiencies are carried out. The net electric power of the PB $W_{\mathrm{el,net}}$ is defined as follows:

$$\boldsymbol{W_{\mathrm{el,net}} = W_{\mathrm{el,gross}} - W_{\mathrm{el,par}}} \tag{6.1}$$

where:

$W_{\mathrm{el,gross}}$ is the gross electrical power calculated by multiplying the mechanical turbine power W_{gross} by the generator efficiency η_{gen}.

$$\boldsymbol{W_{\mathrm{el,gross}} = W_{\mathrm{gross}} \cdot \eta_{\mathrm{gen}}} \tag{6.2}$$

$W_{\mathrm{el,par}}$ is the parasitic power that includes the electricity of the following consumers:

- Condenser fan (only in supercritical configuration, as explained in Section 5.5.3)

$$\boldsymbol{W_{\mathrm{el,fan}} = \frac{\dot{m}_{\mathrm{air}} \cdot \Delta p_{\mathrm{air}}}{\rho_{\mathrm{air}} \cdot \eta_{\mathrm{fan}}}} \tag{6.3}$$

  with:

  Δp_{air} : air pressure drop, assumed to be equal to 125 Pa;
  η_{fan} : fan total efficiency, assumed to be equal to 0.8 [98].

- Condensate pump (CP)

$$\boldsymbol{W_{\mathrm{el,CP}} = \frac{\dot{m}_{\mathrm{PB}} \cdot (h_{\mathrm{out}} - h_{\mathrm{in}})_{\mathrm{CP}}}{\eta_{\mathrm{o\&}e}}} \tag{6.4}$$

- Feed pump before the solar field (FP)

$$\boldsymbol{W_{\mathrm{el,FP}} = \frac{\dot{m}_{\mathrm{PB+TES}} \cdot (h_{\mathrm{out}} - h_{\mathrm{in}})_{\mathrm{FP}}}{\eta_{\mathrm{o\&}e}}} \tag{6.5}$$

- Recirculation pump (only in saturated configuration) (RP)

$$\boldsymbol{W_{\mathrm{el,RP}}} = \frac{\boldsymbol{\dot{m}_{\mathrm{REC}} \cdot (h_{\mathrm{out}} - h_{\mathrm{in}})_{\mathrm{RP}}}}{\boldsymbol{\eta_{\mathrm{o\&}e}}} \tag{6.6}$$

The thermal efficiency η_{th} of the cycles was already defined in Chapter 4. It is important to highlight here that this cycle efficiency cannot provide accurate informations about the whole system plant, since it is referred only to the PB without considering the contribution of all the parasitic consumers. In case of a solar thermal power plant, the thermal efficiency should be redefined as

$$\boldsymbol{\eta_{\mathrm{th}}} = \frac{\boldsymbol{W_{\mathrm{gross}}}}{\boldsymbol{\dot{Q}_{\mathrm{in,PB}}}} \tag{6.7}$$

where W_{gross} is the mechanical work of the turbine and $\dot{Q}_{\mathrm{in,PB}}$ the thermal input to the power block. Furthermore, other three kind of efficiencies should be defined:

1) An overall gross efficiency η_{gross} of the power block, defined as:

$$\boldsymbol{\eta_{\mathrm{gross}}} = \frac{\boldsymbol{W_{\mathrm{el,gross}}}}{\boldsymbol{\dot{Q}_{\mathrm{in,PB}}}} \tag{6.8}$$

2) An overall net efficiency η_{net} of the power block, defined as:

$$\boldsymbol{\eta_{\mathrm{net}}} = \frac{\boldsymbol{W_{\mathrm{el,net}}}}{\boldsymbol{\dot{Q}_{\mathrm{in,PB}}}} \tag{6.9}$$

3) An overall solar-to-electricity efficiency $\eta_{\mathrm{sol-to-el}}$ of the whole system defined as:

$$\boldsymbol{\eta_{\mathrm{sol-to-el}}} = \frac{\boldsymbol{W_{\mathrm{el,net}}}}{\boldsymbol{DNI_{\mathrm{eff}} \cdot A_{\mathrm{eff}}}} \cdot \frac{\boldsymbol{\dot{Q}_{\mathrm{in,SF}}}}{\boldsymbol{\dot{Q}_{\mathrm{in,PB}}}} = \boldsymbol{\eta_{\mathrm{net}} \cdot \eta_{\mathrm{SF}}} \tag{6.10}$$

6.1 Design results

Table 6.1 summarizes the design performances obtained in EBSILON for both analyzed configurations.

Table 6.1: Performance parameters at nominal conditions for both analyzed configurations

Parameters	Supercritical configuration with MM	Saturated configuration with D4
W_{gross}	1173 kW	981 kW
$W_{el,gross}$	1126 kW	941 kW
$W_{el,CP}$	82 kW	27 kW
$W_{el,FP}$	25 kW	46 kW
$W_{el,RP}$	-	59 kW
$W_{el,fan}$	25 kW	-
$W_{el,net}$	992 kW	809 kW
$\dot{Q}_{eff,SF}$	6132 kW	6164 kW
$\dot{Q}_{in,PB}$	4083 kW	4104 kW
$\dot{Q}_{in,TES}$	2049 kW	2060 kW
η_{th}	28.7 %	23.9 %
η_{gross}	27.6 %	22.9 %
η_{net}	24.3 %	19.7 %
$\eta_{th,SF}$	73.4 %	73.80 %
$\eta_{sol-to-el}$	17.8 %	14.6 %

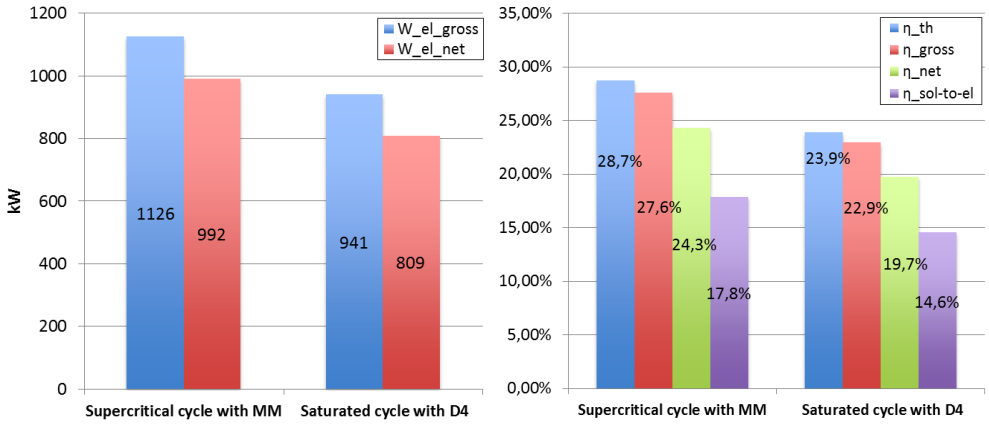

Figure 6.1: Graphical comparison of the gross and net electric power and efficiencies at nominal conditions for both analyzed configurations

According to the obtained values and to their graphical comparison (Figure 6.1), the supercritical configuration with MM leads to higher efficiencies and power output values in comparison with the saturated one. These results are principally due to the lower condensing temperature of the cycle. The total power consumption of the parasitics is quite equal in both configurations, even if it came from different type of consumers. In case of the saturated configuration, the power consumption of the CHP system is not taken into account as it is considered at the expense of the secondary system.
It should be highlighted that this evaluation is only valid from a point of view of the generating electricity. In accordance with the thermodynamic constraints adopted for the configuration with D4, the condensing temperature is still high and the heat reject could be suited for other applications.

6.2 Off-design analysis

Every CSP power plant is subjected to different operations so that the plant operates in conditions different from those given at full output power. An off-design case can be defined as a case, for which the DNI_{eff}, or more precisely, the heat input in the considered thermodynamic cycle is not equal to the one at the design point. In most CSP applications, in contrast to conventional power plants, the off-design operation is actually the normal mode of operation. For instance, the DNI_{eff}, the heat input from the Sun and the air dry-bulb temperature steadily vary from hour to hour and from day to day. It is clear that the part load operation plays also an important role in the overall plant strategy. Heat and mass balances and performances in off-design mode are estimated by accounting for the constraints imposed by the available heat transfer areas in the regenerator and the condenser, as well as the characteristic curves of pumps and turbines. Furthermore, two important constraints on the cycle layouts in off-design are imposed:

- For the supercritical cycle, the turbine inlet temperature is maintained fixed at the design value (280°C), while for the saturated cycle it is equal to the saturated temperature value with a vapor quality *x* of 1;
- For both cycles, the condenser pressure is maintained constant at its design value. In order to make this possible, in case of the supercritical configuration, the air mass flow rate changes, while in the saturated case the value is set.

As mentioned in Section 5.5.1, the turbine operates for both configurations with a sliding pressure control. Hence, in response to a load variation, the cycle follows the change of the mass flow rate and is adjusted automatically without the use of valves, varying the turbine inlet pressure and the vapor flow rate.

The aim of the steady-state off-design calculations carried out is a sensitivity analysis of the simulation models at different DNI_{eff} input values. The sensitivity analysis is then used in the following subsections to evaluate the integration and the perfomances of the indirect two-tank storage system in charging and discharging modes.

6.2.1 Case-study: supercritical cycle configuration

As mentioned before, for the supercritical configuration, the control strategy aims at keeping a constant temperature of 280°C at the outlet of the solar field. The mass flow is allowed to fluctuate in order to follow the available irradiation. Due to the sliding pressure control, at low DNI_{eff} values the supercritical cycle layout cannot be maintained. In fact, the process 2*-3 (Figure 6.2) would enter in the two-phase region. In order to avoid the two-phase region and related control problems, a pressure greater than the critical pressure must always be ensured. At low DNI_{eff} values this can be realized by a throttle or a nozzle control governing.

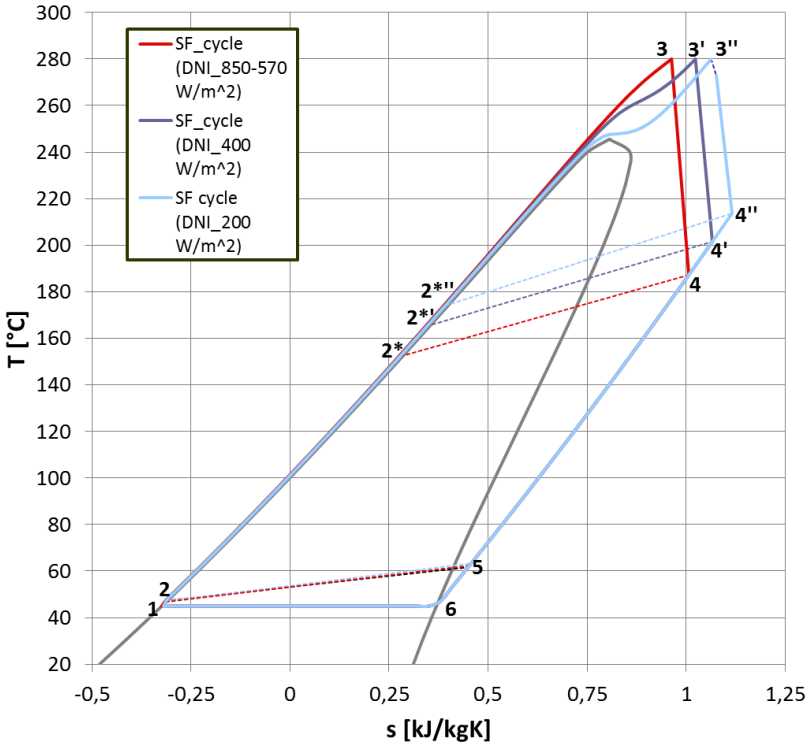

Figure 6.2: Supercritical off-design cycle layouts

As shown in Figure 6.3, in a throttle governing the inlet turbine pressure is reduced just at the turbine entry by a throttle valve, while the enthalpy of the steam remains constant.

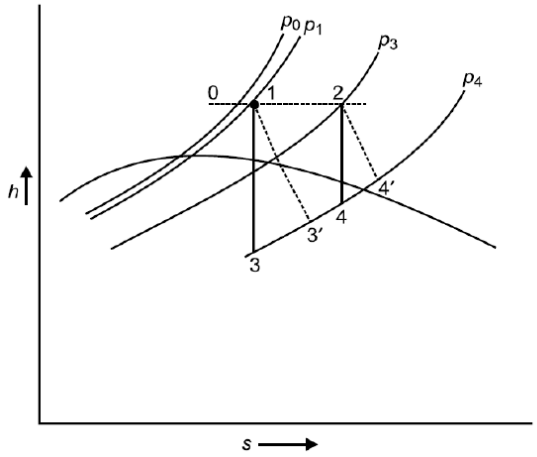

Figure 6.3: Qualitative throttle regulation in h-s diagram [103]

In a nozzle governing, at some part load condition one group of nozzles may be shut off while the other nozzles are fully operated. Therefore, the flow in the turbine is regulated by varying the throat area, rather than regulating the pressure. This type of regulation leads to slightly higher performances in comparison with the throttle one.

Figure 6.4 shows the changes of the turbine inlet pressure and of the mass flow rates in the SF and in the storage system circuit that occur in the plant for different DNI_{eff} values, while Figure 6.5 reports the changes of the gross and net electrical power. From here, interesting observations can be inferred:

- For DNI_{eff} values between 850 W/m^2 (design value) and 570 W/m^2, there is enough thermal power available to run the power block at full load and to charge the storage system. It is important to highlight that a controller is used in order to regulate the charging mode and maintain the mass flow rate in the PB constant at its design value. Since the mass flow rate in the PB and the turbine inlet pressure do not change, the gross electrical power remains also approximately constant. Only the thermal input to the storage system decreases, because the mass flow rate used for the charging process decreases. For this reason, the consumption of the feed pump decreases and, thus, the net electrical power increases.

- For DNI_{eff} lower than 570 W/m^2, the solar field does not provide enough thermal power to operate the power block at full load. The mass flow rate decreases and the power block operates in part-load. Hence, the storage system cannot be charged. As a consequence of the decreased mass flow and pressure, the power output and the power consumption also decrease.

- For DNI_{eff} values higher than 850 W/m^2 (design value), the mass flow rate in the solar field is higher and thus, the turbine works in overcharge increasing its pressure. It is allowed to get a 10% extra over the nominal power of the turbine and a 10% extra over the mass flow rate used for charging the storage system. These constraints can be respected until a DNI_{eff} value of 930 W/m^2 is reached.

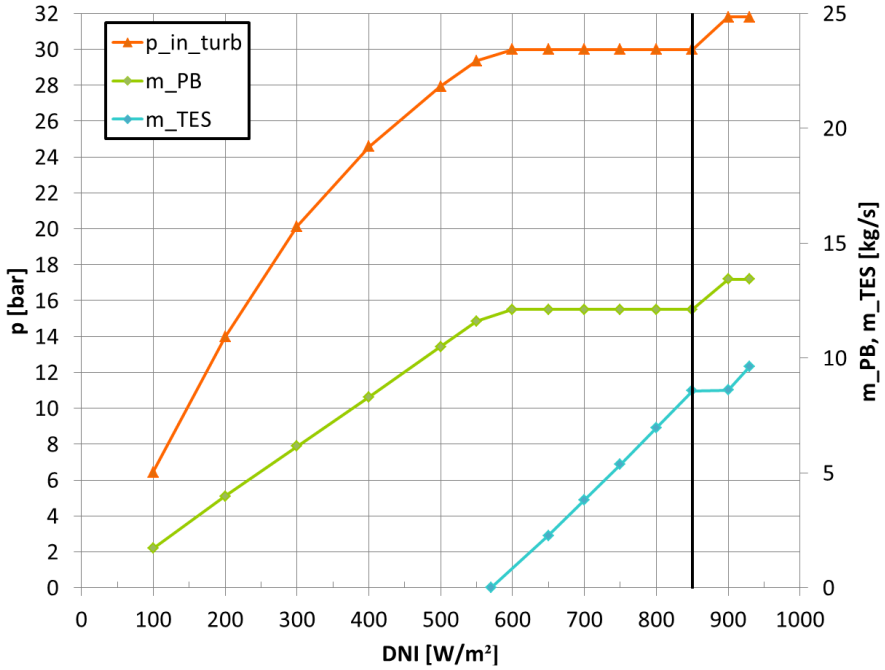

Figure 6.4: Turbine inlet pressure and mass flow rates as function of DNI_{eff} for the supercritical configuration with MM

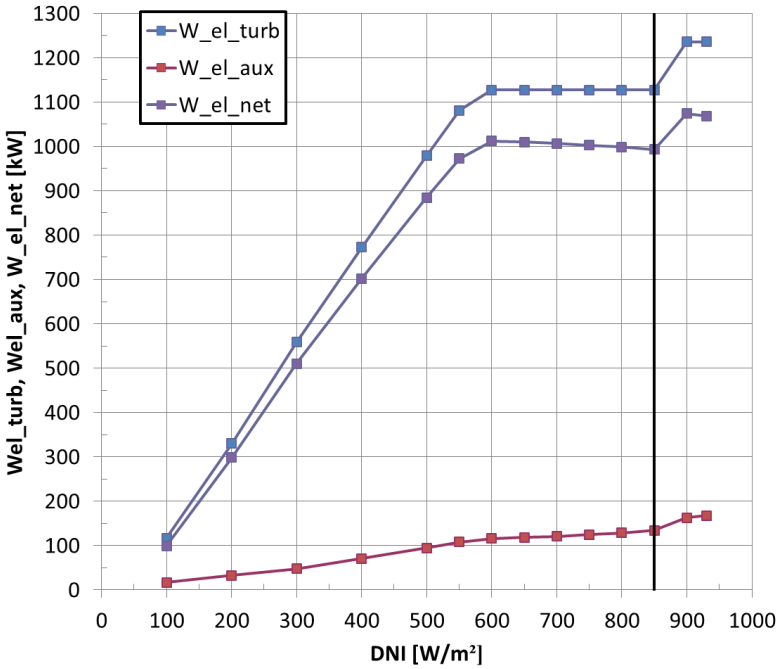

Figure 6.5: Gross and net electrical power output and electrical consumption as function of DNI_{eff} for the supercritical configuration with MM

Figure 6.6 shows the evolution of the efficiency terms as function of different DNI_{eff} values. As already mentioned, an important performance index is the solar-to-electricity efficiency. It can be noticed that in this system the solar-to-electricity efficiency starts to decrease for DNI_{eff} values lower than 450 W/m^2 and higher than 850 W/m^2.

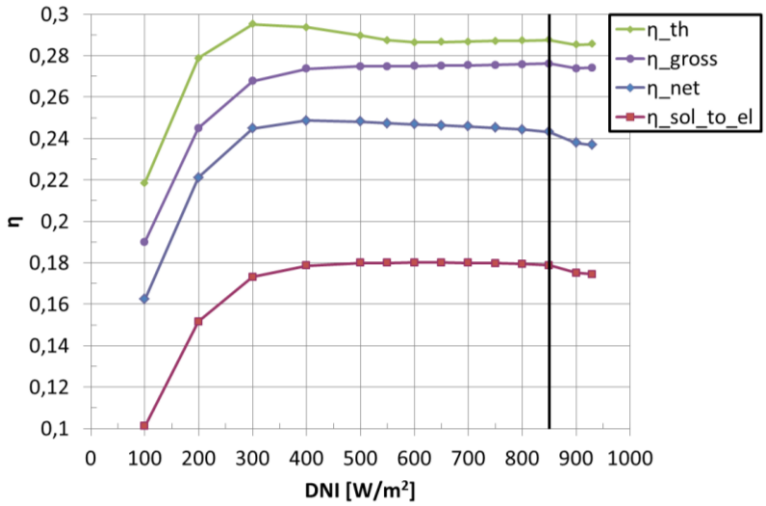

Figure 6.6: Efficiency terms as function of DNI_{eff} for the supercritical configuration with MM

Charging mode analysis

In order to ensure reliable operation of the heat exchanger in the charging mode, a margin on the minimum mass flow rates that flow in the heat exchanger should be set. The heat transfer characterstics are reported in a T-Q diagram, as shown in Figure 6.7.

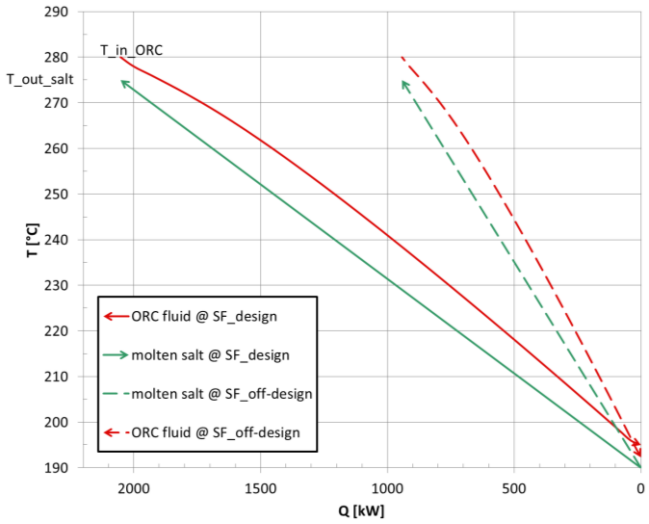

Figure 6.7: T-Q diagram of the charging process in the heat exchanger of the storage system circuit in the supercritical configuration

According to the figure, it can be noted that the charging process can always be performed since there is heat transfer rate in excess (wheter in design or in off-design conditions).

Discharging and storage-only operation analysis

Referring to Figure 6.8, in case of the supercritical configuration, the molten salt enters the heat exchanger at 275°C and leaves it at 190°C. For counter current heat transfer, the cold organic fluid enters the exchanger at the regenerator outlet temperature and exits at 270°C. In order to recover the maximum thermal power of the TES system at these fixed temperatures, a mass flow rate of molten salt equal to 30 kg/s is required. This value allows for a net power output equal to 96% of the design one. The heat transfer at these fixed temperatures can be performed also in part-load until the pinch-point remains positive. The control strategy allows for a decrease of the mass flow rate of the molten salt down to approximately 80% of its design value. The outlet temperature of the molten salt is maintained fixed, in order to avoid that the temperature of the cold tank

increases. In fact, with an increased temperature of the cold tank, the storage capacity will decrease.

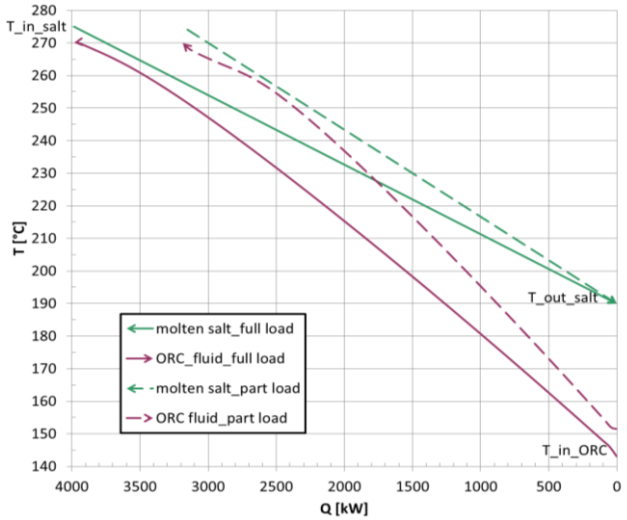

Figure 6.8: T-Q diagram of the discharging process in the heat exchanger of the storage system circuit in the supercritical configuration

Figure 6.9 shows in the T-s diagram the cycle layouts performed with the storage-only operation. For a comparison the cycle layout performed with the solar field at nominal conditions is also represented.

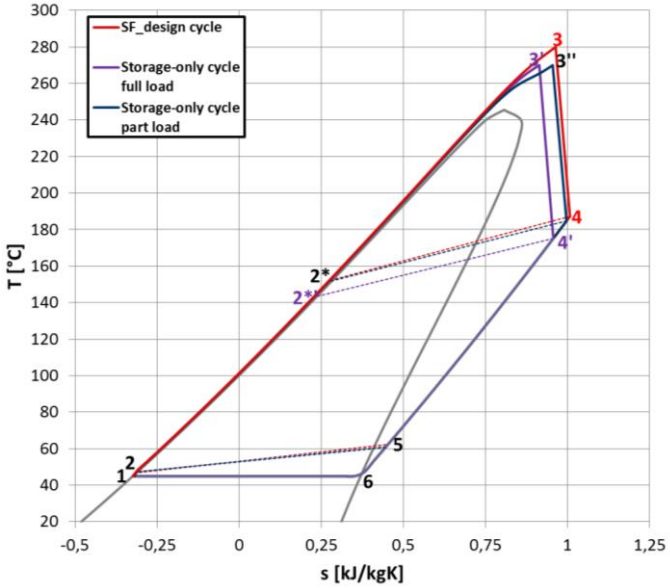

Figure 6.9: Comparison between the supercritical cycle layout perfomed with the solar field at nominal conditions and the ones performed with the storage-only operation in a T-s diagram

Hence, the turbine inlet pressure, the mass flow rate of the organic fluid and the power output can be parameterized as a function of the mass flow rate of the molten salt, as reported in Figure 6.10.

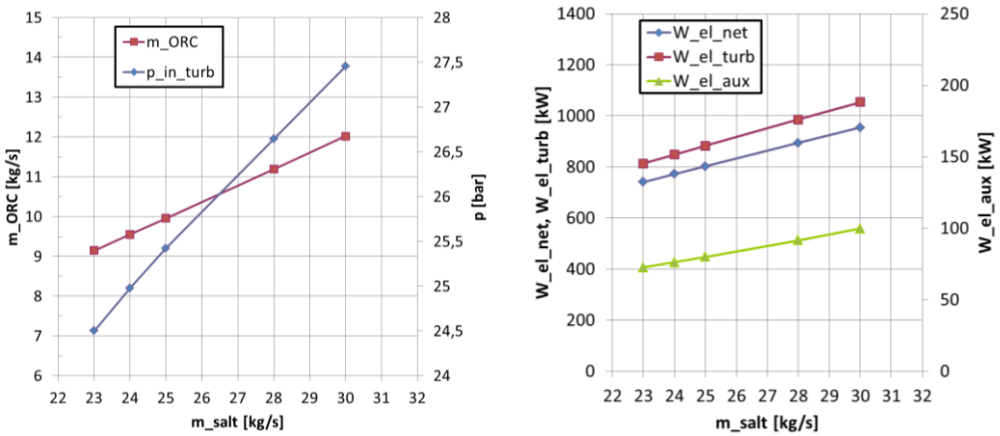

Figure 6.10: Turbine inlet pressure, organic mass flow rate and power terms as function of the mass flow rate of the molten salt for the storage-only operation

Furthermore, in order to evaluate the performances of the plant when the heat source is represented by the TES system, η_{th}, η_{gross}, and η_{net} are calculated. Figure 6.11 shows the defined performance indexes as function of the mass flow rate of the molten salt.

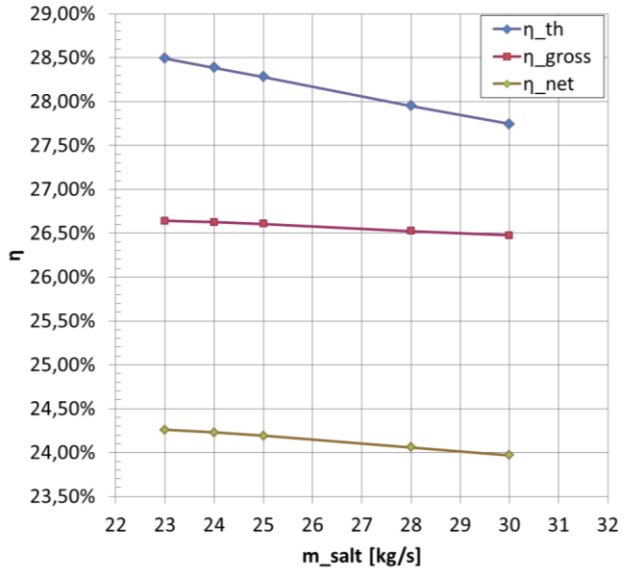

Figure 6.11: Efficiency terms as function of the mass flow rate of the molten salt for the storage-only operation mode

6.2.2 Case-study: saturated cycle configuration

In case of the saturated configuration, the control strategy aims at providing saturated vapor condition at the outlet of the solar field (Figure 6.12).

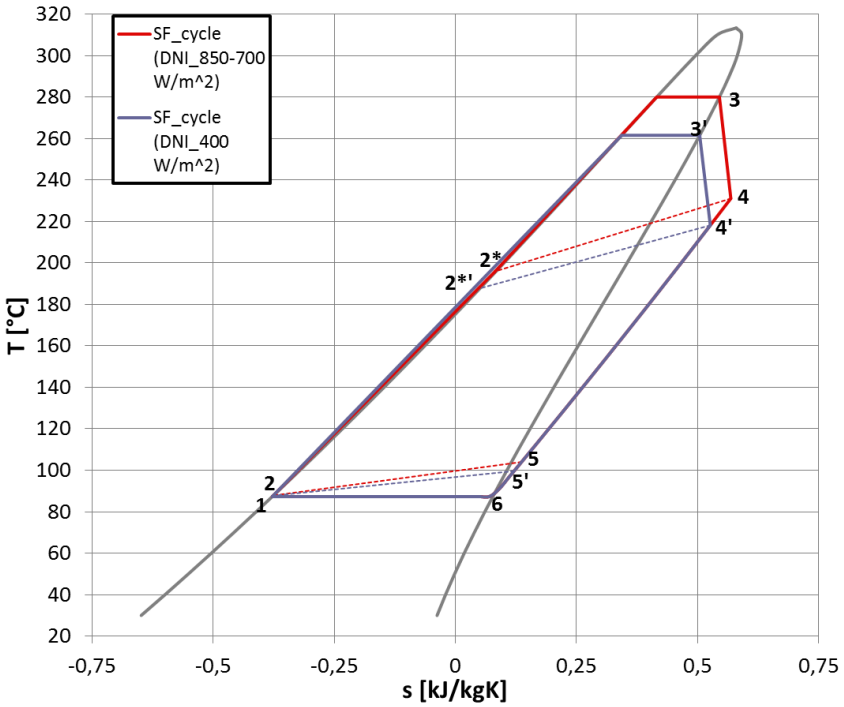

Figure 6.12: Subcritical saturated off-design cycle layouts

The sliding pressure control of the turbine can be maintained for each DNI_{eff} value and there is no need to use a throttle or a nozzle governing. The evaluations in the change of the parameters and performances are quite similar as the ones for the supercritical configuration (Figure 6.4 and Figure 6.5). Nevertheless some differences can be drawn. As shown in Figure 6.13 and Figure 6.14, the first difference is that in the saturated configuration the power block can be run at full load until a DNI_{eff} value of 600 W/m^2, instead of 570 W/m^2. Furthermore, for the saturated cycle configuration the evolution of the recirculation mass flow rate is shown in Figure 6.13. Another important difference is that for DNI_{eff} values lower than 600 W/m^2, all the efficiency terms decrease more rapidly, as shown in Figure 6.15.

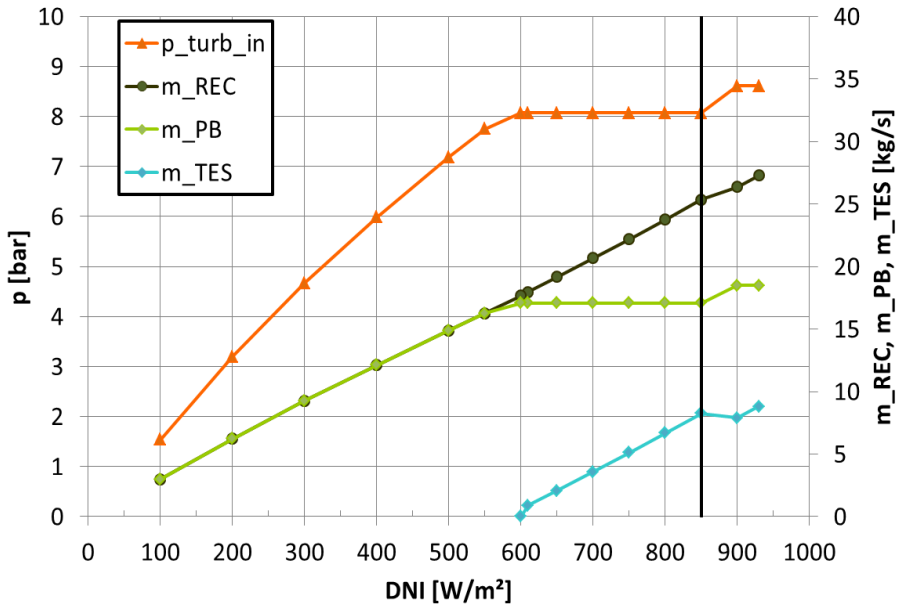

Figure 6.13: Turbine inlet pressure and mass flow rates as function of DNI_{eff} for the saturated configuration with D4

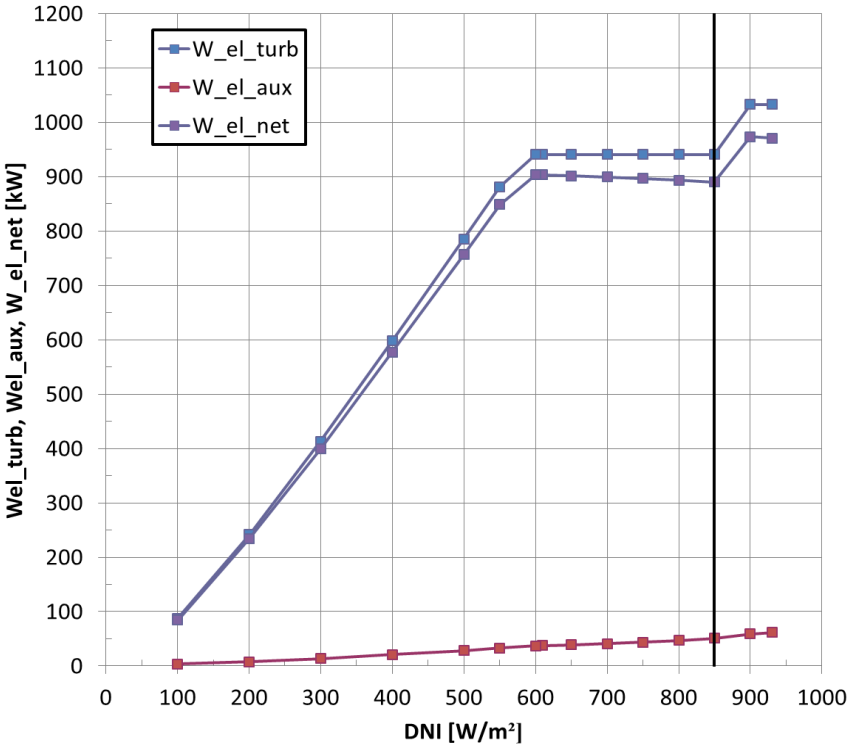

Figure 6.14: Gross and net electrical power output and electrical consumption as function of DNI_{eff} for the saturated configuration with D4

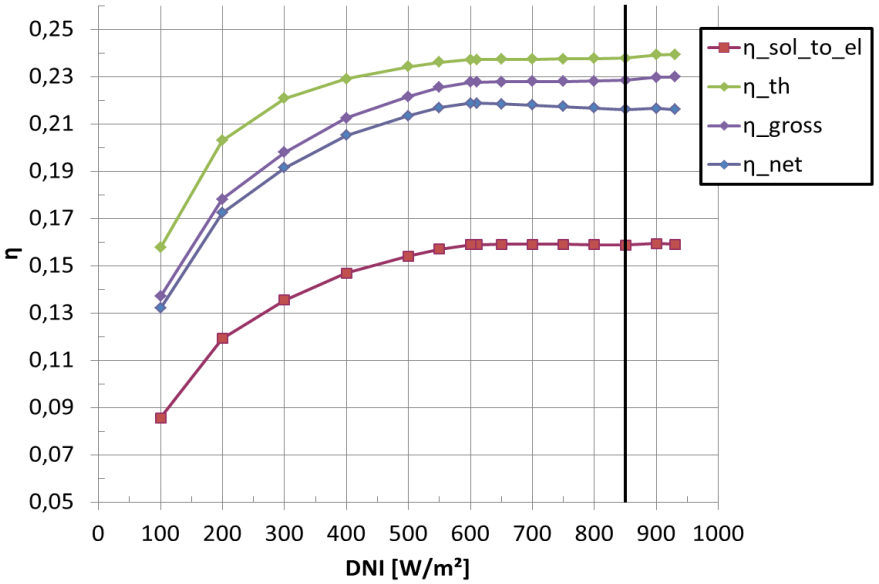

Figure 6.15: Efficiency terms as function of DNI_{eff} for the saturated configuration with D4

Charging mode analysis

According to the Figure 6.16, it can be noted that the charging process in case of the saturated configuration can always be performed and the conclusions drawn for the supercritical case in the previous subsection are still valid.

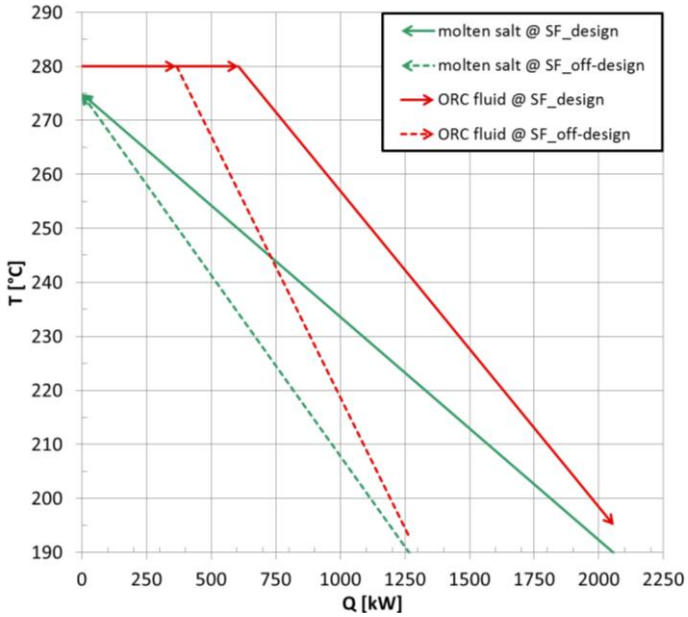

Figure 6.16: T-Q diagram of the charging process in the heat exchanger of the storage system circuit in the saturated configuration

Discharging and storage-only operation analysis

Referring to the T-Q diagram for the saturated configuration (Figure 6.17), it can be noted that the vaporizing stream is represented by a horizontal line. Moreover, as a consequence of the constraint on the pinch-point (ΔT_{pp} = 5°C), the organic fluid exits the heat exchanger at a temperature deeply lower than that of the supercritical cycle.
In order to maintain a saturated layout, in this case only one specific mass flow rate of the fluid ensures a proper thermal match with the heat source. In this case the cycle performed is shown in a T-s diagram in Figure 6.18 and is characterized by a turbine inlet temperature of 228.76°C. In such case, the corresponding net power output would be very strongly decreased from the nominal one (approximately 30% of the design capacity). A comparison of the performance indexes between the cycle perfomed with the SF at nominal conditions and the one performed with the storage-only operation is listed in Table 6.2.

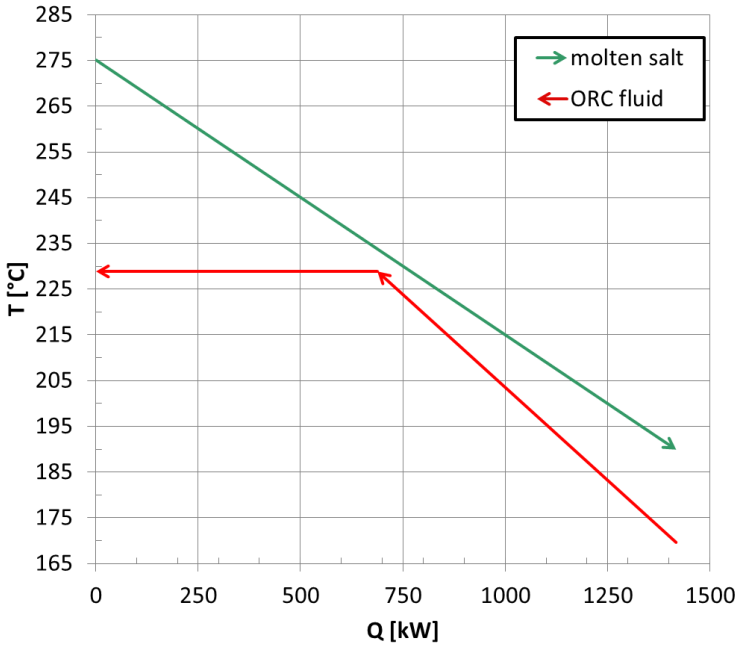

Figure 6.17: T-Q diagram of the discharging process in the heat exchanger of the storage system circuit in the saturated configuration

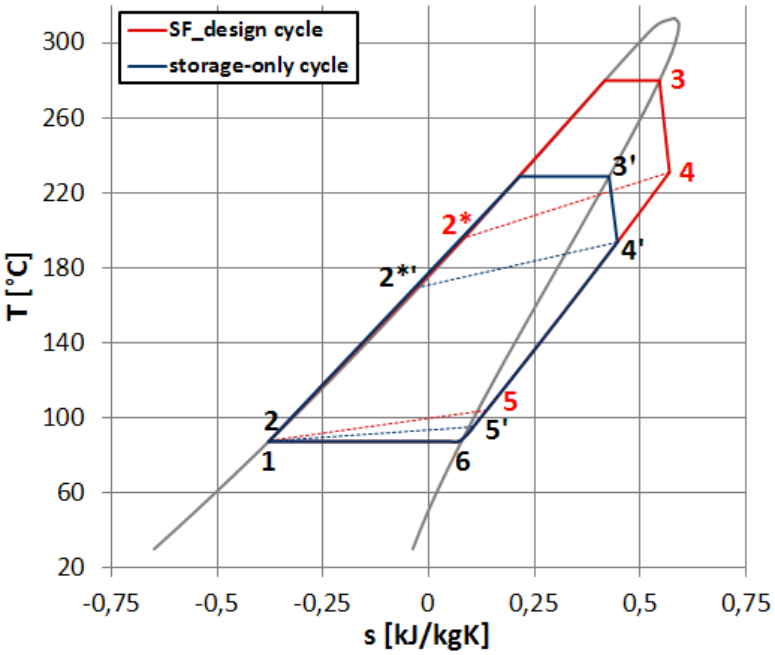

Figure 6.18: Comparison between the saturated cycle layout perfomed with the solar field at nominal conditions and the one performed with the storage-only operation in a T-s diagram

Table 6.2: Comparison between the performance indexes of the solar field at nominal conditions and the one of the storage-only operation for a saturated configuration

Performance index	SF design cycle	Storage-only operation cycle
W_{gross}	981 kW	291 kW
$W_{el,gross}$	941 kW	255 kW
$W_{el,net}$	809 kW	250 kW
η_{th}	23.9 %	20.5 %
η_{gross}	22.9 %	18.0 %
η_{net}	19.7 %	17.6 %

6.3 Simulation of typical days

In order to evaluate the feasibility of the control strategies mentioned in Section 5.8, a simulation of one day in three different seasons is carried out for both plant configurations using the simulation results for design and off-design cases. The data of the effective direct normal irradiation are taken from the EBSILON database for a summer day (21st June 2009), a winter day (19th December 2009) and a mid-season day (25th March 2009) in Lleida, Spain. Table 6.3 shows the specification of the chosen site.

Table 6.3: Specification of the site

Site	Lleida, Spain
longitude	0.56°E
latitude	41.58°N
Annual DNI	1758 kWh/m^2
Average annual	14.6°C

6.3.1 Simulation of a summer day

Figure 6.19 presents the DNI, DNI_{eff} and the IAM· cos(θ_i) data for the specific daytime on 21st June 2009.

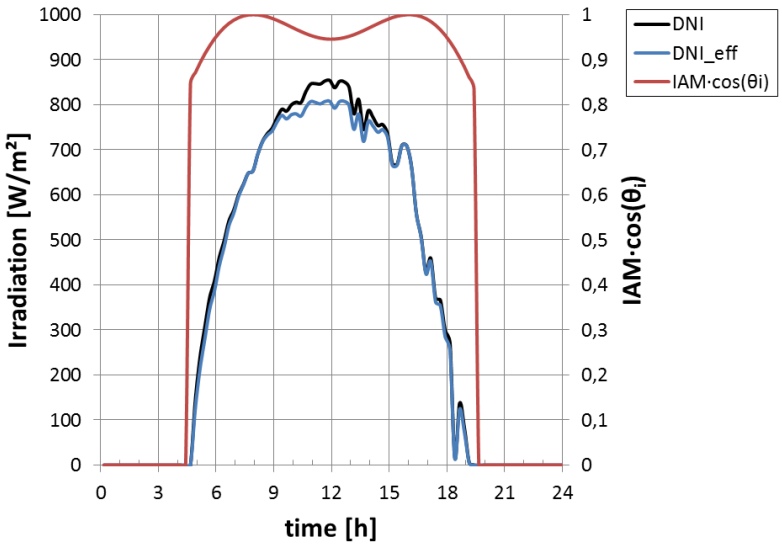

Figure 6.19: DNI, effective DNI and IAM·cos(θ_i) on 21st June 2009 in Lleida

Relevant system parameters for the both, supercritical and saturated configurations are listed in Table 5.7. As described in Section 5.8 various operating points can occure. As a simplification, a mode where the power block

is operated by the solar field and by the storage system at the same time is not considered. Thermal and electrical power for both systems are shown in Figure 6.20, while in Figure 6.21 the evolution of the charge-level of the TES is presented. It must be noted that in case of the saturated configuration (represented on the right), during storage-only operation the system is in low part-load due to the constraints, that are explained in Section 6.2.2. This deep part-load operation allows for electricity production until the early morning hours (2 a. m.) but at a lower efficiency. In contrast to that, the supercritical cycle works at almost full-load during storage-only operation. Therefore, the plant operation already ends at 21:00.

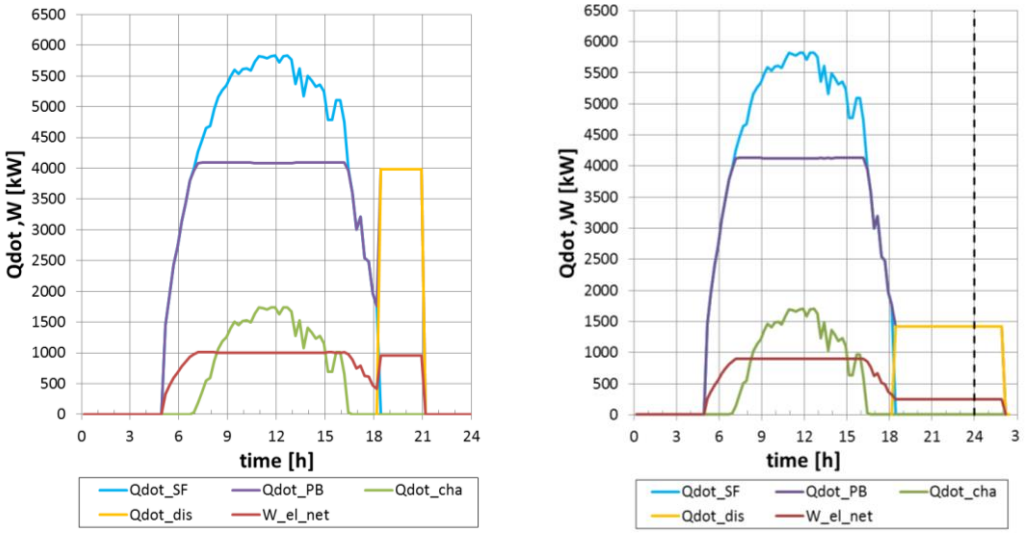

Figure 6.20: Thermal and electrical power for the supercritical (left) and saturated (right) configurations at a location of 41.58°N, 0.56°E for the meteorogical data of a summer day (21st June 2009)

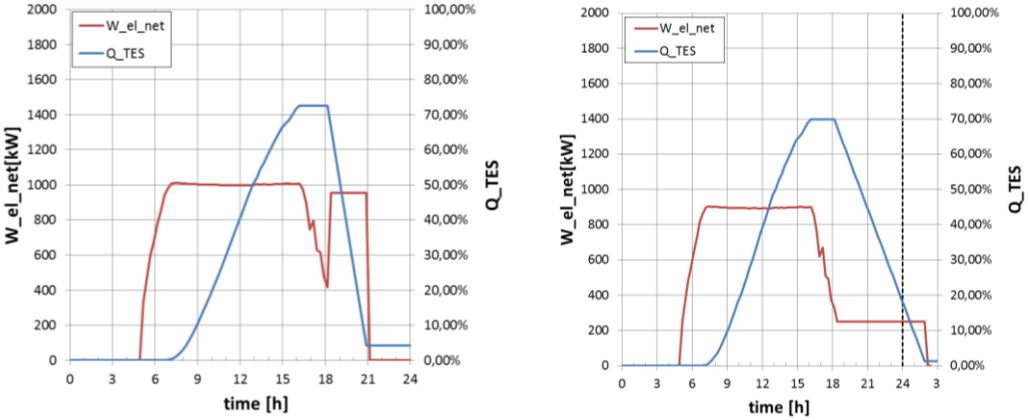

Figure 6.21: Net electric power output and thermal capacity for the supercritical (left) and saturated (right) configuration at a location of 41.58°N, 0.56°E for the meteorogical data of a summer day (21st June 2009)

By observing the results, the following conclusions can be drawn:

- The daily thermal power from the solar field and net electricity output is higher in the supercritical configuration than in the saturated one.

- The daily solar-to-electricity efficiency is also higher in the supercritical case than in the saturated one: 17.1% compared to 14.1%.

- In the supercritical cycle, the power block works almost at nominal load, entailing a high efficiency. Due to that, systems with large storage capacities could be realized offering the possibility of base-load operation.

- In the saturated cycle, the power block works at low part-load during storage-only operation. This operating mode leads to a lower efficiency and, furthermore, systems with large storage capacities cannot be realized since there would not be enough time for the discharge operation during the night.

Table 6.4 summarizes the obtained results for a typical summer day.

Table 6.4: Results of the daily calculation for a typical summer day (21st June 2009)

Description	Supercritical configuration	Saturated configuration
Daily DNI·net aperture area	85 724 kWh	
Daily DNI_{eff}·net aperture area	84 098 kWh	
Daily thermal power from solar field	60 810 kWh	60 675 kWh
Daily net electricity output	14 697 kWh	12 126 kWh
Average solar field thermal efficiency	70.9%	70.8%
Average solar-to-electricity efficiency	17.1%	14.1%

6.3.2 Simulation of a winter day

Figure 6.19 presents the DNI, DNI_{eff} and the IAM· $\cos(\theta_i)$ data for the specific daytime on 19th December 2009.

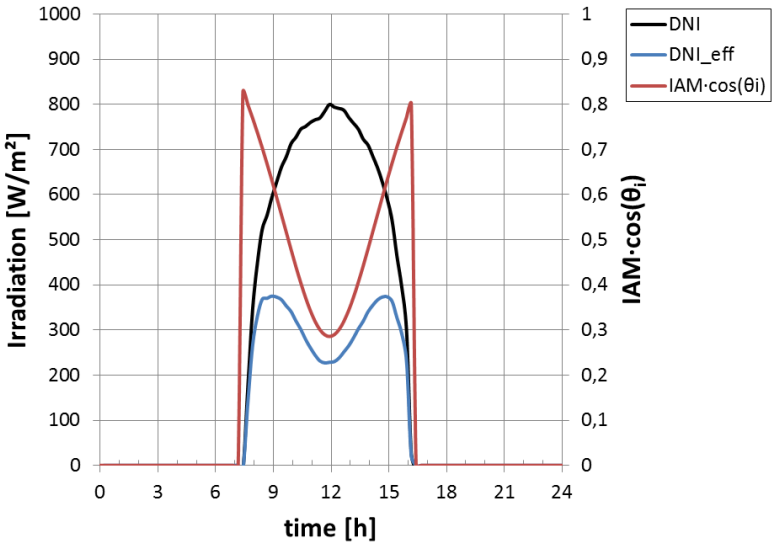

Figure 6.22: DNI, effective DNI and IAM·cos(θ_i) on 19th December 2009 in Lleida

Thermal and electrical power for both systems are shown in Figure 6.20. It must be noted that the thermal power input in such day is not high enough to run the systems at full-load. Both systems are run in part-load from 8 a. m. till 4 p. m. and the storage system remains completely empty.

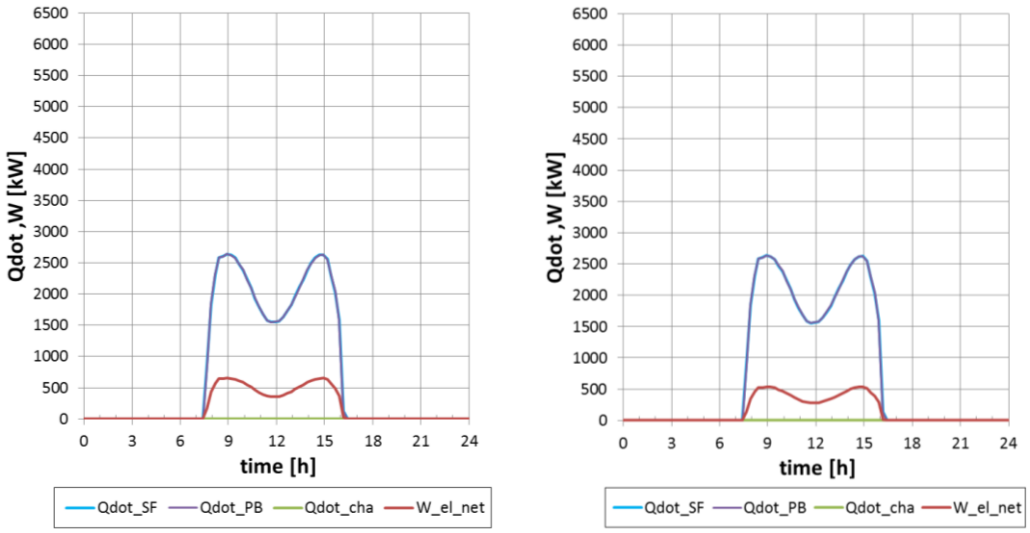

Figure 6.23: Thermal and electrical power for the supercritical (left) and saturated (right) configurations at a location of 41.58°N, 0.56°E for the meteorogical data of a winter day (19th December 2009)

Table 6.5 summarizes the obtained results for a typical winter day. As a consequence of the low DNI_{eff} values, the electricity outputs and the efficiency terms are highly decreased.

Table 6.5: Results of the daily calculation for a typical winter day (19th December 2009)

Description	Supercritical configuration	Saturated configuration
Daily DNI·net aperture area	52 172 kWh	
Daily DNI_{eff}·net aperture area	25 318 kWh	
Daily thermal power from solar field	17 926 kWh	17 942 kWh
Daily net electricity output	4 347 kWh	3 469 kWh
Average solar field thermal efficiency	34.4%	34.4%
Average solar-to-electricity efficiency	8.3%	6.6%

6.3.3 Simulation of a mid-season day

Figure 6.24 presents the DNI, DNI_{eff} and the IAM· $\cos(\theta_i)$ data for the specific daytime on 25th March 2009.

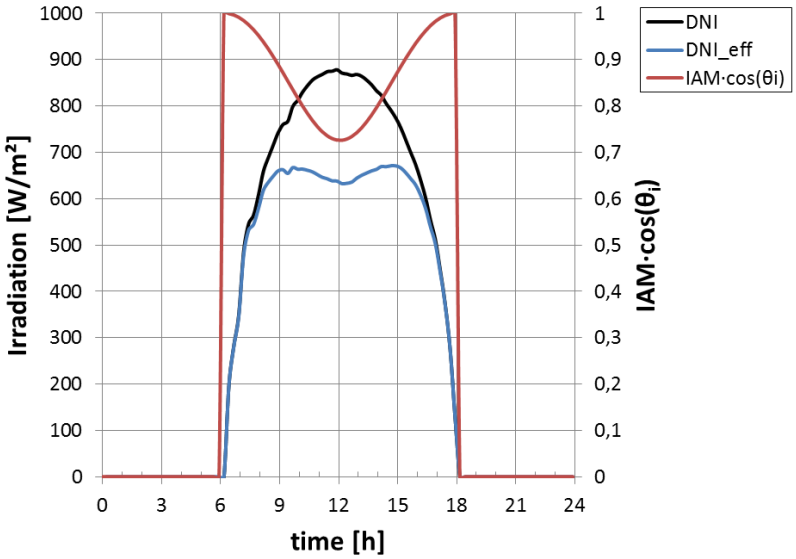

Figure 6.24: DNI, effective DNI and IAM·cos(θ_i) on 25th March 2009 in Lleida

Thermal and electrical power for both systems are shown in Figure 6.25, while in Figure 6.26 the evolution of the charge-level of the TES is presented. It must be noticed that similar conclusion of Section 6.3.1 can be drawn. The main difference is that in such day the DNI_{eff} is lower compared to that in a summer day. The charge-level of the TES system reaches approximately 30% of its total capacity.

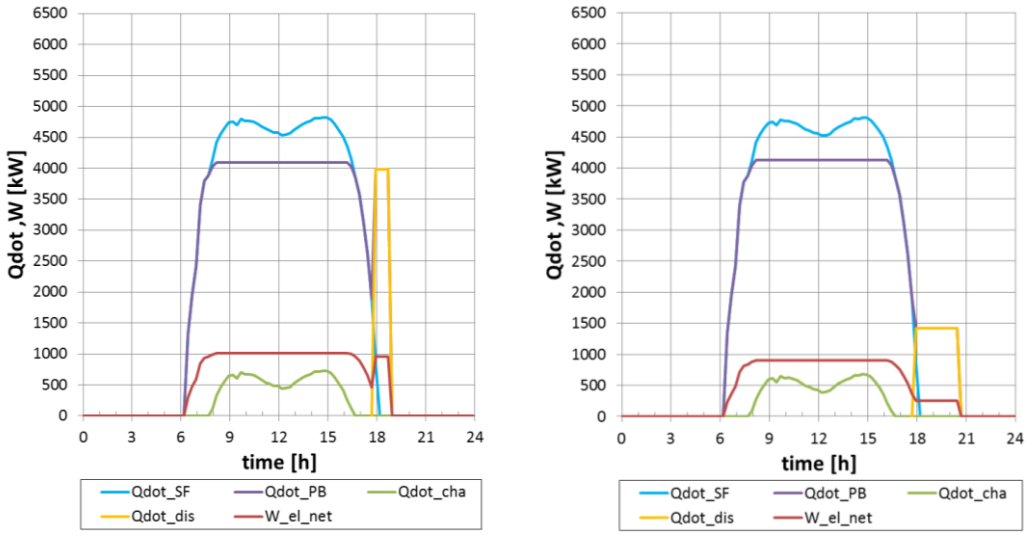

Figure 6.25: Thermal and electrical power for the supercritical (left) and saturated (right) configurations at a location of 41.58°N, 0.56°E for the meteorogical data of a mid-season day (25th March 2009)

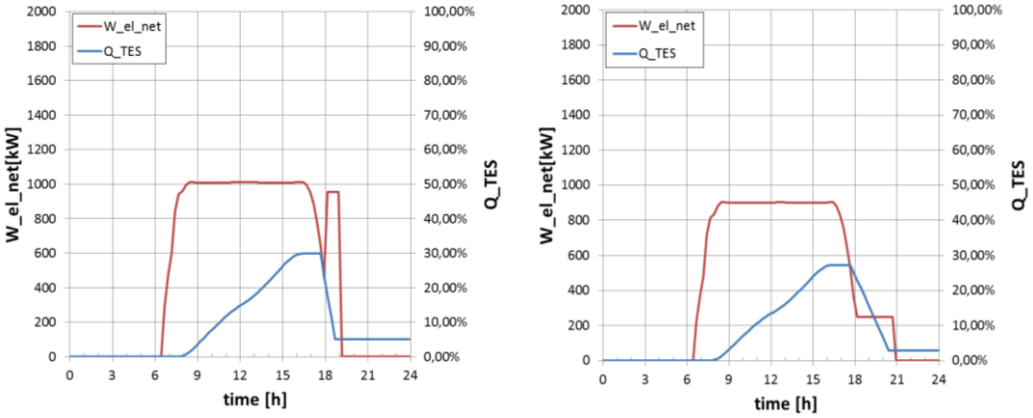

Figure 6.26: Net electric power output and thermal capacity for the supercritical (left) and saturated (right) configuration at a location of 41.58°N, 0.56°E for the meteorogical data of a mid-season day (25th March 2009)

Table 6.6 summarizes the obtained results for a typical mid-season day.

Table 6.6: Results of the daily calculation for a typical mid-season day (25th March 2009)

Description	Supercritical configuration	Saturated configuration
Daily DNI·net aperture area	78 288 kWh	
Daily DNI_{eff}·net aperture area	66 954 kWh	
Daily thermal power from solar field	48 778 kWh	48 610 kWh
Daily net electricity output	11 736 kWh	10 207 kWh
Average solar field thermal efficiency	62.3%	62.1%
Average solar-to-electricity efficiency	15.0%	13.0%

Conclusions

In the present thesis ORC processes for direct steam generation in parabolic trough power plants have been investigated and evaluated. Focus has been set on providing new solutions for power cycles that combine the direct steam generation of an organic medium in a parabolic trough plant.

In Chapter 1 state-of-the art CSP plants are discussed, focusing on the different types of parabolic trough systems including integrated storage system.
New technologies are currently being developed that shall increase the efficiency and reduce the cost of next-generation trough plants. While in the sector of large-scale plants Direct Steam Generation and Molten Salt systems are developed, ORC systems could offer a promising option for small-scale off-grid and co-generation applications.
In Chapter 2 a technical background about ORC has been given. An ORC offers simple cycle design and specific properties, which reduce the complexity of the turbine design. These advantages make organic Rankine cycles particularly attractive for small-scale parabolic trough solar applications. There is a variety of ORC fluids with different thermodynamic characteristics available being suited for different working temperature ranges. Therefore, Chapter 3 is focused on the choice of the organic working fluid. The research has been concentrated on finding the most suitable fluids for a solar DSG application in accordance with the multitude of constraints related to the thermodynamic properties of the fluids, as well as considerations of health, safety and environmental impact. In particular, the organic fluid that circulates through the solar field must be environmental-friendly and meet basic requirements such as safety and technical suitability. Only few fluids meet the selection criteria of Section 3.1. Therefore, a trade-off has been made and a set of possible working fluid candidates have been identified using heuristic knowledge about the processes based on similar systems. The investigated fluids have been selected in order to deal with different maximum temperature values between 200°C and 400°C, typical values reached from existing parabolic trough systems. When low-temperature applications (< 250°C) are considered, fluids like R245fa and SES36, currently employed in geothermal applications and characterized by a low critical temperature, can be used. For high-temperature applications (> 250°C), fluids with the highest possible critical temperature should be selected in order to allow operating a subcritical ORC with limited pressure. Among the investigated fluids with a high critical temperature, cyclic and linear siloxanes have been selected as the most promising also due to their environmental friendly characteristics and their maximum achievable temperatures (300°C for linear siloxanes and 340°C for cyclic siloxanes [75]).

In order to take advantage of the achievable temperatures of the PTCs and in accordance with the research fields of the Line Focus Systems division of DLR, the main interest has been set on high temperature processes. Therefore, in Chapter 4 the basic single-pressure cycle layouts with siloxanes have been analysed, focusing in detail on a saturated process with the fluid D4 and a supercritical process with MM. It must be mentioned that the process with D4 can guarantee the respect of the specific optimization criteria, defined in Section 4.3, only with relatively high condensing temperature (87.3°C). For that reason this fluid should be normally taken with high condensing temperatures for combined heat and power systems (CHP). On the other hand, the supercritical cycle with MM allows operating with actual air-cooled condensers (condensing temperature of 45°C), achieving high performances in terms of specific net work. Analysis has also concluded that for a supercritical cycle with a fixed turbine inlet temperature, the cycle efficiency has its maximum value with a inlet pressure close to the critical pressure value and decreases as the pressure increases. Subsequently, the integration of TES system in the solar ORC processes has been discussed. Most of the investigated TES systems are still proof-concepts for DSG applications, as e.g. the PCM storage system. Among all the possible combinations, only the one with the indirect two-tank storage system has been indicated to be technically feasible for both a saturated and a supercritical process. Nevertheless, for those two case-studies the thermal match between the heat source and the fluid has shown to be rather different. It might be outlined that, compared to the supercritical configuration, in the saturated one the need to store as well sensible as latent heat leads to a higher decrease of the steam parameters between charging and discharging processes. In order to evaluate the performances of a solar thermal DSG power plant based on those two chosen configurations and coupled with an indirect two-tank storage system, computer modeling and simulations have been carried out using the software EBSILON®Professional 10.05 in Chapter 5. Both plant configurations have been properly sized with the same solar field (6 collector loops of the model Eurotrough ET150) and TES system (4 hours at full load capacity). EBSILON is a very stable tool for power plant simulations with traditional water steam cycles. However, the combination of components of the solar library in combination with direct steam generation of an organic fluid led to convergence problems. In order to make design and off-design simulations successfully converge, a trade-off in the layout of both models has been made. Some pipes have been physically decoupled and boundary conditions have been set using transmitter elements. Chapter 6 has been devoted to the evaluation of the simulation results. First simulation has been performed at nominal conditions, which showed that the supercritical configuration could reach higher efficiencies ($\eta_{\mathrm{sol-to-el}}$=17.8%) and power outputs ($W_{\mathrm{el,net}}$=992 $\mathrm{kW_{el}}$) compared to the the saturated one (respectively, $\eta_{\mathrm{sol-to-el}}$=14.6%; $W_{\mathrm{el,net}}$=809 $\mathrm{kW_{el}}$). This

is mostly due to the adopted constraint on the condensing pressure of the cycles. In a second step, the behavior in part-load operation during lower irradiation conditions has been evaluated. The net power generation has achieved the maximum and minimum value for the highest and lowest values of the mass flow rates in the PB, respectively. As expected, the results have shown that the efficiency decreases as both mass flow rates and pressure decrease. In conclusion, specific interest has been dedicated to assess the integration of the indirect two-tank storage system in charging and discharging modes. Off-design results have shown that charging well occurs since there is enough thermal power available to run the power block at full load ($\dot{Q}_{\mathrm{in,PB}}$ =4083 $\mathrm{kW_{th}}$ and $\dot{Q}_{\mathrm{in,PB}}$ =4104 $\mathrm{kW_{th}}$ for supercritical and saturated configuration, respectively). On the other hand, discharging and storage-only operations occur with some thermodynamic limitations imposed by the pinch-point in the heat exchanger. The case-study of the supercritical configuration has shown that discharging at fixed temperatures could be performed until the pinch-point remains positive. A net power output equal to 96% of the design one has been reached when the mass flow rate of molten salt has been set equal to 30 kg/s. In the saturated case, only one specific combination of molten salt and ORC mass flow rate has been found feasible during the discharge mode, due to pinch point limitations. The corresponding net power output has been found to be 30% of the design capacity. It must be concluded that the integration of an indirect two-tank storage system is a feasible but not optimal solution. As demonstrated in the simulation for a typical summer day, only the supercritical configuration offers the possibility to integrate large storage systems for base-load operation. In future studies the integration of storage systems shall be further optimized. Research shall be centered on technological issues, such as material requirements and detailed process component design. Furthermore, a techno-economical analysis about materials and equipments used are required in order to prove the feasibility of the systems as a whole. This study led to the conclusion that direct steam generation of an organic fluid in parabolic trough solar plants with an integrated indirect two-tank storage system is theoretically feasible. In order to assess the dynamic behaviour of the whole plants, the implementation of a detailed control strategy is required and could constitute a future research study. In addition, an annual simulation to assess the electric energy production together with an economic analysis to estimate the levelized cost of the electricity produced by the systems should be carried out.

Appendix

Optical and geometrical losses in a PTC

The following section gives a further describtion of the optical and geometrical losses that must be taken into account to calculate the heat that is absorbed by the receiver. As mentioned in Chapter 5, Section 5.3.2, the incoming optical thermal power of the collector $\dot{Q}_{\mathrm{solar}}$ in W/m^2 is given by

$$\dot{\boldsymbol{Q}}_{\mathbf{solar}} = \mathbf{DNI} \cdot \mathbf{cos}(\boldsymbol{\theta}_i) \cdot \boldsymbol{\eta}_{\mathbf{opt,0}} \boldsymbol{\eta}_{\mathbf{clean}} \boldsymbol{\eta}_{\mathbf{shad}} \boldsymbol{\eta}_{\mathbf{end}} \mathbf{IAM}(\boldsymbol{\theta}_i) \cdot \boldsymbol{f}_{\mathbf{tr}} \qquad \text{(A.1)}$$

with:

- DNI : direct normal irradiation;
- $\eta_{\mathrm{opt,0}}$: optical peak efficiency;
- η_{clean} : reflecting mirror cleanliness factor;
- η_{shad} : shading loss factor;
- η_{end} : end loss factor;
- IAM(θ_i) : incident angle modifier as a function of θ_i in degree;
- f_{tr} : focusing state of the collector.

Optical peak efficiency

The incoming solar radiation on the collector aperture is never fully converted into usable heat. As shown in Figure A.1, optical losses occur and are associated with four parameters that are:

1. The mirror reflectivity, ρ: This parameter represents the ratio between the portion of the reflected radiation and the unitary incident radiation. The typical value for this parameter in PTCs is 0.9. Being less than 1, it means that only part of the incident radiation is reflected by the absorber tube and losses occur.

2. The intercept factor, γ: This index quantifies the losses due to either microscopic imperfections of the reflectors or macroscopic shape errors in the parabolic trough concentrators. Thus, a part of the incident sun rays reflected by the mirrors is deviated from the optimal direction and does not intercept the absorber tube. Its typical value for PTCs is around 0.95.

3. Glass/vacuum transmissivity, τ_{glass}: This index is defined as the ratio between the radiation passing through the glass tube and the total incident radiation on it. In fact, part of the incident sun rays reflected by the mirrors and reaching the glass cover of the absorber pipe is not able to pass through it. Its typical value is set around 0.93.

4. The receiver absorbtivity, α: This parameter indicates the amount of energy absorbed by the steel absorber pipe, compared with the total radiation hitting its outer surface. This parameter is typically 0.95.

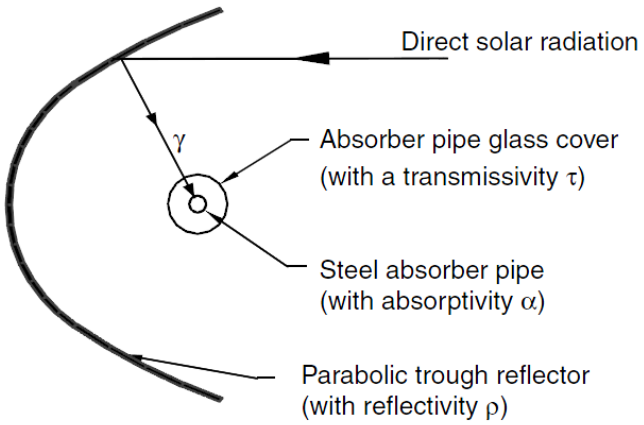

Figure A.1: Optical parameters of a parabolic trough collector [104]

By multiplying these four parameters the optical efficiency can be defined. Considering the optimal case where the collector is perpendicular to the sun'rays ($\theta = 0°$ and $\text{IAM}(0°) = 1$) and all the other efficiencies terms $\eta_{\text{clean}}\eta_{\text{shad}}\eta_{\text{end}}$ are set to 1, the optical peak efficiency is expressed as

$$\boldsymbol{\eta_{\text{opt,0}} = \rho \cdot \gamma \cdot \tau_{\text{glass}} \cdot \alpha|_{\theta=0°}} \tag{A.2}$$

Cleanliness factor

During the operational life of the system the optical properties of mirrors may decay due to the deposition of dust or soil on their surfaces. The cleanliness factor η_{clean} is defined as the quotient of reflectivity of the clean mirror ρ_0 and the actual reflectivity ρ.

$$\boldsymbol{\eta_{\text{clean}} = \frac{\rho_0}{\rho}} \tag{A.3}$$

Shading loss factor

The shading phenomenon occurs generally during the morning and in the evening. As shown in Figure A.2, a part of the collector's aperture gets shaded from the next one, thus preventing the direct beam to reach the collector.

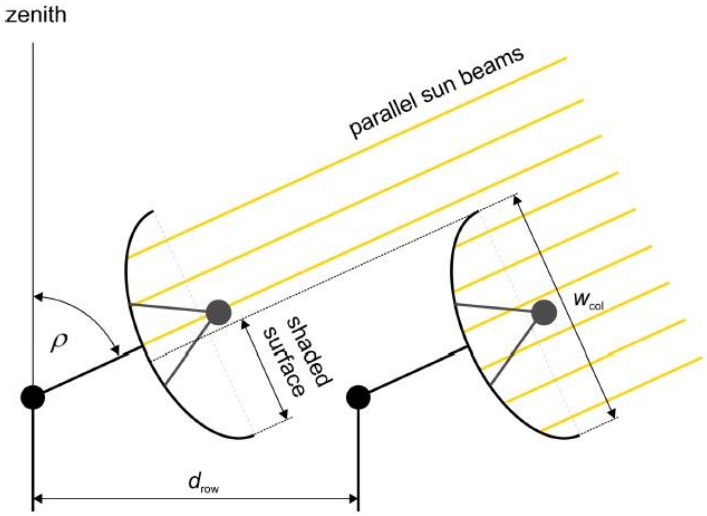

Figure A.2: Shaded collectors [91]

In order to express the losses due to shading, the efficiency factor η_{shad} is used. It can be defined as

$$\boldsymbol{\eta_{\text{shad}} = 1 - \max\left(0, \frac{n_{\text{row}} - 1}{n_{\text{row}}} \cdot \frac{w_{\text{col}} - d_{\text{row}} \cos\rho}{w_{\text{col}}}\right)} \tag{A.4}$$

where n_{row} is the number of collector rows in parallel which have the potential to shade each other, w_{col} is the collector's aperture width, d_{row} the distance between the collector rows and ρ the collector tracking angle.

Endloss factor

End losses occur when the incident angle θ_i (the angle between the normal to the aperture plane of the collector and the sun's vector, both contained on a plane perpendicular to the collector axis) is higher than 0°. Thus, as shown in Figure A.3, the solar radiation does not hit the mirrored surface perpendicularly. As the mirror field and the receiver tube are not infinite, parts of the tube are sometimes inactive, while a part of the light is reflected outside the tube. In the case of several collectors in a row, if the reflected solar radiation hits the receiver of the neighbouring collector, end losses can be partly compensated.

The endloss efficiency η_{end} is defined as

$$\boldsymbol{\eta_{\text{end}} = 1 - \frac{f \cdot \tan\theta_i}{l_{col}} + f_{\text{endgain}}} \tag{A.5}$$

with:

f : focal length (vertical distance between receiver axis and mirror surface)
l_{col} : collector length
θ_i : incidence angle of direct solar radiation
f_{endgain}: end gains that occur when there are more than one collector in a row

The factor f_{endgain} can be calculated with the number of collectors in one row $n_{col,row}$ and their distance d_{col}, as expressed in Equation (A.6).

$$\boldsymbol{f_{\text{endgain}} = \frac{n_{\text{col,row}} - 1}{n_{\text{col,row}}} \cdot \frac{\max(0, f \cdot \tan\theta_i - d_{\text{col}})}{l_{\text{col}}}} \tag{A.6}$$

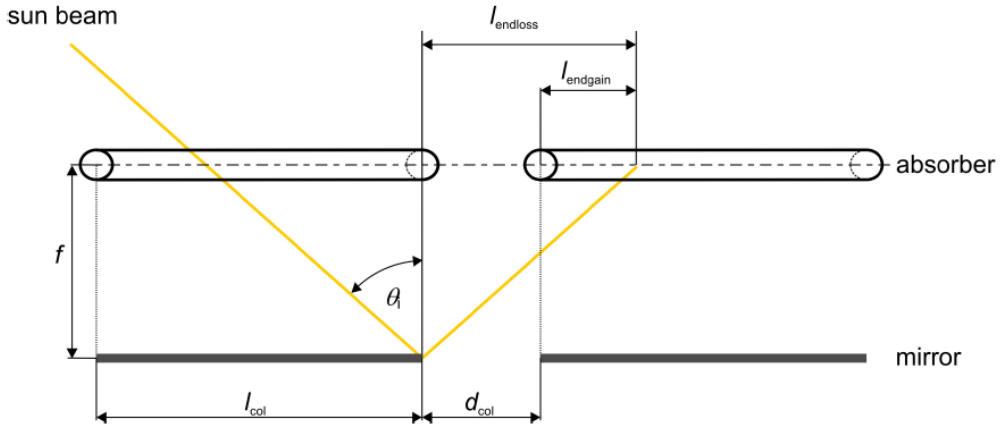

Figure A.3: End effects [91]

References

[1] *International Energy Agency IEA*. 2012; Available from: http://www.iea.org/.

[2] Kalogirou, S.A., *Solar energy engineering: processes and systems*2009: Academic Press.

[3] IEA, *Solar Energy Perspectives.* 2011.

[4] Al-Sulaiman, F.A., *Energy and sizing analyses of parabolic trough solar collector integrated with steam and binary vapor cycles.* Energy, 2013. **58**: p. 561-570.

[5] *Turboden*. Available from: www.turboden.eu.

[6] Šúri, M., et al., *Comparison of direct normal irradiation maps for Europe*. Proceeding of the SolarPACES, 2009.

[7] Price, H., et al., *Advances in parabolic trough solar power technology*. Journal of solar energy engineering, 2002. **124**(2): p. 109-125.

[8] Fernández-García, A., et al., *Parabolic-trough solar collectors and their applications.* Renewable and Sustainable Energy Reviews, 2010. **14**(7): p. 1695-1721.

[9] Giostri, A., et al. *Comparison of Two Linear Collectors in Solar Thermal Plants: Parabolic Trough vs Fresnel*. in *Proceedings of the ASME 2011 International Conference on Energy Sustainability*. 2011.

[10] Abbas, R., et al., *Solar radiation concentration features in Linear Fresnel Reflector arrays.* Energy Conversion and Management, 2012. **54**(1): p. 133-144.

[11] NREL. *NREL: Concentrating Solar Power Projects - Ivanpah Solar Electric Generating System*. 2013; Available from: http://www.nrel.gov/csp/solarpaces/project_detail.cfm/projectID=62.

[12] J., T.-K.K. and B. M, *Erneuerbare Energien, Band 2*2009: Neuruppin.

[13] Kalogirou, S.A., *Solar thermal collectors and applications.* Progress in energy and combustion science, 2004. **30**(3): p. 231-295.

[14] Laboratories, S.N. *Sandia, Stirling Energy Systems set new world record for solar-to-grid conversion efficiency*. 07.02.2014]; Available from: https://share.sandia.gov/news/resources/releases/2008/solargrid.html.

[15] SolarPaces. *Technology Characterization Solar Dish Systems*. 07.02.2014]; Available from: http://www.solarpaces.org/CSP_Technology/docs/solar_dish.pdf.

[16] *Solutia Therminol VP-1 Product Data Sheet*.

[17] Group, E.W., *Solar thermal energy production: guidelines and future programmes of ENEA. ENEA Report*, 2001, ENEA/TM/PRESS/2001-07.

[18] Kearney, D., et al., *Assessment of a molten salt heat transfer fluid in a parabolic trough solar field.* Journal of solar energy engineering, 2003. **125**(2): p. 170-176.
[19] ENEA. *Archimede Project*. 07.02.2014]; Available from: http://www.archimedesolarenergy.it/enea_archimede_project.htm.
[20] Zarza, E., et al., *Direct steam generation in parabolic troughs: Final results and conclusions of the DISS project.* Energy, 2004. **29**(5-6): p. 635-644.
[21] Zarza, E., et al., *The DISS Project: Direct Steam Generation in Parabolic Trough Systems. Operation and Maintenance Experience and Update on Project Status.* Journal of Solar Energy Engineering, 2002. **124**(2): p. 126.
[22] Zarza, E., et al., *INDITEP: The first pre-commercial DSG solar power plant.* Solar Energy, 2006. **80**(10): p. 1270-1276.
[23] Zarza, E., et al., *DISS-phase I project.* Final project report, Editorial CIEMAT, Madrid, Spain, 1999.
[24] Hellwig, U., J. Peterseim, and P. Widera, *Water Circulation Calculation for Concentrated Solar Thermal Plants.*
[25] Chemieingenieurwesen, V.-G.V.u. and V. Gesellschaft, *VDI Heat Atlas*2010: Springer.
[26] Eck, M., et al., *Field test of water-steam separators for direct steam generation in parabolic troughs.* Journal of solar energy engineering, 2008. **130**(1): p. 011002.
[27] Feldhoff, J.F., et al., *Status and first results of the DUKE project - Component qualification of new receivers and collectors*, in *19th SolarPACES Conference*2013: Las Vegas, NV, USA.
[28] Steinmann, W.-D. and R. Tamme, *Latent Heat Storage for Solar Steam Systems.* Journal of Solar Energy Engineering, 2008. **130**(1): p. 011004.
[29] Laing, D., et al., *Thermal energy storage for direct steam generation.* Solar Energy, 2011. **85**(4): p. 627-633.
[30] Steinmann, W.-D. and M. Eck, *Buffer storage for direct steam generation.* Solar Energy, 2006. **80**(10): p. 1277-1282.
[31] Feldhoff, J.F., et al., *Comparative system analysis of direct steam generation and synthetic oil parabolic trough power plants with integrated thermal storage.* Solar Energy, 2012. **86**(1): p. 520-530.
[32] Canada, S., et al., *Parabolic Trough Organic Rankine Cycle Solar Power Plant.* 2004 DOE Solar Energy Technologies, 2005.
[33] Canada, S.B., D, et al., *Status of APS 1-MWe Parabolic Trough Project.* 2005 DOE Solar Energy Technologies, 2005.
[34] *Holaniku at Keahole Point Micro CSP Thermal Plant, United States of America*. 07.01.2014]; Available from: http://www.power-technology.com/projects/holanikuatkeaholepoi/.

[35] Quoilin, S., *An introduction to thermodynamics applied to Organic Rankine Cycles.* 2008.
[36] Quoilin, S., et al., *Techno-economic survey of Organic Rankine Cycle (ORC) systems.* Renewable and Sustainable Energy Reviews, 2013. **22**: p. 168-186.
[37] Tchanche, B.F., et al., *Low-grade heat conversion into power using organic Rankine cycles – A review of various applications.* Renewable and Sustainable Energy Reviews, 2011. **15**(8): p. 3963-3979.
[38] Chen, H., D.Y. Goswami, and E.K. Stefanakos, *A review of thermodynamic cycles and working fluids for the conversion of low-grade heat.* Renewable and Sustainable Energy Reviews, 2010. **14**(9): p. 3059-3067.
[39] Wang, J., J. Zhang, and Z. Chen, *Molecular Entropy, Thermal Efficiency, and Designing of Working Fluids for Organic Rankine Cycles.* International Journal of Thermophysics, 2012. **33**(6): p. 970-985.
[40] Angelino, G. and P. Colonna di Paliano, *Multicomponent Working Fluids For Organic Rankine Cycles (ORCs).* Energy, 1998. **23**(6): p. 449-463.
[41] Wang, X.D. and L. Zhao, *Analysis of zeotropic mixtures used in low-temperature solar Rankine cycles for power generation.* Solar Energy, 2009. **83**(5): p. 605-613.
[42] Schuster, A., S. Karellas, and R. Aumann, *Efficiency optimization potential in supercritical Organic Rankine Cycles.* Energy, 2010. **35**(2): p. 1033-1039.
[43] Group of Energy Conversion Systems (Gecos), *State of the art of ORC.* Technical Report, Politecnico di Milano, 2013.
[44] Gaia, M. *"30 Years of Organic Rankine Cycle Development*. in *First International Seminar on ORC Power Systems, Keynote Lecture*. 2011.
[45] Angelino, G., M. Gaia, and E. Macchi, *A review of Italian activity in the field of organic Rankine cycles.* VDI-Berichte, 1984(539): p. 465-482.
[46] Baskharone, E.A., *Principles of turbomachinery in air-breathing engines*2006: Cambridge University Press.
[47] Obernberger, I., P. Thonhofer, and E. Reisenhofer, *Description and evaluation of the new 1,000 kWel Organic Rankine Cycle process integrated in the biomass CHP plant in Lienz, Austria.* Euroheat & Power, 2002. **10**(1): p. 18-25.
[48] Lund, J.W., *Combined Heat and Power Plant–Neustadt-Glewe, Germany*. Geo-Heat Center Quarterly Bulletin, 2005. **26**(2): p. 31-34.
[49] Canada, S., et al., *Parabolic Trough Organic Rankine Cycle Solar Power Plant.* 2004 DOE Solar Energy Technologies, 2005.

[50] Quoilin, S., et al., *Performance and design optimization of a low-cost solar organic Rankine cycle for remote power generation.* Solar Energy, 2011. **85**(5): p. 955-966.
[51] Lai, N.A., M. Wendland, and J. Fischer, *Working fluids for high-temperature organic Rankine cycles.* Energy, 2011. **36**(1): p. 199-211.
[52] Saleh, B., et al., *Working fluids for low-temperature organic Rankine cycles.* Energy, 2007. **32**(7): p. 1210-1221.
[53] Shengjun, Z., W. Huaixin, and G. Tao, *Performance comparison and parametric optimization of subcritical Organic Rankine Cycle (ORC) and transcritical power cycle system for low-temperature geothermal power generation.* Applied Energy, 2011. **88**(8): p. 2740-2754.
[54] *Ozone-Depletion and Chlorine-Loading Potential of Chlorofluorocarbon Alternatives*. Available from: http://www.ciesin.org/TG/OZ/odp.html.
[55] *GWP - Definition*. Available from: http://en.wikipedia.org/wiki/Global-warming_potential.
[56] *IPCC*. Available from: http://www.ipcc.ch/.
[57] ASHRAE, A., *Standard 34-2001, Designation and safety classification of refrigerants.* American society of heating, refrigerating, and air-conditioning engineers, Atlanta, GA, 2001.
[58] Drescher, U. and D. Brüggemann, *Fluid selection for the Organic Rankine Cycle (ORC) in biomass power and heat plants.* Applied Thermal Engineering, 2007. **27**(1): p. 223-228.
[59] Borsukiewicz-Gozdur, A. and W. Nowak, *Comparative analysis of natural and synthetic refrigerants in application to low temperature Clausius–Rankine cycle.* Energy, 2007. **32**(4): p. 344-352.
[60] Zhang, F.-Z. and P.-X. Jiang, *Thermodynamic analysis of a binary power cycle for different EGS geofluid temperatures.* Applied Thermal Engineering, 2012. **48**(0): p. 476-485.
[61] Walraven, D., B. Laenen, and W. D'haeseleer, *Comparison of thermodynamic cycles for power production from low-temperature geothermal heat sources.* Energy Conversion and Management, 2013. **66**(0): p. 220-233.
[62] Badr, O., P. O'Callaghan, and S. Probert, *Rankine-cycle systems for harnessing power from low-grade energy sources.* Applied Energy, 1990. **36**(4): p. 263-292.
[63] Invernizzi, C., P. Iora, and P. Silva, *Bottoming micro-Rankine cycles for micro-gas turbines.* Applied Thermal Engineering, 2007. **27**(1): p. 100-110.
[64] Lemort, V., et al., *Contribution à l'étude des cycles de Rankine de récupération de chaleur, VIIIème Colloque Interuniversitaire Franco-*

Québécois sur la Thermique des Systèmes, Montréal, Canada, 2007, ART-05-03.

[65] Liu, B.-T., K.-H. Chien, and C.-C. Wang, *Effect of working fluids on organic Rankine cycle for waste heat recovery.* Energy, 2004. **29**(8): p. 1207-1217.

[66] Dai, Y., J. Wang, and L. Gao, *Parametric optimization and comparative study of organic Rankine cycle (ORC) for low grade waste heat recovery.* Energy Conversion and Management, 2009. **50**(3): p. 576-582.

[67] Lakew, A.A. and O. Bolland, *Working fluids for low-temperature heat source.* Applied Thermal Engineering, 2010. **30**(10): p. 1262-1268.

[68] Quoilin, S., et al., *Thermo-economic optimization of waste heat recovery Organic Rankine Cycles.* Applied Thermal Engineering, 2011. **31**(14): p. 2885-2893.

[69] Tchanche, B.F., et al., *Fluid selection for a low-temperature solar organic Rankine cycle.* Applied Thermal Engineering, 2009. **29**(11–12): p. 2468-2476.

[70] Facão, J., A. Palmero-Marrero, and A.C. Oliveira, *Analysis of a solar assisted micro-cogeneration ORC system.* International Journal of Low-Carbon Technologies, 2008. **3**(4): p. 254-264.

[71] Angelino, G. and C. Invernizzi, *Experimental investigation on the thermal stability of some new zero ODP refrigerants.* International journal of refrigeration, 2003. **26**(1): p. 51-58.

[72] *EPA raises GWP Tariff on R245fa*. Available from: http://www.infinityturbine.com/ORC/News/Entries/2012/5/2_Price_spikes_in_USA_for_R245fa.html.

[73] Fröba, A. and e. al, *Thermophysikalische Eigenschaften eines Kältemittelgemisches aus R365mfc (1,1,1,3,3-Pentafluorbutan) und Galden ® HT 55(Perfluorpolyether).* DKV Conference 2005, 2005.

[74] Bombarda, P. and M. Gaia. *Geothermal binary plants utilising an innovative non-flammable, azeotropic mixture as working fluid*. in *Proceedings 28th NZ Geothermal Workshop*. 2006.

[75] Fernández, F.J., M.M. Prieto, and I. Suárez, *Thermodynamic analysis of high-temperature regenerative organic Rankine cycles using siloxanes as working fluids.* Energy, 2011. **36**(8): p. 5239-5249.

[76] Colonna, P., A. Guardone, and N.R. Nannan, *Siloxanes: A new class of candidate Bethe-Zel'dovich-Thompson fluids.* Physics of Fluids, 2007. **19**(8): p. 086102.

[77] *Dow Syltherm 800 Product Data Sheet*.

[78] Angelino, G. and C. Invernizzi, *Cyclic methylsiloxanes as working fluids for space power cycles.* Journal of Solar Energy Engineering;(United States), 1993. **115**(3).

[79] *CoolProp*. Available from: http://coolprop.sourceforge.net/.

[80] Mago, P.J., et al., *An examination of regenerative organic Rankine cycles using dry fluids.* Applied Thermal Engineering, 2008. **28**(8–9): p. 998-1007.
[81] Astolfi, M., et al., *Binary ORC (organic Rankine cycles) power plants for the exploitation of medium–low temperature geothermal sources – Part A: Thermodynamic optimization.* Energy, (0).
[82] Astolfi, M., et al., *Binary ORC (Organic Rankine Cycles) power plants for the exploitation of medium–low temperature geothermal sources– Part B: Techno-economic optimization.* Energy, 2014.
[83] Colonna, P. and J. Larjola, *Siloxanes as Working Fluids for Mini-ORC Systems Based on High-Speed Turbogenerator Technology.* Journal of Engineering for Gas Turbines and Power, 2013. **135**: p. 042305-1.
[84] Angelino, G., C. Invernizzi, and E. Macchi, *Organic working fluid optimization for space power cycles*, in *Modern Research Topics in Aerospace Propulsion*1991, Springer. p. 297-326.
[85] Stenglein, M., et al., *Novel Approach of Thermal Energy Storage Systems in Concentrated Solar Power Plants with Direct Steam Generation.*
[86] Tamme, R., et al., *Latent heat storage above 120 C for applications in the industrial process heat sector and solar power generation.* International Journal of energy research, 2008. **32**(3): p. 264-271.
[87] DLR, *Personal Communication.*
[88] *NIST*. Available from: http://www.nist.gov/srd/nist23.cfm.
[89] Pawellek, R., T. Löw, and T. Hirsch. *EbsSolar—A Solar Library for EBSILON® Professional*. in *Proceedings of the SolarPACES 2009 Conference*. 2009.
[90] *German Institute for Standardization, DIN 5034, part 2*, Beuth Verlag.
[91] Schenk, H. and M. Eck, *Yield analysis for parabolic trough solar thermal power plants - a basic approach.* DLR Report, 2012.
[92] Benz, N., *Parabolrinnenkollektoren: Feldtest, Optimierung und Weiterentwicklung von Receivern (PARFOR).* 2008.
[93] Forristall, R.E., *Heat transfer analysis and modeling of a parabolic trough solar receiver implemented in engineering equation solver*2003: National Renewable Energy Laboratory.
[94] Burkholder, F. and C.F. Kutscher, *Heat loss testing of schott's 2008 PTR70 parabolic trough receiver*2009: National Renewable Energy Laboratory.
[95] Friedel, L. *Improved friction pressure drop correlations for horizontal and vertical two-phase pipe flow*. in *European two-phase flow group meeting, Paper E*. 1979.
[96] Kelly, B. and D. Kearney, *Parabolic trough solar system piping model.* Final Report, National Renewable Energy laboratory, 2006.

[97] Price, H. *A parabolic trough solar power plant simulation model*. in *ASME 2003 International Solar Energy Conference*. 2003. American Society of Mechanical Engineers.
[98] Bonacina, L., *Ottimizzazione energetica e analisi economica di impianti geotermici binari in applicazione cogenerativa*, 2011, Politecnico di Milano: Milano.
[99] Stodola, A., *Dampf-und Gasturbinen: mit einem Anhang über die Aussichten der Wärmekraftmaschinen*. Vol. 1. 1922: J. Springer.
[100] Menny, K., *Strömungsmaschinen*, in *Hydraulische und thermische Kraft- und Arbeitsmaschinen*2006, Teubner: Wiesbaden. p. Online-Ressource (X, 327S. 227 Abb, digital).
[101] Macchi, E. and A. Perdichizzi. *Theoretical prediction of the off-design performance of axial-flow turbines*. in *Proceedings Atti del XXXII Congresso Nazionale ATI, Roma*. 1977.
[102] Astolfi, M., et al., *Technical and economical analysis of a solar–geothermal hybrid plant based on an Organic Rankine Cycle.* Geothermics, 2011. **40**(1): p. 58-68.
[103] Singh, O., *Applied Thermodynamics*. 3rd ed2009: New Age International.
[104] Goswami, D.Y. and F. Kreith, *Handbook of energy efficiency and renewable energy*2007: Crc Press.